CrossMark

EURECA Conceptual Design Report

The EURECA Collaboration

G. Angloher[n], E. Armengaud[b], C. Augier[g], A. Benoit[f], T. Bergmann[k], J. Blümer[i,j], A. Broniatowski[e], V. Brudanin[h], P. Camus[f], A. Cazes[g], M. Chapellier[e], N. Coron[c], G.A. Cox[i], C. Cuesta[s], F.A. Danevich[l], M. De Jésus[g], L. Dumoulin[e], K. Eitel[j], A. Erb[o], A. Ertl[o], F. von Feilitzsch[o], D. Filosofov[h], N. Fourches[b], E. García[s], J. Gascon[g], G. Gerbier[b], C. Ginestra[s], J. Gironnet[g], A. Giuliani[e], M. Gros[b], D. Hauff[n], S. Henry[p], G. Heuermann[i], J. Jochum[r], S. Jokisch[j], A. Juillard[g], C. Kister[n], M. Kleifges[k], H. Kluck[i], E.V. Korolkova[q], V.Y. Kozlov[j], H. Kraus[p], V.A. Kudryavtsev[q], J.-C. Lanfranchi[o], P. Loaiza[m], J. Loebell[r], I. Machulin[u], S. Marnieros[e], M. Martínez[s], A. Menshikov[k], A. Münster[o], X.-F. Navick[b], C. Nones[b], Y. Ortigoza[s], P. Pari[a], F. Petricca[n], W. Potzel[o], P.P. Povinec[t], F. Pröbst[n], J. Puimedón[s], F. Reindl[n], M. Robinson[q], T. Rolón[s], S. Roth[o], K. Rottler[r], S. Rozov[h], C. Sailer[r], A. Salinas[s], V. Sanglard[g], M.L. Sarsa[s], K. Schäffner[n], B. Schmidt[i], S. Scholl[o], S. Schönert[o], W. Seidel[n], B. Siebenborn[i], M. v. Sivers[o], C. Strandhagen[r], R. Strauß[o], A. Tanzke[n], V.I. Tretyak[l], M. Turad[r], A. Ulrich[o], I. Usherov[r], P. Veber[d], M. Velazquez[d], J.A. Villar[s], O. Viraphong[d], R.J. Walker[b,i], S. Wawoczny[o], M. Weber[k], M. Willers[o], M. Wüstrich[o], E. Yakushev[h], X. Zhang[p], A. Zöller[o]

[a]CEA, Centre d'Études Nucléaires de Saclay, IRAMIS, 91191 Gif-sur-Yvette Cedex, France
[b]CEA, Centre d'Études Nucléaires de Saclay, IRFU, 91191 Gif-sur-Yvette Cedex, France
[c]CNRS, Institut d'Astrophysique Spatiale, Université Paris 11, Orsay 91405, France
[d]CNRS, Université de Bordeaux, ICMCB, 87 avenue du Dr. A. Schweitzer, Pessac cedex, 33608, France
[e]Centre de Spectroscopie Nucléaire et de Spectroscopie de Masse, UMR8609 IN2P3-CNRS, Univ. Paris Sud, Orsay Campus, 91405, France
[f]Institut Néel, CNRS, 38042 Grenoble cedex 9, France
[g]IPNL, Université de Lyon, Université Lyon 1, CNRS/IN2P3, 4 rue E. Fermi, Villeurbanne 69622, France
[h]Laboratory of Nuclear Problems, JINR, Dubna 141980, Russian Federation
[i]Karlsruhe Institute of Technology, Institut für Experimentelle Kernphysik, Karlsruhe 76128, Germany
[j]Karlsruhe Institute of Technology, Institut für Kernphysik, Karlsruhe 76021, Germany
[k]Karlsruhe Institute of Technology, Institut für Prozessdatenverarbeitung und Elektronik, Karlsruhe 76021, Germany
[l]Institute for Nuclear Research, MSP 03680 Kyiv, Ukraine
[m]Laboratoire Souterrain de Modane, CEA-CNRS, Modane 73500, France
[n]Max-Planck-Institut für Physik, 80805 München, Germany
[o]Physik-Department E15, Technische Universität München, Garching 85747, Germany
[p]University of Oxford, Department of Physics, Keble Road, Oxford OX1 3RH, UK
[q]University of Sheffield, Department of Physics and Astronomy, Sheffield S3 7RH, UK
[r]Eberhard-Karls-Universität Tübingen, Tübingen 72076, Germany
[s]Laboratorio de Física Nuclear y Astropartículas, Pedro Cerbuna 12, Universidad de Zaragoza, Zaragoza 50009, Spain
[t]Comenius University, Department of Nuclear Physics and Biophysics, Bratislava 84248, Slovakia
[u]NRC "Kurchatov Institute", Kurchatov sq. 1, Moscow, Russia

A R T I C L E   I N F O

A B S T R A C T

The EURECA (European Underground Rare Event Calorimeter Array) project is aimed at searching for dark matter particles using cryogenic bolometers. The proponents of the present project have decided to pool their strengths and expertise to build a facility to house up to 1000 kg of detectors, EURECA, consisting in the first instance of germanium and $CaWO_4$ crystals. The shielding will be provided through a large water tank in which the cryostat with detectors will be immersed. The EURECA infrastructure will be an essential tool for the community interested in using cryogenic detectors for dark matter searches. Beyond European detectors, it will be designed to host other types of similar cryogenic detectors, requiring millikelvin operating temperatures. In particular, this includes the germanium detectors currently in use by the SuperCDMS team, following the current collaborative work performed by the EURECA and SuperCDMS collaborations. EURECA

will have two stages. The first phase aims at a sensitivity of $3 \cdot 10^{-10}$ pb and will involve building the infrastructure, cryostat and shielding, and operating 150 kg of detectors. The second phase will be completed with 850 kg of additional detectors, the relative weight between the different detectors being decided by the collaboration according to the physics reach. A sensitivity of $2 \cdot 10^{-11}$ pb is aimed for at the second stage. EURECA will ideally benefit from the planned extension of the deepest underground laboratory in Europe – LSM. With a site-independent design, it can also be hosted in other locations at similar or deeper sites such as SNOLAB.

1. Executive summary

The EURECA (**E**uropean **U**nderground **R**are **E**vent **C**alorimeter **A**rray) project is part of the quest for understanding the composition of our universe and in particular the large fraction, 26.8% [1], of its unknown mass-energy density called dark matter. This question, raised 80 years ago, has still no answer and there is a fierce race towards the direct detection of dark matter particles. Many astrophysical observations converge on the assumption that it would consist of particles still unknown, as yet undetected and fugitive, present since the early moments of the universe.

Many experiments around the world, all located in underground environments, aim to track down the presence of these particles. Among these, EDELWEISS, located at the LSM laboratory, and CRESST, installed at the Gran Sasso laboratory, are cryogenic experiments involving solid state detectors cooled to very low temperatures.

The experiments at the LHC have not shown any hints so far, as of March 2013, of SUSY, the favoured theory providing a natural candidate for dark matter. However, the question of the existence of dark matter in the universe and the question of which theory describes best beyond standard model physics are different. As such, direct detection dark matter experiments remain much in a situation where the attainment of continual improvement on upper limits for WIMP-nucleon cross sections through enhancing the detectors' sensitivities remains a very important objective.

In the present situation, where we do not yet have experimental proof of SUSY, nor convincing evidence of the existence of WIMPs by direct detection experiments, the next generation of direct detection experiments, providing an increase of sensitivity by two orders of magnitude, will be needed to tackle the issue of the dark matter nature. The recent avatars of low mass WIMP hints, not considered yet as evidence [2], confirm that several experiments with complementary detection principles will be needed to establish a conclusive demonstration of signal identification. The specific strengths of cryogenic detectors, namely their very good energy resolution, excellent discrimination against background and the redundancy offered by the use of multiple target nuclei in the same cryogenic infrastructure, equip EURECA with a significant advantage for the identification of a dark matter signal.

The proponents of the present project, mostly originating from the EDELWEISS, CRESST and ROSEBUD collaborations, therefore have decided to pool their strengths and expertise to build a facility to house up to 1000 kg of detectors, EURECA, consisting in the first instance of germanium and CaWO$_4$ detectors. The detectors will be mounted in subunits of towers, housed in a 6-m^3 cryostat, with shielding provided by a large water tank. Innovative cryogenics will rely on European expertise in the field, and together with adaptable cabling and electronics options, the EURECA infrastructure will be an essential tool for the community interested in the use of cryogenic detectors for dark matter searches. Beyond European detectors, it will be designed to host other types of similar cryogenic detectors, requiring millikelvin

operating temperatures. In particular, this includes the germanium detectors currently in use by the SuperCDMS team, following the current collaborative work performed by the EURECA and SuperCDMS collaborations.

EURECA will have two stages. The first phase aims at a sensitivity of $3 \cdot 10^{-10}$ pb and will involve building the infrastructure, cryostat and shielding, and operating 150 kg of detectors. The second phase will be completed with 850 kg of additional detectors, the relative weight between the different detectors being decided within the collaboration according to the physics reach. A final sensitivity of $2 \cdot 10^{-11}$ pb is aimed for.

EURECA will ideally benefit from new space provided by a new planned extension of the LSM, a cavity project called DOMUS. Furthermore, the site of Fréjus is best suited to this research being the deepest in Europe. With a site-independent design, it can be hosted in other locations at similar depths or even deeper sites like SNOLAB.

Such a unique facility, planned to operate long-term, will be designed to ensure an exceptionally radio-pure environment in order to provide optimal sensitivity for dark matter searches currently under design.

2. Science

This section describes the current context of dark matter searches and the place that EURECA, the European Underground Rare Event Calorimeter Array, will occupy within the scientific landscape. Table 1 summarises the objectives of EURECA, split into two phases, starting with a target mass of 150 kg in Phase 1 and reaching the design value of 1000 kg in Phase 2:

Table 1
Objectives of EURECA

EURECA	Goals
Phase 1	
Cross section (SI)	$3 \cdot 10^{-10}$ pb
Mass to be operated	150 kg
Residual background (all sources)	10^{-2} evts/kg/y in ROI
Duty cycle	70%
Time of operation	1 year
Phase 2	
Cross section (SI)	$2 \cdot 10^{-11}$ pb
Mass to be operated	1000 kg
Residual background (all sources)	$<10^{-3}$ evts/kg/y in ROI
Duty cycle	70%
Time of operation	3 years

The regions of interest (ROI) referred to in Table 1 are as defined for the EURECA target composition and thresholds used to obtain the sensitivities shown in Fig. 1. The following sections describe the conceptual design to reach the above physics goals.
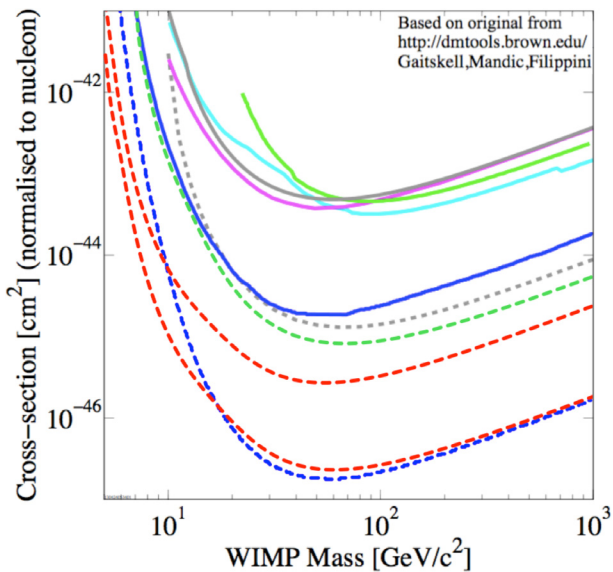
Figure 1. The sensitivities obtained by the experiments EDELWEISS-II (green) [6], CDMS (grey) [10], EDELWEISS-CDMS combined (cyan) [11], ZEPLIN-III (magenta) [12] and XENON100 (blue) [13]; the potential sensitivity of EDELWEISS-III (dashed green) with a 12 000 kg· d background-free exposure; and the position that the proposed experiments of SuperCDMS (dashed grey) [14], XENON1T (dashed blue) [15] and EURECA (Phase 1: upper dashed red, Phase 2: lower dashed red) will play in their improvement. The sensitivity for EURECA Phase 2 is as presented in Table 1, with one event/t/y assuming a 50:50 mass split of Ge:CaWO4, 5- (15-)keV threshold for 200 kg (300 kg) of Ge and a 10-keV threshold for CaWO$_4$ as presented in this CDR. Sensitivity for Phase 1 is 15% scaled by mass from Phase 2, for 70% duty cycle of one year. (For interpretation of the references to colour in this figure legend, the reader is referred to the web version of this article.)

2.1. Scientific environment

The EURECA project is part of the quest for understanding the composition of our universe and in particular the large fraction, 26.8%, of its unknown mass-energy density called dark matter [1]. This question, raised 80 years ago, still has no answer and there is a fierce race towards the direct detection of dark matter particles.

Many astrophysical observations converge on the assumption that it would consist of particles still unknown, as yet undetected and fugitive, present since the birth of the universe. While theoretical models have provided many candidates, which span 50 orders of magnitude of mass and cross section, the most motivated candidates are the weakly interacting massive particle (WIMP), the axion and possibly a sterile neutrino. In any case, dark matter requires physics beyond the standard model of particle physics.

The favoured candidate for dark matter is a WIMP related to new physics at the TeV scale. Among the various WIMP candidates at this scale, the most appealing is the lightest super-symmetric (SUSY) particle (LSP), the neutralino, which is embedded in a consistent model, e.g. the minimal supersymmetric standard model (MSSM). The MSSM postulates that the effective scale of SUSY breaking is around a TeV and that there is an additional symmetry called R-parity which would keep the lightest SUSY particle stable. Other extensions of the standard model provide suitable WIMP dark matter candidates, e.g. the light Kaluza-Klein particle (LKP) in extra-dimensional theories [3] and the lightest T-odd particle (LTP) in Little Higgs models [4].

The parameter space of WIMPs is largely covered by the proposed cryogenic direct dark matter search, which could probe dark matter particles with a mass in the range from GeV to TeV with a spin-independent WIMP-nucleon cross section down to a few 10^{-11} pb.

Current data, obtained at the LHC, do not show any hint of SUSY particles in proton-proton collisions for a total integrated luminosity of 10.5 fb^{-1} [5] up to an energy of $\sqrt{s} = 8$ TeV. No indication of

particles predicted by extra-dimensional models or by Little Higgs models have shown up either. However, the remaining parameter space is planned to be investigated after the restart of the LHC in 2015, with final integrated luminosity goals of 250 fb^{-1} by 2020 and 3000 fb^{-1} by 2030.

Nonetheless, the discovery of a candidate particle for dark matter at the LHC alone does not prove that it is the CDM particle required by cosmology. For that purpose, the detection of cosmological WIMPs is necessary. Conversely, the detection of cosmological WIMPs would show new physics but not prove that they are SUSY particles. For that purpose, identification and investigation at accelerators is necessary. The synergy between the LHC and the next generation of dark matter searches is obvious and constitutes an exciting perspective.

In the present situation, where we do not have experimental proof of physics beyond the Standard Model at the LHC, nor convincing evidence of the existence of dark matter particles by direct detection experiments, the EURECA project, by operating cryogenic detectors of up to one ton target mass and addressing an increase of sensitivity by two (three) orders of magnitude at high (low) mass, as shown in Fig. 1, is an essential tool to tackle the mystery of dark matter.

2.2. Scientific case

Many experiments around the world, all located underground, aim at tracking down the presence of dark matter. EDELWEISS [6,7], located at the Laboratoire Souterrain de Modane (LSM) under the Fréjus mountain, and CRESST [8,9], installed at the Gran Sasso laboratory, are 'cryogenic' experiments involving solid state detectors cooled to very low temperatures. They still have not shown evidence of these particles and will be limited in the coming years in their sensitivity by the size of the cryostats housing the detectors.

Cryogenic detectors, as demonstrated by the latest published results, exhibit excellent capability for their exploitation in facilities for the direct detection of dark matter particles. The quality of the next generation of cryogenic germanium detectors, with significantly improved discrimination power against background events, is such that one can anticipate to run masses of the order of 100-1000 kg without significant background.

The teams of the EDELWEISS and CRESST collaborations, together with other European teams, in particular from the ROSEBUD collaboration, leading innovative R&D on new scintillating detectors, have decided to pool their strengths and expertise to build a facility to house up to 1000 kg of detectors: EURECA.

Such an extremely sensitive search should be carried out in the best possible environment, that is in the deepest site in Europe, to reduce as much as possible the cosmic muon-induced backgrounds. This led the EURECA collaboration to favour the Fréjus site as the ideal location of the experiment.

With the current baseline design, consisting of a shield of a large water tank in which will be immersed the cryostat housing the detectors, EURECA is too large to fit within the existing cavity of the Fréjus laboratory. It will ideally benefit from the extension of the laboratory, the Deep Observatory for Multidisciplinary Underground Science (DOMUS), planned to be dug in conjunction with the already started safety tunnel (digging from France reached the position of the current LSM laboratory in March 2013) of the Fréjus road tunnel. In case of cancellation of this extension project, an alternative design of a mixed water/dense shield may allow EURECA to fit within the available space of the lab.

EURECA will consist of a single cryostat, installed in a dedicated water tank and will have two stages. The first phase will involve a cryostat and shielding with 150 kg of detectors while the second phase will be completed with 850 kg of additional detectors. The two-phased approach provides us with the opportunity to have a staged production of the large number of individual detectors.

The specifics of the set-up will be to house detectors with several

target nuclei in order to be able to prove that the observed rates and energy spectra of a possible candidate show the expected correlation of a WIMP signal. It will be designed to operate various types of cryogenic detectors: germanium bolometers currently developed within EDELWEISS, measuring heat and ionisation signals; and $CaWO_4$ scintillating bolometers allowing measurement of light and heat signals, developed by CRESST. R&D is ongoing to characterise other scintillating targets, specifically those including nuclei with enhanced sensitivity to spin-dependent interactions, and low-mass WIMPs. Depending on the achieved performance, one of these materials could be incorporated as an additional target in EURECA, most likely in the second phase.

For germanium detectors developed within EDELWEISS, the increase of sensitivity will be obtained in three ways: decrease of the local radioactive background by selection of materials and improved surface treatment, increased rejection capability against gamma rays and betas, and improvement of energy resolutions allowing lower thresholds. These three avenues of development are being pursued within EDELWEISS-III, and the obtained results allow to extrapolate to the required sensitivity for EURECA.

Scintillation-phonon detectors provide an excellent suppression of gamma background. So far this potential could not yet be fully shown due to effects related to an alpha background, this is why efforts to increase the sensitivity are therefore dominated by avoiding and tagging the alpha related backgrounds.

Different types of recoiling nuclei can to some extent be distinguished within one detector module. With the presently used $CaWO_4$ detectors of the CRESST experiment, oxygen recoils can clearly be distinguished from tungsten recoils by their different light yield (ratio between light and phonon signal). Thus, such detectors are capable of partially discriminating a neutron background from a signal caused by a WIMP heavier than ~ 20 GeV.

The detectors mentioned above use different read out schemes, which will need flexibility in the design of wiring and electronics housing of the EURECA cryostat. Such flexibility will also be a key feature allowing to house other types of detectors.

Other types of detectors are being developed within a parallel project lead by the American team of SuperCDMS, the successor of the CDMS collaboration. This program, whose goal is to operate 150 kg of germanium detectors, is very similar to EURECA Phase 1. Indeed, the very similar quality of data obtained so far by the EDELWEISS and CDMS collaborations led the two teams to combine both data sets to produce an improved limit relative to each individual result [11]. The success of this collaborative work led the two collaborations to start more concrete work on the design of their next generation of the projects described above, in order to possibly exchange detectors and further combine future data sets.

Other 100-kg to tonne-scale projects are being pursued with liquid noble gases. Self-shielding effects and capability of the localisation of interactions are distinctive features of liquid noble gas two-phase technology. The most advanced are XENON1T (two-phase liquid Xe, 1000-kg fiducial mass), LUX (two-phase liquid Xe, 100-kg fiducial mass), and XMASS (single-phase liquid Xe, 100-kg fiducial mass).

With their low threshold and good energy resolution, the cryogenic detectors exhibit very good potential for reliably detecting low-mass WIMPs. The very different detection techniques make the two approaches complementary, a strong and decisive advantage in case a possible candidate is seen by one of the detectors and needs to be cross-checked and confirmed by the other.

In summary, such a unique setup in Europe, planned to operate long-term, will be designed to provide an exceptionally good radio-pure environment. It will be designed to house, in the first instance, detectors dedicated to the search for dark matter. In particular, electronics and cabling will be designed to operate different types of cryogenic detectors, whether semiconductors such as germanium, or scintillating type as $CaWO_4$, or any other cryogenic detectors.

3. Infrastructure

Although EURECA can be placed in any suitably sized underground location, discussion here follows the preferred location of the LSM extension (DOMUS). A view of the overall layout of the proposed new space is shown in Fig. 2. Here we describe the interfaces between the host laboratory and the EURECA facility. Table 2 summarises some of the key features of the EURECA infrastructure.
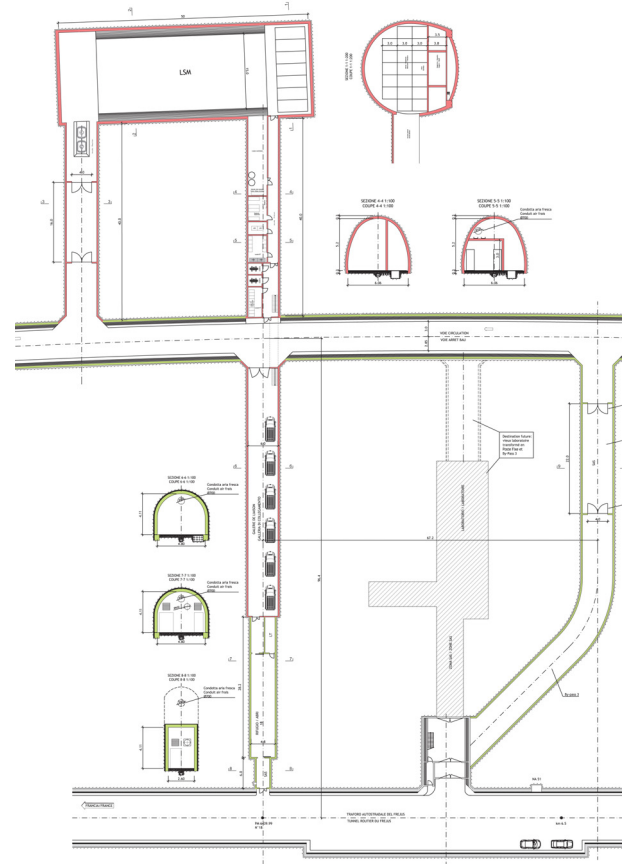

Figure 2. Position of the new facility, towards the top of the image, with respect to the existing road (lowermost) and laboratory space (shaded).

Table 2
Key features of the EURECA infrastructure

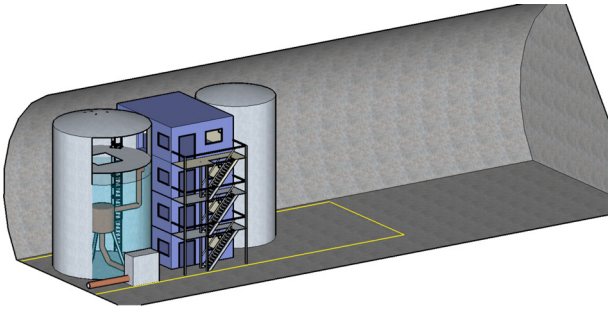| Infrastructure	Baseline option
	Space
EURECA volume	10 × 24-m footprint × 12-m height
Cryostat	2-m diameter × 2-m height
Water shield tank	8-m diameter × 12-m height
Water buffer	6.5-m diameter × 12-m height
Infrastructure building	6 × 8-m footprint × 12-m height, 3 or 4 storeys
Cleanroom suite	48-m^2 footprint × 3-m height
Cryogenics	6 × 5-m footprint × 3-m height
	Power, volume, flows and data rate
Power peak	270 kW
Power running	230 kW
Low-Rn air flux	150 m^3/h
Water volume	400 m^3
Cooling need	equivalent to 8 m^3/h of water
Shielding water recirculation	2 m^3/h
Data bandwidth	1 Gb/s

Figure 3. Layout of the main water tank (left) containing the cryostat, adjacent infrastructure and cleanroom tower, and water storage tank (right) within the 50-m-long hall of the DOMUS lab. Proximity cryogenics are shown within the cold box connected to the cryostat. Clearance of at least 1 m has been included between the cavern walls and the experimental infrastructure. The yellow line indicates the floor space available within the current LSM, although with the reduced height of only 10 m. (For interpretation of the references to colour in this figure legend, the reader is referred to the web version of this article.)

3.1. General experiment infrastructure

A schematic for the housing of the experiment is shown in Fig. 3. The detectors will be placed in a cryostat within a water tank to shield against neutrons and gamma-rays. A building is located next to the tank through which access to the cryostat will be provided. An additional tank will be placed in the vicinity of the experiment for storage of water when access to the cryostat is required. Some elements of the cryogenics system will be located in immediate proximity to the cryostat, housing the detectors. The other elements of the cryogenic systems, especially large plant (compressors, cryogenic machines) prone to contribute noise and vibration, will be placed at some distance from the cryostat. Further details are provided below.

3.1.1. Housing of the experiment

The detector cryostat will be surrounded by at least 3 m of ultra-pure water, in each direction, within a stainless steel water tank. Next to this will be the infrastructure tower which will include space for storage of materials, slow control and DAQ systems, water purification plant, and a cleanroom. The cleanroom is placed at the top of the tower and serves as access to the water tank with cleanroom integrity extending into the water tank. The tank is sealed at the point of entry by means of an airlock to preserve the low-Rn atmosphere. All connectors (electrical, cryogenic, vacuum) through the water contain bends, or include sufficient solid shielding, to prevent a direct path for neutrons. An additional water tank is located by the side of the tower for use as a water storage location when access to the cryostat is needed. The extra tank will be matched in height to the water tank to minimise the amount of floor space used, but will be of a smaller volume since no internal access is required.

For a cryostat with a height and diameter each of 2 m, the water tank would need to have a diameter of 8 m and a height of 12 m. This includes a clearance of about 4 m above the water level for access and cranes. An alternative size for the water shield is presented in Appendix A. The thickness of the tank walls will be up to 20 mm, with the precise thickness to be determined through standard design procedures (for example FEA analysis) in the TDR. The internals of the water tank will require surface passivation after thorough cleaning, with electro-polishing being a likely method for the latter.

With a water tank of 8-m diameter, the adjacent tower could have similar dimensions. A footprint of 8×6 m provides adequate cleanroom space (see Section 3.3). A vertical space of 12 m could accommodate four floors. A building this tall within a curved cavern shown in Fig. 4, would allow space for the cleanroom overpressure fans to be placed on top of the building. Sufficient space would then also exist to allow a flow of air to cool the overpressure fans. The lowermost floor
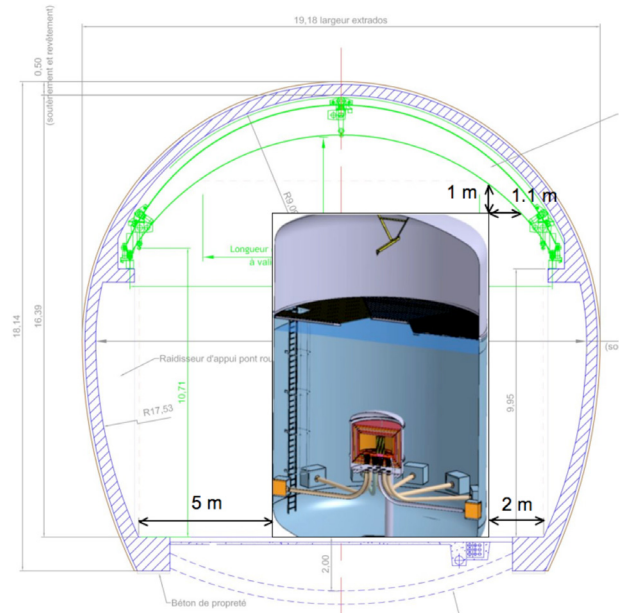

Figure 4. Position of the water tank within the cross section of the new DOMUS laboratory, approximately to scale. The widest part of the hall is 18.2 m. The cylindrical envelope for the water tank is to scale within the cross section, and has a height of 12 m and a diameter of 8 m.

could house most of the water purification plant. An exception to this would be the Rn-stripping column (if used), which would likely be too tall to be housed within a single level. The middle floor or floors could be dedicated to slow control and DAQ, whilst the uppermost floor or floors could contain the cleanrooms. All levels could also provide some form of storage.

A non-detailed analysis using the laboratory cross-section shown in Fig. 4 and assuming a regular cylindrical shape for the water tank suggests siting the tank with a 1-m clearance from the crane beam would allow a horizontal distance of 2.0 m to the wall on one side, and 5.0 m on the other side. Note that the 1-m clearance shown in Fig. 4 is most limited in the vertical direction, leaving a horizontal clearance of 1.1 m between the top of the tank and the crane beam. Structural integrity using FEA will be investigated, with close attention to the top of the water storage tank where the water level may approach closer to the top of the tank. If floor space is considered more precious, a different shape for the top of the water shield tank should be considered, allowing the experimental housing to be situated nearer to the side of the cavern. Sloping, or stepping, the top section of the water tanks above the water level would allow the tank to be placed nearer the cavern wall, but depends in part on the requirements on the reach of the crane internal to that tank. This depends on whether the crane needs the capability of horizontal movement across the full radius of the tank, and whether this is needed around the full arc of 2π.

The detector unit, inside the water tank, the water tank itself and the cryogenic unit (see below) are placed on a common platform, constructed from a 1-m-thick slab of concrete, as they will be connected via the rigid cryoline. Vibrations from the pumps and compressors will be transferred via the tubes and also this platform. The whole mass will be supported by air springs that must support a mass of approximately 700 t. Suitable dampers are available from seismologic protection systems for buildings (see e.g. [16]) that can support an axial force of up to 6000 kN. A possible strategy could be offered by a semi-active system or an active feed-forward vibration isolation system. Seismometric measurements can determine the level of vibration and piezo-electric actuators could then compensate for the movements [17].

3.1.2. Cryogenic systems

A cryogenic unit, positioned immediately adjacent to the water tank for close proximity to the cryostat, houses the 1-K pot and still, the heat exchangers and the ^{3}He condenser. The valves for the fast precooling of the detector array will also be situated inside this cryogenic unit. The unit will have dimensions of about 1.5×2.5 m, and will be mounted on the same base plate as the detector array, connected by a rigid cryo-line.

The remainder of the cryogenic system consisting of pumps, compressor and gas storage will be placed in a separate cavern up to 100 m from the detectors to reduce microphonics. Possible locations are the sides of access tunnels or a separate cavity cut into the rock. 5 m^3 is required for gas storage, with the compressor approximately $2.5 \times 2 \times 2$ m, and a further $1.5 \times 1 \times 2$ m required for oil filtration. A footprint of at least 6×5 m would be required for these items, if all of them are on the same level.

The lines to the ^{3}He and ^{4}He pumps, as well as the liquid helium (LHe) transfer line, will pass between the main cavern and the acoustically decoupled cryogenic facility. The cryogenic unit will be decoupled from vibration by flexible sections and damping structures that are optimised for the spectrum of the vibration of the pumps and the helium liquefier. These flexible sections will also allow the necessary movement of the platforms by several cm when emptying or filling the water shielding tanks.

Full details of the cryogenic system are provided in the dedicated Section 4.

3.1.3. Underground storage of detectors and other materials

Cosmic rays (neutrons and protons) interacting with different materials at the surface produce radioactive isotopes. Some of these isotopes have a relatively long half life and, after materials and components are moved underground and installed in the detectors, may contribute to the background event rate compromising the detector sensitivity. The prime concern for the EURECA experiment is the Ge crystals and copper. Both these materials will be present in large quantities. Irradiation of copper by cosmic rays will produce ^{60}Co amongst other radio nuclides with shorter half lives, whereas exposing Ge to cosmic rays will give several isotopes, the most problematic being ^{68}Ge and ^{65}Zn.

The estimates of neutron flux intensity at different depths and copper activation show that copper can be safely stored at a shallow depth of about 10 m.w.e. This will give a saturation activity of less than 0.3 μBq/kg which is well below the tolerated upper limit of about 10 μBq/kg. Copper can be stored in an underground storage place in one of the institutions and quickly moved to the processing site and then underground reducing the time of irradiation by cosmic rays.

Induced activity in Ge crystals is more problematic and a greater depth for storage is required. The exposure to cosmic rays at the surface should be minimised and the crystals will be stored underground before and after detector preparation. The decays of ^{68}Ge and ^{65}Zn give peaks at about 10 keV. In case of a high event rate at these energies, we will remove the region around these activation lines from the dark matter data analysis.

More details are given in Appendix B.

3.1.4. Heavy lifting equipment

Cranage will be needed both inside the water tanks for removal of the cryostat thermal shielding, and access to the bolometer towers; and externally for use as the tanks are built up and components of the infrastructure are added. The crane inside the tower is therefore likely to be rated to a safe working load of no greater than 1 t. This may be increased if the internal shielding cannot be split into smaller components (see below regarding internal gamma shielding). For example, a 15-cm-thick Cu shield of diameter 1.6 m would weigh nearly 3 t. Further details of the cleanroom crane are in Section 3.3. The crane

outside the water tank, in the main experimental hall, will need to be of a higher rating, up to 8 t.

Placement of a lift passing along the outside of the building to allow the easy transport of goods up to the upper floors would be beneficial. A working load of 1 t may be sufficient for this.

Access will be needed for heavy equipment to be placed in locations such as the cleanroom (laminar flow cabinets, other furniture), or side caverns (cryogenic plant). Some movement of equipment will be with portable floor cranes and pallet-trucks, which are readily available with working loads of up to at least 3 t.

3.2. Interfaces with the host laboratory

3.2.1. Electricity

Power consumption and heat loads from a number of items detailed in this section are to be considered. The power consumption of the current LSM is approximately 200 kW, with electricity supplied at 400 kVA. An estimation for the power drawn by many items is included in Appendix C. This suggests the power requirements for EURECA will be around 450 kVA (270 kW). Items included in that list are summarised here.

The total power drawn from the cryogenic plant is estimated to be 130 kW. Items considered for this are the compressor, vacuum pumps, refrigerator, electronics and the possibility of water cooling, if needed, at a total rate of 8 m^3/h. Other items likely to draw large amounts of power are the water shield purification plant (20 kW), low-Rn air supply (30 kW), DAQ and slow control (12 kW), and cleanroom plant (9 kW). Further details about each of these are contained in their dedicated Sections below.

3.2.2. Computing infrastructure

Computing will be needed for control of DAQ (detector and veto), slow control (detector and water purification) and cryogenics as well as for general use for communications, monitoring, log book entries, etc. EDELWEISS-III will provide a testbed for the EURECA DAQ, which will in turn dictate part of the computing infrastructure requirements. The DAQ will operate at room temperature and require air cooling. More details are given in Section 7.1.

Allocation must be made for local data storage and slow control machines to include data logging. Both cryogenic and water purification data, along with information about ambient conditions (temperature, pressure, Rn levels, etc.) will be stored.

3.2.3. Cooling water and drainage

The amount of cooling water required depends on the amount of heat produced, and cannot be accurately known until a design of the cryogenic system has been finalised. Initial estimates have quoted that parts of the cryogenic plant need either water cooling at a rate of 8 m^3 of water per hour, or 14 000 m^3 of air per hour. The fire-fighting circuits have previously provided water for cooling systems which was disposed of after use.

3.2.4. Laboratory cooling

The heat produced by the cryogenic plant, vacuum pumps, computing, DAQ, water and air purification

plants will need to be extracted from the laboratory. The first order estimate of power consumption is shown in Subsection 3.2.1. A power consumption corresponding to 30% of the total electrical power has been assumed for provision of cooling. It will be possible to provide a more precise figure once detailed designs of the cryogenics, DAQ and water purification plant have been finalised. These will be included within the future TDR.

3.2.5. Low-radon air supply

We work with the assertion that only the water tanks and cleanroom will need a low-Rn air supply. SuperKamiokande operates
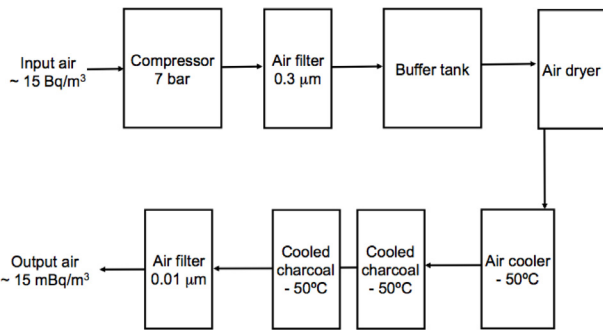
Figure 5. Schematic of the low Rn air facility.

Figure 6. Schematic of the water purification plant. The abbreviations are: UF, ultra-filtration; RO, reverse osmosis; EDI, electrodeionisation; and UV, ultraviolet.

within a regime whereby only the volume above the water is supplied with low-Rn air, with a residual Rn concentration in air of a "few" mBq/m^3 [18]. In this instance, a system of the same scale as that operating in the LSM for NEMO and EDELWEISS could provide the necessary flow of low Rn air.

The current system consists of a compressor, air buffer and dryer at one location, with a footprint of approximately 6 × 1 m; and several filters, an air cooler and a series of carbon adsorption columns at another location, with a footprint of approximately 5 × 2 m. The air cooler, and the tonne of carbon, are cooled to −50 °C. Power drawn by this is estimated to be around 30 kW when running for both EDELWEISS and NEMO. The system provides 150 m^3/h of air with a factor 1000 reduction for Rn, to less than 15 mBq/m^3. A schematic of the current Rn reduction facility is shown in Fig. 5.

Further details about Rn progeny deposition are provided in Section 3.3.

The current Rn monitoring system in use at the LSM could be used for monitoring the local environment of EURECA. If a greater sensitivity is required (dependent on simulations to show how low a Rn concentration in air we need), it would be possible to increase the size of the electrostatic collection vessel and operate the PIN detector at a higher voltage, as was done with the SuperKamiokande Rn detector. Further, a number of similar systems at different locations around the cavern could be in operation simultaneously.

3.2.6. Low-radon water supply

Simulations have shown that it is necessary to include a 3-m thickness of water to efficiently suppress the gamma background. This is in excess of the 70 cm of water necessary to reduce the neutron background to below the sensitivity of the detector. Requirements for Rn in water are to be less than 100 mBq/m^3. GERDA used a similar volume of water and obtained U, Th, K, Pb contaminations below ppt levels, with a very efficient removal of particles with sizes >1 μm [19]. EURECA will operate with a similarly low level of contaminants in the water.

Working with the baseline of a water tank of diameter 8 m and a height of 12 m containing 8 m depth of water, EURECA requires around 400 m^3 of ultra-pure water for one cryostat. An additional tank capable of storing the entire capacity of water from the shielding tank will also be required.

We will require a two-stage purification process. A schematic of the water purification plant is shown in Fig. 6. Feed water is initially passed through a system consisting of filtration and reverse osmosis several times before entering a second stage. Up to 70% of the water maybe lost during the initial stage. The second stage consists of ultrafiltration, electrodeionisation and membrane degasification, and forms part of the continuous purification loop which will be necessary to maintain the cleanliness of the water. UV treatment and/or cooling may also be necessary during the second stage, to limit bacterial growth which would reduce optical depth. For the first stage purification, a footprint of around 4 × 2 m is envisaged, depending
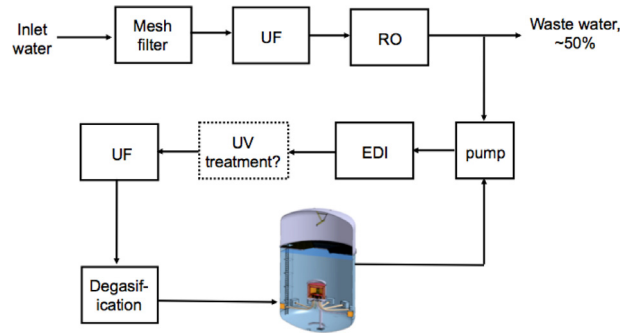
on final design. The second stage may (again subject to final design) fit into a footprint of around 6 × 4 m. However, if a buffer tank is used within the (second stage) purification loop, an additional space of the order 10 m^3 may be needed.

Of particular concern are the levels of Rn in water. This is not only for Rn daughters acting as a source of background within the water but also for the possibility of outgassing of the water increasing the Rn concentration within the air of the cleanroom, which will be at times open to the water tank. Borexino use a 6-m tall, approximately 40-cm diameter Rn-stripping column. Water flows in one direction (downwards), with a counterflow of N_2, to achieve a Rn level of 3 mBq/m^3 (reduction to this level achieved after many cycles through the purification loop) [20]. The footprint for their system is about 1 × 1 m. An alternative, as used by SuperKamiokande, would be to use a vacuum degasifier with the pre-treatment of Rn-reduced air to increase the degasification efficiency.

For monitoring the Rn concentration in water, a similar system to that currently employed at the LSM for monitoring Rn in air can be used, which is based on the design employed by SuperKamiokande [21]. With this detector, water is passed through a membrane degasifier allowing gas to flow into a chamber of Rn-reduced air which is fed into the monitor as with the 'standard' Rn-in-air detector. Quoted sensitivity is around 1 mBq/m^3 of Rn in water for a one-day measurement. It would be beneficial to have at least two such detectors; one monitoring the Rn concentration within the water tank, and the other at the outlet of the Rn degasification unit.

It may be necessary to install an additional resin-based Rn filter within the first-stage purification process. Such a step would depend on the quality of the feed water, likely dependent on its origin.

An input flow rate of up to 10 m^3/h is foreseen with recirculation dependent on contamination arising from the system.

For the cryostat outer shell, a number of possibilities exist. Ideally Cu would be used. However, Cu is known to corrode in deionised water [22], necessitating a polymer (or other) coating. Hence, PMMA (acrylic, Perspex), as discussed in Section 4 is chosen as outer shell for the cryostat.

It may be possible to use stainless steel for the pipework. However, the use of polymers is preferred to prevent metallic contamination within the water. Metallic particulates can aid the transport of bacteria. PVDF and PE are both favoured in ultrapure water systems. Materials containing fluorine used here would be sufficiently far from the detectors for it to be of no concern with (α, n) reactions.

The local firefighting service supplied water for cooling at the LSM in the past, and we assume that this can be extended into supplying the water also for the shielding. In the past, cooling water was disposed of after use, and did not form part of a closed circuit.

3.3. Cleanrooms

We plan for at least two cleanroom areas, one within the water tank and the other at the top of the infrastructure tower. The latter will be used for detector preparation and it will be through this that access to the water tank will be provided. An option exists for having either the water tank and the cleanroom as two separate cleanrooms, each with its own low-Rn air supply and vent; or having the air supply to the water tank, in turn overpressurising the cleanroom. The two must be mechanically decoupled to prevent unnecessary vibration of the detector, but also seal against the outside to maintain cleanliness within. Additional cleanroom space may be available for general facility use elsewhere within the underground laboratory.

In addition to the clean area, extra space must be available for changing rooms, and the storage of both cleanroom and everyday clothing. A clean-off area and a materials hatch will require space as they will need a double airlock system.

External to the cleanroom, space must be made available for the interfaces between inside and outside the cleanrooms. Provision must be made for gas cylinder placement, liquid nitrogen (LN$_2$) dewar storage (if boil-off of LN$_2$ is to be used as a purge gas), and the supply and disposal of water.

3.3.1. Cleanroom around cryostat

Since there exists a requirement for the cryostat to be shielded by ultra-pure water, then the water tank must be considered to be a cleanroom. Access to the cryostat will be via the water tank, initially through the adjacent man-tower, the upper floor of which will function as a cleanroom. A likely category would be ISO 6 to 7 (class 1000 to 10 000, respectively).

Low-Rn air could be introduced at the top of the water tank, further filtered to the requirements of the cleanroom. An overpressure will be maintained within the tank, although the option of using boil-off from LN$_2$ will be considered during detector operations. Careful consideration must be given to dead zones of air within the tank. It may be necessary to pipe the clean air down to the bottom of the tank while the cryostat is open. The water will already have a low concentration of Rn.

The entrance from the cleanroom will lead onto a platform in the tank above the level of the water. This is envisaged to be a solid structure of stainless steel. Two trapdoors will be located in the floor, one at the edge providing access to the bottom of the water tank; the other in the centre allowing access to the cryostat.

A crane will be included within the water tank, likely with a load limit of 1 tonne. The crane will be used for moving shields, and for the detector towers. The minimum movement necessary for the crane will need to be defined (for detector tower placement) as will the reach of the crane. If access is required to the whole volume, modifications will be needed to the platform at the top of the tank to enable it to be temporarily moved.

Space must be available for the six detector thermal shields. One option would be to include a floor stage at around the level of the opening of the cryostat. Adequate drainage would have to be considered, e.g. use of a grilled floor, as would access of the crane.

3.3.2. Cleanroom for detector mounting and preparation

The cleanroom located at the top floor of the tower will be for detector mounting and preparation. This will be a ISO 7 cleanroom containing laminar flow cabinets of ISO 5.

Since we will have multiple target materials, and therefore the possibility of multiple groups working within one area, there should be at least two of these dedicated areas. Return air from the cleanroom will be passed to the input of the air handling unit, to minimise the input of low-Rn air.

Storage and mounting space within this cleanroom will be needed for individual detectors, those mounted onto base plates, and those mounted in towers. Considering that individual towers of detectors may be up to 1-m long and up to 30-cm diameter, adequate storage space needs to be planned.

Apparatus for cleaning will be needed. This includes an ultrasonic bath, a clean (deionised and filtered) water supply for rinsing, a water disposal route, fume hoods and storage cabinets for work with hazardous chemicals and solvents such as dichloromethane, and a gas supply. Mains water can be input to the cleanroom, with small scale filtering occurring therein. Gas cylinders and/or LN$_2$ dewars could be placed external to the building and gas piped into the cleanroom.

A building of dimensions 6 × 8 m has been presented within Section 3.1. If this provides insufficient floorspace for the cleanroom, alternatives of a larger footprint or partially submerging the building will be considered. Cleanroom overpressure and HEPA-filtered fans will be placed on top of the building.

3.3.3. Radon prevention

^{222}Rn decay leads to deposition of the relatively long-lived progeny ^{210}Pb onto surfaces exposed to Rn. ^{210}Pb decays mainly by emission of two βs and an α before reaching the stable ^{206}Pb. In order to reduce the background to below one event/tonne/year in the WIMP-search region of interest (ROI), special care must be taken to reduce such deposition onto surfaces which are in direct view of the detector crystals. A low-Rn environment must be supplied for mounting the detectors into the EURECA cryostat.

The ^{222}Rn level inside the current LSM laboratory is 10–15 Bq/m^3 due to the ventilation system supplying air from outside of the mountain at 7000 m^3/h (two laboratory volumes per hour). Low-Rn air is also supplied to areas of the current laboratory to a maximum rate of 150 m^3/h with a measured concentration at the exit of the low-Rn facility of less than 15 mBq/m^3. Further details of the system are presented in Section 3.1. An average Rn level in the proximity of the EDELWEISS-II cryostat at the LSM of less than 100 mBq/m^3 has been achieved, with air supplied from this system at a rate of 0.5 m^3/h.

We plan to use a similar Rn reduction system to that already in place as an input to the cleanroom overpressure fans. Since the required air flow through the cleanroom is in excess of the low-Rn air flow by a factor of around 10, we will recycle the low-Rn air such that the fan filter units draw air in from the room itself, a standard cleanroom practice.

Calculations have been performed to estimate the amount of Rn progeny deposited on a surface for given exposure times and concentrations of Rn. Further details are given in Appendix D. For an initially clean surface exposed to 100 mBq/m^3 of Rn for 90 days, we would expect to obtain 2.5 αs and 5 βs in the ROI per tonne per year with a rejection power for both of 1.7 × 10^4 [23,24]. This activity is a factor of ∼10 too high. Possible methods of reducing the amount of Rn within the cleanroom to an acceptable level would be by increasing the flow rate of air through the Rn trap, and installing up to two additional charcoal filters. The final specifications for this improvement will be detailed at a later stage. The 90 days provides an example time for assembly of the detectors.

Within the water tank, sources of Rn may arise from the PMTs and stainless steel of the tank. A membrane degassing unit (see [21] for an example) will be included within the water purification circuit to lower the level of Rn to below the required 100 mBq/m^3.

3.4. Electromagnetic Shielding

The detailed design of EURECA's experimental installation will consider electromagnetic compatibility (EMC) from the earliest stages. It will be seen as part of the global infrastructure, as well as the cryostat and electronics designs. Additionally, the International Electrotechnical Commission (IEC) provides test standards and technical reports on EMC. The most relevant of these are within the IEC 61000

numbered documents. General regulations and good practice provide sufficient guidance for the design and implementation of general experiment infrastructure.

Special consideration is necessary for the space housing the detectors and front-end electronics at the centre of the cryostat. Here, requirements typically go beyond the general good practice described above and are described in more detail in the relevant section on electronics. Broadly, the detector accommodation will need to be designed and implemented as a Faraday cage. In addition, further shielding against magnetic interference may become necessary if this noise contribution is identified as being too high. Typical sources of magnetic contributions are vacuum and recirculation pumps and other motors and compressors. These should be located at sufficient distance from the detector compartment.

3.5. Muon veto system

The water tank housing the cryostat will be the shielding for any neutron and gamma activity from the concrete of the laboratory (see Section 3.6) and will act as an active shield for cosmic muons. For that purpose, the water tank will be equipped with PMTs. The detailed parameters of the PMT setup (e.g. PMT size, number, position, trigger threshold) will be defined in an optimising process based on MC simulations. The optimisation process will include the exact geometry of the support structure of the cryostat, the infrastructure and cabling pipes from the tank wall to the cryostat and will examine different solutions for the tank surface such as highly reflective foils. A likely configuration will consist of the order of 100 8-inch encapsulated PMTs fixed on a mounting structure at the tank wall, bottom and top. All PMTs will have to be leak checked to ensure compatibility with long term use. From first simulations (Section 8.4), the signal threshold corresponding to an energy deposit of 0.2 GeV has to be achieved to suppress any muon-induced neutron background in the bolometer array.

The simulations show that less than five single nuclear recoils induced by cosmic muons are expected for a 3 tonne· years exposure. All the background events linked to single nuclear recoils in EURECA crystals show energy deposits >0.2 GeV in the water tank. For such energy deposits, an efficiency far in excess of 90% is typical for such water Cherenkov vetoes, thus any muon-induced single nuclear recoil is expected to be vetoed. As stated in Section 8.4, an upper limit on the unvetoed single nuclear recoils is 0.3 events/year assuming an 0.2 GeV energy threshold for the veto system.

Each PMT will be supplied with an individual high voltage based on a HV system (MPOD 2H LX HV-EX mainframe housing 10 boards with 16 or 32 HV channels each) to individually adjust the PMT response. Calibration and stability/purity control will be ensured by laser pulses, movable bulbs and radioactive sources. Several options for the deadtime-free signal readout and data acquisition are currently under investigation.

The muon veto data stream (as digitised traces) will be integrated into the main data acquisition system (see Section 6).

3.6. Monte Carlo simulations for the shielding design

Alpha and beta particles have short ranges within materials. The 5-mm-thick copper screens will be sufficient to shield from these sources of radiation.

Neutrons and gammas from rock can be efficiently shielded by various materials. A suppression of gamma-ray and neutron fluxes by about six orders of magnitude is required to reduce the non-discriminated background below the level of detector sensitivity. In our simulations we have considered background radiation from rock and concrete of the lab walls. Fig. 7 shows the attenuation of the gamma-ray flux from concrete beyond the water shield, as in the baseline design of EURECA. Our results show that 3 m of water is
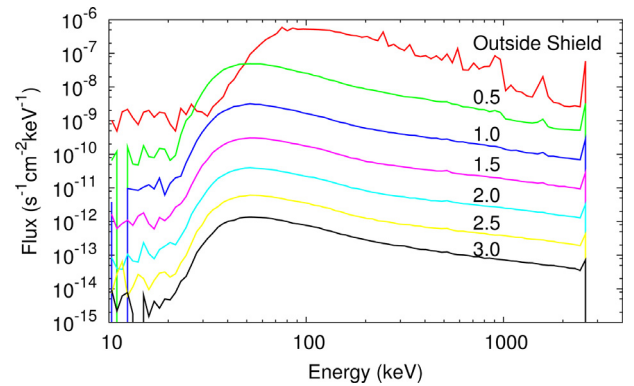

Figure 7. Gamma-ray spectra from the Th decay chain contained in the concrete of the laboratory walls attenuated by different thicknesses of water shielding (given in metres).

required to attenuate the gamma-ray flux from the lab walls so the remaining gamma-ray induced background (before discrimination) in the region of interest will be about 2000 per year in a tonne of target. This leads to a size of the water tank of about 8 m in diameter and 8 m in height for a tonne-scale experiment. With 3 m of water shield the neutron flux from rock and concrete of the lab walls will be suppressed to a level well below the detector sensitivity. More details of simulations are given in Appendix F.

4. Cryogenics and cryostat

4.1. Cryogenics

The cryogenic solution for cooling EURECA is presented in this section. Table 3 summarises the aims of the cooling system.

Table 3
Baseline design for the EURECA cryostat and cryogenics.

Cryogenics and cryostat	
Base temperature	7 mK
Cooling power at base temperature	20 μW
Cooldown time	20 days to base temperature
Cryostat size	2 m diameter, 2 m height
Cold volume	1.5 m diameter, 1.5 m height

The base temperature to be provided by the EURECA cryogenic system will be 7 mK to cool a detector mass of 1 t. Detectors equipped with NTD-Ge sensors can operate with excellent sensitivity at 20 mK; but 10 mK operating temperature (with margin) is required for the operation of $CaWO_4$ detectors, equipped with transition edge sensors (TESs). The critical temperature of tungsten TESs is around 15 mK with a spread of a few mK. For reliable stabilisation of the operating temperature for TESs, a base temperature of 10 mK is required at the detector holders, and thus 7 mK is specified as the base temperature for the cryogenic system.

This low temperature will be created by a dilution refrigerator (DR). Circulated low-temperature gas within the DR circuit will further cool two intermediate low-temperature stages: a heat intercept at 50 mK and a thermal shield at 500 mK. Additional thermal shielding will be maintained at 1.8 K and 60 K by a He refrigerator, which will also provide pre-cooling to all cryogenic components during the first stage of cool-down. A diagram of the cryogenic circuit is shown in Fig. 8.

A cooling power of 20 μW at 10 mK on the detector side is required to manage the heat release due to thermal relaxation of the bulk material at low temperature. Such high cooling powers have already been reached previously, for example in the investigation of
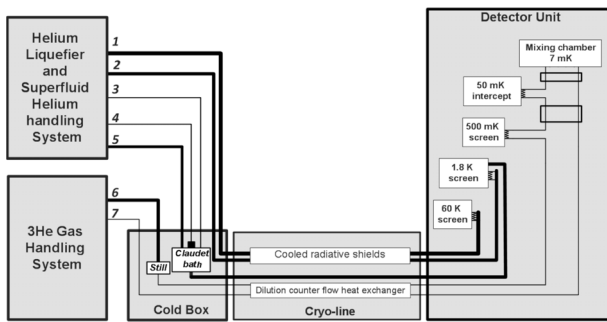
Figure 8. Diagram of the cryogenic system for EURECA. Numbered items refer to: 1, pressurised gaseous helium cooling loop; 2, pre-cooling helium loop; 3, liquid helium supply; 4, superfluid helium supply; 5, pumping line (16 mbar, return from Claudet bath); 6, dilution ^{3}He pumping line (return); 7, dilution ^{3}He supply.

polarisation of ^{3}He [25] and with the current design of the CUORE cryostat [26]. A feasibility study on the design of the EURECA dilution refrigerator has been carried out within the recent design study for EURECA [27].

Based on completed studies [17,27,28] our design includes the following features:

- A thermal shield below room temperature at 60 K; the thermal load is driven by the radiative load from room temperature; the cooling power is provided by a pressurised helium loop.
- A 1.8 K level, cooled by a pressurised superfluid helium link in order to minimise the micro-vibrations (avoiding boiling helium); the heat load is driven by the conduction from the supporting struts and cabling, and the heating introduced by the electronics front-end.
- The dilution refrigerator is optimised to minimise the conductive load on the coldest stage:
  - A closed 500 mK shield intercepts the bulk of the conductive load from structural elements and the detector wiring.
  - An intermediate 50 mK stage limits the conductive loads on the last stage.
  - An enclosure of the detector compartment at 10 mK.
- Low-temperature dilution refrigerator components are located in a common cold box with the He refrigerator (i.e. the still and the ^{3}He pre-cooling).

For comparison, the CUORE experiment [29,30] has a similar requirement for the cooling of 1 t of detectors with a cooling power of 5 μW at 12 mK. CUORE uses several 40-K and 4-K cryo-coolers to establish a number of intermediate stages. For the EURECA design, we decided against the use of cryo-coolers to minimise potential issues with vibrations. In addition, the EURECA solution of using a combination of a He refrigerator and a dilution refrigerator is favoured for reasons of fast cool-down and high efficiency.

4.1.1. Requirements

The main drivers for the cryogenic design are:

- A base temperature of 7 mK for a detector temperature of 10 mK is chosen for detector sensitivity. The large cooling power (20 μW) is driven by the estimated thermal relaxation process in the pure copper used for part of the low-background shielding.
- A cold space volume of up to 1.5-m diameter and 1.5-m height to accommodate 1 t of detectors, and internal shielding against radioactivity.
- An allocation of cooling power at a temperature <4 K for the SQUID-based cold electronics, or other front-end electronics (1.5 W at the 1.8-K stage).
- Material selection for the cryogenic parts inside external shielding.

- Minimisation of the vibrations exported from the cryogenic equipment, i.e. the compressors and pumps, the fluids' circulation and phase changes.
- Lifetime of the equipment longer than 20 years, with typical measurement periods >1 year.
- A cool-down time <5 days to reach 1 K and a further <15 days to reach operational conditions.

4.1.2. Overall cryogenic system

The cryogenic system is composed of five main elements, which are the cryostat, containing the detectors, a cryo-line, through which the cooling to the cryostat is provided, a cold box, housing cryogenics, a DR and a He refrigerator.

The cryostat will contain the detectors mounted below the mixing chamber, with front-end electronics mounted above. The cryo-line connects the cryostat, placed within the water tank, to the cold box. Our design is based on a total allowable length of the cryo-line of 20 m, although the aim is to keep the overall length below 10 m to reduce heat and pressure losses, and the required amount of ^{3}He. Further details are given below.

4.1.3. Helium refrigerator

The He refrigerator will provide cooling of the thermal stages at 60 K and 1.8 K, and will also be used for the initial pre-cooling of the colder stages. Cooling of the 60 K shield will be achieved with He gas at 40 K, pressurised to 7-15 bar. As an example, a flow of 20 g/s (5 mol/s) with a temperature elevation of 20 K gives a cooling power of 2200 W.

For the 1.8-K stage, a direct Joule-Thomson expansion of He to 16 mbar will create a 1.8-K bath. This will be combined with a Claudet bath (see Appendix E.1) to provide pressurised superfluid He (He II) to the cryostat at 1.25 bar. The use of the Claudet bath stops microphonic noise produced by He boiling within the pipe. A cooling power of 10 W extracted from the He II heat pipe creates an evaporation rate of 0.05 g/s/W (0.013 mol/s/W). This flow is low compared to the 40-K cooling loop, allowing to have a direct extraction of the 1.8-K vapours without circulation in the regenerative heat exchangers.

A small commercial He refrigerator, with modifications, is an optimal solution for the EURECA cooling system. The smallest liquefiers available from the main manufacturers provide 100 W at 4 K [31], which is needed for cooling down to a temperature of 4 K within about 4 days. Further, it has sufficient cooling capacity during normal running. At 1.8 K the cooling power is typically a quarter of that at 4 K. Two weeks of cooling are expected for reaching operational conditions. Incorporating such a He refrigerator into the cooling system allows simplification of the thermal architecture of the system through access of cooling stages within the refrigerator and linking them directly to corresponding shields and stages within the EURECA cryostat.

The He refrigerator consists of a 5 m^3 gas tank for the closed cycle ^{4}He storage, a compressor and pumps. These items will be placed at a significant distance from the detectors to limit noise generated by the high level of vibration, particularly from the compressor. The only limit is the pumping speed for the low-pressure flows (1.8-K He bath and dilution still). Additional items include heat exchangers, two gas-bearing turbo expanders, a Joule-Thomson valve and the control system, all contained within the cold box.

A suitable unit is a modified HELIAL ML series fridge, manufactured by Air Liquide [31]. This draws 75 kW at full power, during cool-down, reducing to 50 kW under part load once the system is at the operational temperature. An additional pump will be required for the 1.8 K He II within the Claudet bath. The compressor is of dimensions 2225 × 1960 × 1885 mm^3, and requires a dedicated oil removal plant of size 1500 × 800 × 2100 mm^3. A volume of

about 7 m^3 is needed within the cold box for the items related to the He refrigerator.

With the modified He refrigerator, the fast cooling phase can be managed entirely by this system using the same compressor and pumps. The cold box of the He refrigerator can also accommodate several elements of the DR: the ^{3}He pre-cooling and the still. Compared to smaller cryocoolers, the thermodynamic cycle of a liquefier (the Claude cycle) is ~10 times more efficient. The Claudet bath, combined with a fast cool-down to 1.8 K, is the main justification to use a small He refrigerator, derived from a liquefier design.

An example of a He refrigerator coupled with a cryostat with a superfluid thermal link is the NeuroSpin cryogenic system [32]. More details of this system are provided in Appendix E.1.

4.1.4. Dilution refrigerator

The DR cools three progressively colder stages at 500 mK, 50 mK and 7 mK. It is composed of a gas handling unit (placed with the compressor of the He refrigerator), a heat exchanger and still within the cold box, and the mixing chamber located within the cryostat.

Due to the 20 µW cooling power requirement combined with the low temperature of 7 mK, the performance of the dilution refrigerator depends critically on the properties of the sintered material used for the discrete counter-flow heat exchangers. The classical choice is to use sintered Ag heat exchangers. However, commercial Ag powders are known to exhibit radioactivity incompatible with low-background requirements. Power consumption by the DR is likely to be up to 20 kW during cool-down, estimated to be 15 days for 1 t of detector material, starting from a temperature of 1.8 K. This will reduce to 10 kW during low-temperature operation.

A design based on sintered Cu has been tested for EURECA [17], showing 10 cm^3 of sintered Cu is necessary to achieve the requirements. Examples are shown in Appendix E.2. Based on these results we conclude that the EURECA thermal requirements are well within the state-of-the-art. The procurement of commercial powder and details of the sintering process will be defined and characterized during the technical design for EURECA.

Several commercial powders have been identified and the following properties will be studied before the final decision on purchasing the powder is made:

- Porosity characterisation, optimisation of the sintering process.
- Measurement of the Kapitza resistance.
- Measurement of the radioactivity level.

4.2. Power budget and detector tower thermal requirements

The estimated thermal load on both stages is given in Table 22. At this stage of the design, comfortable margins for cooling power (>100%) have been included. Table 4 summarises the cooling powers and their required gas flows for the different temperature stages.

The ^{3}He isotope molar flow is driven by the cooling power requirement on the lowest temperature stage (10 mK). The estimation given here includes a 100% margin. The contributions to each stage are shown in more detail in Tables 22 and 23 in Appendix E.3.

EURECA detectors will be mounted in arrays of towers which will be heat sunk to each of the temperature stages. The design figures for the different stages of the towers are at 75 K, 3 K, 700 mK, 60 mK and 10 mK. The power budget at each stage both on the cooling-system side and the detector side is shown in Table 5 with further details of the contribution to the 10 mK stage listed in Appendix E.3. Contributions to the heat load are from dissipation of the readout electronics, dissipation and heat release in the detectors, and conduction through the wiring, neglecting the radiative load from the detector towers. Section 5.3 provides details concerning the mounting of detectors within towers.
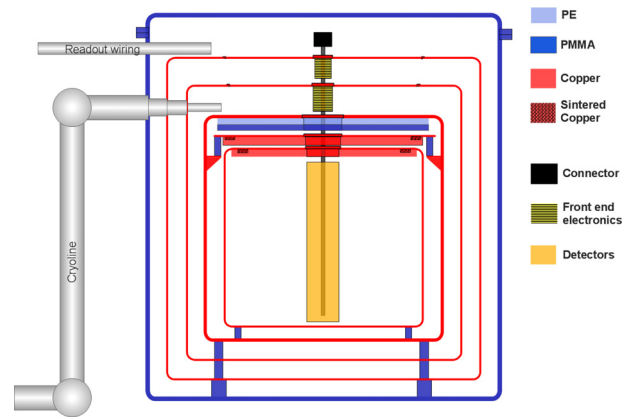

Figure 9. EURECA cryostat sketch showing the thermal shields, Cu, PE and PMMA shielding against radioactivity and other elements. One example of a top-loading detector tower is shown. The cryogenic line connects the He refrigerator with the dilution refrigerator through several cooling loops.

4.3. Cryostat design

A detailed design for the cryostat will be carried out for the Technical Design Report. Here we present a concept of the cryostat emphasising only its main features.

4.3.1. Main features

The cryostat will be installed within a high-purity water tank. The various cryogenic stages are thermally linked to the He refrigerator and dilution refrigerator through a cryo-line.

In addition to the outer vacuum container (OVC) at ambient temperature, thermal shields are placed at temperatures of 60 K, 1.8 K, 500 mK, 50 mK and 10 mK. Fig. 9 shows a schematic of the cryostat cross section. The He refrigerator provides cooling for the 60 K and 1.8 K stages in addition to the required cooling power for the readout electronics, operating at a temperature of around 100 K. The detector volume is protected by copper, polyethylene (PE) and acrylic (PMMA) shielding. The cold-plate, operating at the base temperature of 10 mK is one part of the copper shielding. The bulk of the copper shielding, as well as the PE and PMMA will be thermally connected to the 50 mK temperature level. The cooling power for the detector towers is provided by conduction through the cold-plate onto which the cooling elements will be mounted. Around 10 cm^3 of sintered material will be used to couple the cold-plate to the low temperature He mixture.

The 60 K shield limits the heat transfer to the 1.8 K stage and provides a large cooling power for the readout electronics. It is actively cooled by high pressure gaseous He supplied at 40 K, at up to 15 bar. The main thermal load is the radiation from the 300 K external wall. The temperature gradient along the shield is an issue to be considered to control the thermal load at the 1.8 K stage. Two options are considered: either a single wall cooled by a heat exchanger mounted along the cylindrical part of the shield, or a double-walled stage cooled by the cold-plate.

Table 6 presents an overview of all temperature stages of the cryostat. Figures for the heat balance are presented in Table 7. Calculations for Table 7 assume an emissivity of the copper shields of 10%, which is a conservative value for uncoated pure copper. The external wall (PMMA) has an emissivity of 100%.

4.3.2. Cryostat mechanical infrastructure

The cryostat will have a diameter of 2 m and a height of 2 m.

The inner 10-mK volume will have a diameter of 1500 mm and a minimum height of 1500 mm. This is sufficient to contain 1 t of

Table 4

Gas flows and cooling powers for each of the different temperature stages within EURECA. Gas flows are of ^{4}He for 60 K and 1.8 K stages, and of ^{3}He for the sub-K stages.

Stage	60 K	1.8 K	500 mK	50 mK	10 mK
Flow	5 mol/s ^{4}He	0.13 mol/s ^{4}He	10 mmol/s ^{3}He	10 mmol/s ^{3}He	10 mmol/s ^{3}He
Cooling power	2.2 kW	10 W	50 mW	600 μW	20 μW

Table 5

Maximum temperatures and power requirements for the detector towers at each of the temperature stages. The default number of towers is envisaged to be 12.

Cooling-side temperature	Detector-side temperature	Power - 12 towers
60 K	75 K	30 W
1.8 K	2 K	1.5 W
500 mK	700 mK	1.5 mW
50 mK	60 mK	30 μW
7 mK	10 mK	0.5 μW

detector material as presented in Section 5 in addition to the shielding for the detectors to limit radioactivity from the cold electronics (Section 8). The dimensions of the intermediate thermal shields are presented in Table 8.

Parameters for the design of the struts are given in Table 9.

For a cylinder of 2-m height and 2-m diameter the buoyancy will be equivalent to 6300 kg. The enclosure and its supports will be made stiff enough to accommodate the change in forces when water is and is not present.

4.3.3. Detector towers

The thermal contacts between the cryogenic stages and the detector towers limit the useful power available within the towers. With the towers bolted to their shields, a thermal conductance of 50 mW/K is considered as a good thermal contact at 4 K [28,33,34]. The required performance will be achieved through rigorous control of the mounting and of the surface finish. Parameters calculated for Table 7 assumed the following thermal contacts: 7 W/K at 60 K, 50 mW/K at 1.8 K, 10 mW/K at 500 mK.

Further details of the mechanics of the detector towers are given in Section 5.

4.3.4. Materials and internal shielding

Most of the cryostat will be constructed from NOSV copper. NOSV is the name given to this grade of ultrapure copper by the supplier, Aurubis. However, due to its mechanical properties, Cu will need to be reinforced at some locations to achieve satisfactory strength. Since deionised water was found to be corrosive to Cu [22], several options for the OVC material have been considered:

- Pure Cu. Only if the effect on water purity and effects of pure water are fully acceptable.
- Pure Cu with outer passive layer in contact with water. Possibly difficult to achieve full coverage, also risk of mechanical damage during installation. Potential radiopurity issues of passivation layer.
- PMMA (acrylic, Perspex) or PE. The thickness of such material would have to be enough to withstand the water pressure, possibly following a spherical design.
- Alloyed Cu. CuNi (30% Ni [17]) or CuTi.

If the OVC enclosure is made of PMMA (partly due to its low radioactivity), then a thickness of 80 mm will be required to support a differential pressure up to 3 bar. PMMA is known to have a water transmission of ~1.8 g·mm/m^2/day, giving about 0.4 g/day for an 80-mm thickness and surface of 18 m^2. As is common with many water Cherenkov systems, use of an optically reflecting layer is foreseen within the water tank to enhance the light collection of the muon veto. In our case, such a reflective layer constructed from e.g. PE or PTFE will have the additional benefit of curtailing water transmission through the PMMA cryostat jacket.

The struts separating the various stages will also be made from PMMA. If the mechanical behaviour of PMMA under stress and at low temperature is found to cause problems, backup solutions will be used, e.g. titanium alloy, Torlon.

Internal shielding in the form of Cu, PE and PMMA will be required to reduce background radiation from the cold electronics. Current estimates (see Section 8) suggest around 15 cm of Cu, 10 cm of PE and 10 cm of PMMA will be necessary.

4.3.5. Cryostat monitoring & control

A sufficient number of temperature sensors will be installed to monitor temperature at multiple locations around the cryostat, e.g. from the centre to the edge of the cold-plate, and at various temperature levels. Other parameters such as electrical parameters, acceleration, position (horizontal/vertical level) will also be monitored to identify unstable periods of detector operation.

A mass spectrometer head within the vacuum jacket of the cryostat will be included for leak-checking of the cryostat. A spectrometer tuned to different masses will be used if the cryostat volume is too large to use He due to the low pumping speed of this gas. Residual gas from the cryostat vacuum jacket will be analysed continuously to monitor the vacuum space for integrity.

4.4. Cryo-line

The cryo-line runs between the cold box and the cryostat. It will be composed of three straight components separated by 90° bends through which access will be made via a connection box. Its length will be <20 m with an outer diameter of 400 mm.

The cryo-line will be constructed from an outer layer matched in material to the cryostat outer vacuum chamber (see Section 4.3.4 for more details). A diagram showing the cross section of the cryo-line is shown in Fig. 10. A pipe made of PMMA with additional external coating will be used. Two copper screens cooled by high-pressure He at 40 K pumped through 20-mm Cu pipes will be placed inside the PMMA pipe. Another Cu screen will be placed inside these two and will contain one He II heat pipe and one pipe for pre-cooling, both of 20-mm diameter. The cryogen-free dilution heat exchanger will be placed in the middle of the cryo-line and contain the DR exchanger and a fast injection line used for pre-cooling to <10 K.

Including multi-layer insulation within the cryo-line is foreseen as an option, to reduce the heat load, currently estimated to be 300 W for a length of 20 m.

4.5. Cold box

Whilst the compressor and pumps of the He refrigerator will be placed far from the sensitive cryogenic detectors, less-noisy components will be positioned close to the detectors within the cold box. This will contain the heat exchangers, two gas-bearing turbo expanders, a Joule-Thomson valve and the control system of the He refrigerator.

Table 6
Overview of the cryostat temperature levels.

Stage	Material	Comment
OVC	PMMA	Design to support the differential pressure and compatible with ultra high purity water (80-mm thickness)
60 K enclosure	Cu	First thermal shield, cooled by He cryo-loop at 60 K
60 K thermal shield	Cu	Second thermal shield at 60 K (not required if continuous heat exchanger is mounted along first thermal shield
1.8 K shield	Cu	He refrigerator 1.8 K stage, connected by a He II heat pipe through the cryo-line
500 mK enclosure	Cu	Intermediate closed box, protection for the low-temperature stage and residual gas conduction, moderately vacuum-tight
50 mK intercept	Cu plate	Thermalisation stage for the wiring before the last low-temperature stage
10 mK stage	Cu + Ge/CaWO$_4$	Closed volume housing the detectors, moderately vacuum-tight

Table 7
Conductive and radiative loads of the cryostat.

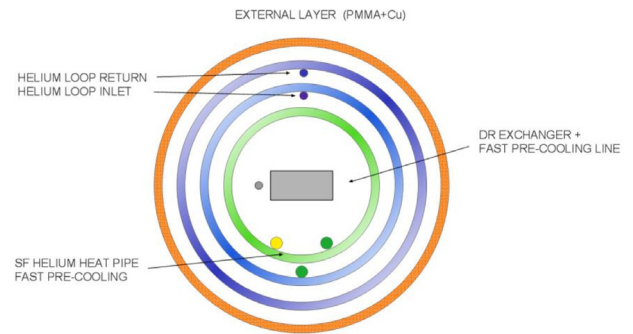| Stage	Temperature	Radiative load	Conductive load (struts)	Total
60 K enclosure	60 K	363 W	5.2 W	368 W
Thermal shield	60 K	–	–	–
1.8 K shield	1.8 K	450 mW	670 mW	1120 mW
500 mK enclosure	500 mK	0.5 μW	3400 μW	3400 μW
50 mK intercept	50 mK	–	85 μW	85 μW
10 mK stage	10 mK	–	0.5 μW	0.5 μW

Table 8
Dimensions and mass of the cryostat and its inner shields. The dimensions have been simplified by assuming perfect cylinders for the shields. The mass estimation includes a 50-mm-high flange of radial distance 20 mm for sealing located external to each shield. Inclusion of 15 cm of Cu and 10 cm each of PE and PMMA shielding, matched in diameter to the cold plate leads to an additional 2400 kg of Cu, 170 kg of PE and 215 kg of PMMA.

Stage	Diameter (mm)	Height (mm)	Thickness (mm)	Mass (kg)	Material
OVC	2000	2000	80	1650	PMMA
60 K enclosure	1780	1790	3	873	Cu
Thermal shield	1714	1734	3		
1.8 K Shield	1648	1678	3	393	Cu
500 mK enclosure	1582	1622	3	365	Cu
50 mK intercept	1516	–	–	65	Cu
10 mK stage	1516	1566	3	339	Cu
Total Mass				1650	PMMA
				2035	Cu
				3685	Total

The DR elements contained within the cold box are the ^{3}He pre-cooling bath and still. The vibrations generated within the cold box should not be an issue due to the high speed of the expansion turbines of >200 kRPM.

The cold box will be placed next to the water shielding tank, allowing at least one metre of clearance around the box. Dimensions of the box will be approximately 2.4 × 1.3 × 2.5 m^3.

Figure 10. Cross section of the EURECA cryo-line.

4.6. Cooldown

The cooldown of the system will be controlled by three cryo-fluid forced circulations. These consist of two operations:

1. Fast cooldown to 4 K.
   - 40 K He gas provided by the He liquefier to cool the external shields.
   - 4 K He pumped into the 1.8 K superfluid line. The full liquefier power will be used to achieve the 4 K temperature of the inner components within four days.
   - Forced circulation of the DR isotope mixture pre-cooled to 4 K within the cold box. A dedicated return line by-passing the counter-flow heat exchanger will be used during the cool-down (not shown on the Figures).

   The cool-down times have been validated through simulations. The He refrigerator power of 100 W at 4 K determines the time required for this stage.
2. Dilution refrigerator cool down. After the fast cool-down to 4 K the superfluid line will be used to provide the cooling power to 1.8 K and the DR will be set to operate in nominal mode. The DR will then drive the cool-down to the nominal 7 mK temperature within two weeks. Thermal relaxation in the copper and hydrogen ortho-para conversion determines the time needed for this stage.

5. Sensitivity, production and mounting of detectors

This section describes how a total target mass of up to about 1000 kg can be built and what the key issues are to reach the required sensitivity.

EURECA aims to have germanium detectors as well as scintillating bolometers within its target. Several options for materials exist

Table 9

Parameters of the struts within the cryostat. The struts in PMMA have been calculated with a 50 MPa maximum compressive strength. The buckling limit is far from the indicated values.

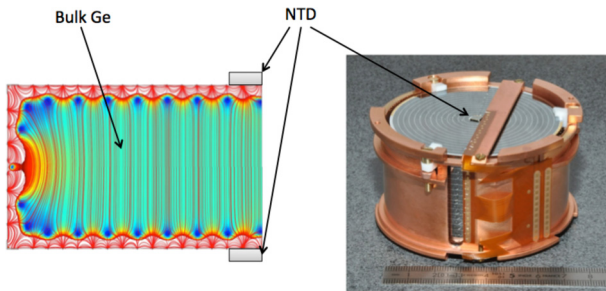| Between stages	Outer Diameter × Inner Diameter × Length (mm)	Number	Surface Area / Length (mm)	Max load (daN)
OVC to 60 K	50 × 40 × 50	8	123	30 000
60 K to thermal shield	50 × 40 × 50	8	123	30 000
Thermal shield to 1.8 K	50 × 40 × 50	8	123	30 000
1.8 to 0.5 K	50 × 44 × 50	8	72.8	18 000
500 to 50 mK	50 × 44 × 50	8	72.8	18 000
50 to 10 mK	50 × 46 × 50	8	49.2	12 000

Figure 11. Left: radial cross section of a germanium detector showing the NTD-Ge and electric field lines defining bulk and surface volumes. Right: photograph of the detector partially mounted in its support.
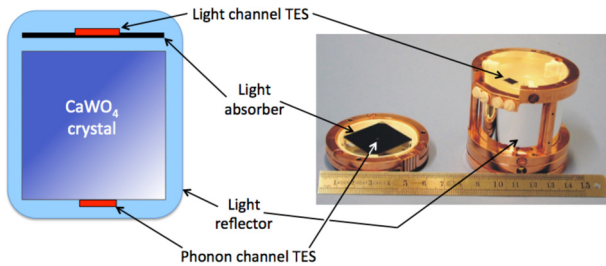

Figure 12. $CaWO_4$ detector showing TESs, light reflector and light absorber.

for scintillating bolometers, for example, $CaWO_4$ as in the CRESST experiment, or sapphire, BGO, LiF as investigated by the ROSEBUD [35] experiment. A decision on the actual material composition of the EURECA target will be made at an appropriate cutoff point. The production and mounting issues, as described in this section, are similar to all materials and the setup will be flexible to host any of them. In the following text only $CaWO_4$ is mentioned, since presently it looks most promising as scintillating material.

EURECA will be based on the detectors presently used by the two dark matter experiments EDELWEISS and CRESST. The detection is in both cases performed with low-temperature devices; however, there is a difference regarding the implementation of background rejection capability. The EDELWEISS detectors are made of germanium and are read out by NTD sensors and electrodes evaporated onto the crystal surfaces. A detector is shown in Fig. 11. The background suppression in this case is realised by simultaneously measuring heat and ionisation to distinguish between electron and nuclear recoils. In CRESST the target material is $CaWO_4$. Here, the background rejection is achieved by measuring phonons and scintillation light at the same time. The $CaWO_4$ scintillating target crystal, as well as the light detector, are readout by superconducting TESs made of tungsten films. A detector is shown in Fig. 12. Both detector types are being optimised, addressing aspects such as radiopurity, scintillation properties, background identification and energy threshold.

A better control of background events from the surface is the way to further increase the sensitivity of both detector types, germanium

and $CaWO_4$. Besides the reduction of surface contamination, this can be achieved by the fully interdigitised (FID) detector design [24,36] in the case of germanium and by scintillating detector holder surfaces in the case of $CaWO_4$. To produce a total target mass of up to 1000 kg we assume a mass of 800 g for germanium crystals and 300 g for $CaWO_4$ crystals as a baseline design. There is work in progress to increase the crystal size to 1600 g for germanium and 1000 g for $CaWO_4$, but already with the baseline option, at least 100 kg of target mass for both germanium and $CaWO_4$ can be produced per year. The detectors will be mounted in 12 towers, each with either 108 germanium detectors or 180 $CaWO_4$ detectors and a mix of up to 1040 kg of germanium and of up to 648 kg of $CaWO_4$ can be built as a target. Table 10 summarises the key numbers for the detectors and detector production.

Table 10

Key numbers for the EURECA detectors and detector production. Separation (or energy) threshold refers to the recoil energy above which the rate of undiscriminated gamma events falls below the target sensitivity.

Sensitivity Requirements		
Separation threshold	10 keV or below	
Background suppression	10^5 or better	
Energy resolution for Ge detectors	650 eV (ionisation), <1 keV (heat)	
Energy resolution for $CaWO_4$ detectors	<1 keV (light), 300 eV (heat)	
Readout		
	Heat	Charge/Light
Ge detectors	NTD sensors	FID Al electrodes
$CaWO_4$ detectors	TES	TES
Detector Mass		
	Baseline design	Advanced design
Ge detectors	800 g	1600 g
$CaWO_4$ detectors	300 g	1000 g
EURECA maximum capacity – baseline desig		
	Target mass	Number of detectors
Ge detectors	1040 kg	1296
$CaWO_4$ detectors	648 kg	2160

Under the usual assumption of coherent WIMP scattering, one expects that the total scattering rate in $CaWO_4$ is dominated by interactions with the heavier tungsten nuclei. However, due to kinematics a heavier nucleus tends to receive a smaller recoil energy, and in a detector with a finite energy threshold the other constituents can also become relevant despite the coherence effect. For low WIMP masses up to about 12 GeV, the scattering off tungsten is completely below threshold, and oxygen and calcium recoils give the only possible signal. On the other hand, above WIMP masses of about 30 GeV, germanium and tungsten recoils completely dominate. When looking for possible WIMP interactions we therefore benefit from considering all nuclei from both materials in order to be sensitive to the largest possible range of WIMP masses and to discriminate against a potential remaining neutron background.

The two types of detectors are to be kept in separate towers, as the two detector types do not have the same geometry and the same readout scheme. $CaWO_4$ temperature sensors are low-impedance TES

while FID sensors are high-impedance NTD germanium, with charge read-out using electrodes. There are also slight differences in cryogenic requirements. NTD germanium sensor performance is a smooth function of their temperature, and are currently adapted to $\sim 18 \pm 3$ mK, while TES require a precise regulation at their transition temperature, currently around 15 mK. There are also differences in calibration requirements since the ionisation channel of germanium detectors is very linear, while both heat and scintillation channels of $CaWO_4$ are non-linear and require a pulser scheme, and the ionisation channel of the FID detectors needs daily resets by exposition to either an intense gamma-ray or IR LED source.

5.1. Present sensitivity and strategy for improvement

5.1.1. Sensitivity improvement with germanium detectors

The sensitivity of the EDELWEISS ID detectors was of the order of one count per 100 kg· day, a factor 1000 away from the EURECA objective of about 1 count per tonne·year. This sensitivity was found to be limited by the insufficient shielding against fast neutrons and by the limited gamma-ray rejection of the ID detector design (limited to a few 10^4). This latter observation led to the development of the FID800 detector design, with a demonstrated gamma suppression of $4 \cdot 10^5$.

In order to achieve a sensitivity at a level of 10^{-10} pb, the expected gamma-ray background needs to be suppressed by a factor 10^5 for recoil energies above 10 keV. This performance has already been surpassed with FID800 detectors. Maintaining this performance down to 10 keV requires baseline resolutions on heat and ionisation signals below 1 keV. This goal has been achieved by EDELWEISS-II. The expected background presented in Section 8 is based on a reduction of the gamma-ray background by a factor of ~ 10 relative to what has been achieved in EDELWEISS-II. Experiments are being performed currently to see if the gamma rejection factor of present-day FID800 detectors reaches the 10^6 level, which would relax the constraints on the gamma-ray background that needs to be achieved.

The other important suppression factor for germanium detectors is that of surface beta events. With the present level of five surface events per detector per day in the first FID detectors, the rejection needed for surface events is of the order of 10^6. This is a factor 15 larger than the measured rejection of ID detectors. A factor two reduction in surface contamination has been achieved in the past, and a further reduction by an order of magnitude is expected from the tuning of the surface treatment of the germanium detectors, as this has been shown in both EDELWEISS and CDMS to be an effective way to improve the charge collection in surface events, resulting in charge yields sufficiently above the values associated with nuclear recoils.

5.1.2. Sensitivity improvement with $CaWO_4$ detectors

The sensitivity of the CRESST detectors was of the order of one count per 10 kg·day. The gamma suppression of the present CRESST detectors has been shown to be better than 10^5 at 45 keV, where this measurement was limited due to the alpha background. This alpha background was found to be the main limitation to the above sensitivity and is discussed below. Independent of this alpha background, given the width of the light-yield distributions and under the assumption there are no 'effects of reduced light', the gamma suppression of the CRESST detectors can be estimated to be better than 10^7 down to 20 keV for oxygen recoils and down to 15 keV for tungsten. Assuming this level of rejection, and given the known actual level of contamination, the sensitivity we are aiming for of about one count per tonne·year in the energy window of interest could be reached even with the present level of radioactive contamination. So far no indication of any surface effect or any other effect reducing the light yield for electromagnetic interactions has been found. Nevertheless it will be useful to reduce the contamination of the crystals,

which is why efforts are undertaken within CRESST to grow scintillating crystals from previously screened materials under well controlled conditions.

However, the high potential for gamma suppression could not yet be fully shown due to the effects related to the alpha background. A recoiling nucleus from an alpha decay hitting the target crystal cannot be distinguished from a tungsten recoil induced by a WIMP. This potentially problematic background can be suppressed if the surrounding surfaces are scintillating; in this case the escaping alpha particle produces additional scintillation light when hitting those surfaces and the event will appear as a high light-yield event, distinct from the low light emitting nuclear recoils. Both detectors of a module are held by thin bronze clamps and are enclosed in a common, highly light-reflective housing in order to collect as much scintillation light as possible. The bronze clamps are also covered with a thin scintillating layer except at the small spot at which they touch the crystal. The light reflector is a polymeric foil which scintillates. Making all surfaces in the vicinity of the detectors scintillating is important in discriminating background events due to contamination of surfaces with alpha emitters. The efforts to increase the sensitivity therefore are currently dominated by providing cleaner clamp material and by developing a method to make the entire clamps scintillating. The current level of alpha-background of 0.1 evt/kg· d needs to be reduced by a factor of around 10^4 to meet the low level needed to obtain the WIMP sensitivity curve shown in Fig. 1.

The energy threshold above which a sufficient separation of nuclear recoils from the electron-gamma background is possible depends largely on the resolution of the light channel at low energies and the level of gamma background. Reducing the threshold pays off much more than reducing the crystal contamination, which is why efforts are being undertaken to further improve the light detection efficiency and resolution. A light-channel resolution at low energies of < 1 keV$_{ee}$ is currently achieved. The phonon channels typically have an energy resolution of ~ 300 eV (FWHM) at low energies and allow triggering at 2 keV with full efficiency. With this performance of the phonon- and light-channels in the presently running detectors, a separation between oxygen and tungsten recoils with $\sim 50\%$ efficiency is possible above 10 keV, which is sufficient for the goals of EURECA. A factor of three to five seems possible through improving the performance of the light channel, until single photon detection sensitivity is reached. If achieved in practice, considerably lower discrimination thresholds than 10 keV would be possible.

5.2. Detector production

5.2.1. Production of germanium crystals and ionisation electrodes

The FID detectors used in the EDELWEISS-III experiment are cylinders with a height of 4 cm and a diameter of 7 cm. Their mass is 800 g. Estimates of price can be reliably based on the current experience with the production of 34 such detectors for EDELWEISS-III. As for the production schedule, it took an average of one week for evaporating the aluminium electrodes on the detectors and to validate their isolation resistance. This step of the production process was the main cause for limiting the production rate at one detector per week because of the availability of only one evaporator. The number of detectors that can be produced per week is given by the number of evaporators and the cost of increasing the number of these machines in an industrial environment has been evaluated.

Germanium crystals of 800 g are our baseline design. One important development to consider for EURECA, in order to reduce the number of readout channels per crystal and reduce the surface-to-volume ratio of the detectors, is to double the crystal mass. The same height of 4 cm would be kept, in order to keep the same electric field strength in the detector volume, but with the diameter increased to 10 cm. The mass per crystal would then be 1.6 kg, and only 300 detectors are needed to obtain a total mass of 0.5 t. The diameter of 10

cm is a development being pursued by the SuperCDMS collaboration. For this important future development, we need to:

1. procure 10-cm-diameter crystals,
2. modify the evaporator currently used to produce EDELWEISS detectors to accept (a) such large diameter and (b) make it possible to hang and rotate such large masses with the necessary precision,
3. verify that the FID fabrication is reliable in terms of leakage currents and quality of gamma and surface rejection,
4. allow for adaptation of crystal quality, surface treatment, height, diameter.

The ionisation and heat sensors of the germanium detectors have a relatively simple design, well adapted to mass production. Once the production yield is satisfactory we will find an industrial partner to prepare two or three evaporators and train competent personnel to be able to produce 300 detectors in one year. Should the 10-cm-diameter crystal solution not be possible, the existing 800-g crystal design will be implemented. Keeping the same production rate in terms of mass of detector per month would then require doubling the number of evaporators. The number of detectors has implications for the readout system (cabling and electronics). The planning on this aspect is based on the 800-g baseline solution, and fitting less electronics and cabling is easily accommodated.

5.2.2. Germanium heat sensors

Systems assembling many hundreds of NTD germanium heat sensors with sufficiently uniform performances have already been made (CUORICINO, CUORE). In EDELWEISS-II it was shown possible to obtain heat sensor sensitivities that vary smoothly with bolometer temperature (typically ~10% per mK), with the advantage of having performances that do not rely critically on achieving the best cryogenic conditions. In the FID detector design, each bolometer is equipped with two NTD germanium sensors. This redundancy enhances the signal-to-noise ratio when the signals from both sensors are combined.

5.2.3. Production of CaWO$_4$ crystals

Present CaWO$_4$ crystals have a mass of 300 g and have cylindrical shape with a diameter and height of 4 cm. Increasing diameter and height to 6 cm will result in a mass of 1000 g per detector module. Mass and fiducial mass are the same for this type of detector. The possibility to produce and use larger target crystals is under investigation. For the discussion here, we assume 300 g per module. For a 100-kg target, 330 detector modules are necessary. The demonstrated delivery rate is about two 1-kg crystals per month [37]. To achieve a target mass of 100 kg or more, other solutions are therefore required.

To obtain a 300-g CaWO$_4$ target crystal, a primary crystal with a minimum length of 60 mm and minimum diameter of 45 mm has to be grown. To make future 1-kg target crystals, the size of the primary crystal would have to be 65 mm in diameter and 80 mm in length. A critical parameter is the light yield of the crystals as scintillators. It depends on the purity and stoichiometry of the starting material, on the oxygen partial pressure in the growth atmosphere and on the conditions during post-growth annealing. The post-growth annealing is carried out under oxygen atmosphere and ameliorates the crystals mechanical, optical and luminescent properties. The light yield should have a minimum value of 100% compared to our currently used reference crystal.

At present we are able to grow crystals with 60 mm length and 45 mm diameter out of which we can manufacture one crystal of the presently used 300-g type. The time required for the complete production process is 2.5 weeks. This includes the growth process, post-growth annealing as well as cutting and polishing of the crystal and the characterisation of its light yield. The currently produced crystals show a light yield of ~ 100% of our reference crystal. For the crystal growth we use a Cyberstar Czochralski furnace equipped with a rhodium crucible (80 mm and 120 mm in diameter). In the first attempts with the larger crucible we were able to grow crystals with 1.6-kg mass, a diameter of 55 mm and 80 mm length. It is therefore conceivable that we will be able to produce target crystals with 1 kg of mass in the near future. Furthermore, the growth of crystals which are long enough that one can manufacture two crystals with 1 kg each is in principle possible. For the growth of one crystal the Czochralski furnace is occupied for three days. This is true for the production of the currently used 300-g crystals but will also not change for future 1-kg crystals. Therefore, to produce 100 kg of the current 300-g crystals within one year, one will need three furnaces, assuming 100% production efficiency and a continuous production during the whole year. For future 1-kg crystals one furnace is sufficient to obtain 100 kg of crystals under the same assumptions.

5.2.4. Production of TES

There are two types of TES, one for the phonon channel and one for the light channel. Both are thin tungsten films which one has to evaporate onto a carrier crystal. In addition there are aluminium and gold structures attached to the tungsten film as phonon collectors, for biasing, cooling and heating the thermometer film. The energy threshold of the phonon and the light channel mainly depends on the operating temperature and thus the critical temperature T_c of the TES. To achieve the required sensitivities, a T_c below 20 mK is needed for the phonon channel. Much more demanding is the required sensitivity for the light channel. A higher T_c of the light channel directly results in higher separation thresholds between gammas and nuclear recoils and between oxygen and tungsten recoils. Therefore a T_c around 15 mK is needed for the light channel.

Tungsten films for reading the thermal signals of the CaWO$_4$ crystals are deposited by electron beam evaporation on thin CaWO$_4$ wafers. A thin SiO$_2$ layer on the CaWO$_4$ wafers serves as a diffusion barrier. A deposited tungsten film is structured via photo-lithography and wet chemical etching into a number of TES, which subsequently receive sputtered aluminium contact pads for electrical and gold pads for thermal connection of the TES. Present light detectors use thermometer and heater structures directly evaporated on silicon or on sapphire wafers. With such thin wafers used as TES carriers, standard deposition equipment can be used (UHV system, coating, etching, bonding, mask aligner, etc). Several UHV evaporation systems and all other thin film etching and structuring equipment are available within the EURECA collaboration partners. The production of several light detectors per week is possible and one can produce TES for one hundred detectors within a year.

Until recently most TES for the phonon channel have been evaporated directly onto the large CaWO$_4$ target crystals, and special equipment for almost all steps in the film deposition and film structuring process was required. The scintillation properties of the crystals suffered from the heating cycle during the evaporation process. To overcome these problems in future, the thermometers will first be deposited onto a small and thin carrier crystal and after production glued onto the CaWO$_4$ target crystal. In recent CRESST runs, such composite detectors showed an even better performance due to the increased light yield. For the future this technique will considerably simplify mass production. After tungsten evaporation onto one 2- or 3-inch wafer, more than 20 thermometers could be cut. The real limiting issue will be a measurement of the T_c of each individual TES. The required numerous cool-downs to 10 mK would definitively limit the effective production rate. In recent years, considerable progress has been achieved in controlling the stability of the resulting T_c over several production runs. A characterisation of one of the TESs fabricated from a large tungsten film should be sufficient. To further facilitate this process we are investigating the possibility of characterising a larger number of TESs in one cooldown by using a multiplexed SQUID readout.
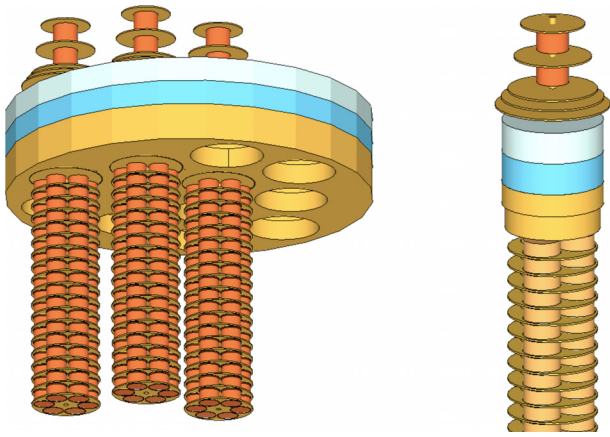
Figure 13. Positioning of detectors along a detector tower. Left shows the 86-mm diameter, 48-mm-high outer casings, as in EDELWEISS-III, with detector trays of 280-mm diameter mounted next to the 1500-mm diameter low background shielding. Right shows the larger casings necessary for the 100-mm diameter germanium crystals within trays of the same diameter.

5.3. Detector mounting and tower geometry

The mechanical stability, heat transport, and optimal packing of the detectors and their front-end electronics and cabling are the key requirements for the interfaces which consist of detector housings, cable paths, supports and thermal links. The choice of materials is limited to the most radio-pure ones; all other materials must be minimized. The residual heat load, vibration control and microphony are also important parameters to control in the design of the interfaces.

5.3.1. Arrangement of germanium detectors

EDELWEISS-III uses 800-g germanium detectors mounted in copper frames of a maximum outer diameter of 86 mm and external height 48 mm, arranged in multi-level arrays with a centre-to-centre detector spacing in each horizontal plane of 90 mm. Centre-to-centre vertical separation is 53 mm. Working with the baseline design of using these same dimensions for EURECA, we assume additional space external to the detector outer casing will not be required, e.g. for the cumulative amount of wiring along the length of the tower. Small modifications can, however, be made. Further, we work here with the baseline solution of placing fully mounted detector towers from the top of the cryostat into the detector compartment.

A 90 mm centre-to-centre spacing allows six 800-g detectors to be placed within a diameter of 280 mm with additional space for structural support. Considering the clearance needed to mount detector towers from the top of the cryostat, a tower centre-to-centre spacing of 360 mm is needed once all spacing for further shielding is taken into account (see Fig. 13). 12 towers, each containing 18 layers, then give a maximum mass of 1040 kg of Ge. A 280 mm diameter tower also allows the possibility of three 1600-g crystals, each with a diameter of 100 mm, to be placed within the same volume. The total height of detectors for a 53 mm pitch is then 960 mm. A further ~600 mm would be necessary for mounting through the thermal and low background shields. Detectors could be mounted onto a tray which is then attached to a central rod. A schematic of the design is shown in Fig. 13.

5.3.2. Arrangement of CaWO₄ detectors

300-g $CaWO_4$ crystals have a diameter of 40 mm and a height of 40 mm. These are currently mounted within holders allowing a horizontal spacing of 64 mm and a vertical spacing of 70 mm. A slight reduction, especially in module height is possible, so we assume in the following a 64 mm vertical and horizontal pitch. 12 detectors can be mounted per level on each of the 280 mm plates. For 15 levels

Table 11
Example options for ratios of germanium and $CaWO_4$ crystals, assuming 800 g and 300 g respectively.

No. of towers Ge:CaWO₄	No. of detectors Ge:CaWO₄	Mass (kg) Ge:CaWO₄
12:0	1296:0	1040:0
10:2	1080:360	865:108
6:6	648:1080	520:324
2:10	216:1800	175:540
0:12	0:2160	0:648

per tower with a 64 mm vertical pitch this will give 180 detectors or 54 kg of $CaWO_4$ per tower. If larger $CaWO_4$ crystals of 60 mm diameter, 60 mm height and 1 kg of mass can be manufactured, one could mount them in a spacing of 84 mm horizontally and vertically. Six of these detectors can be mounted per level. With 11 levels this results in 66 detectors, or 66 kg of $CaWO_4$ per tower. Arranging a split between germanium and $CaWO_4$ towers, assuming each tower has only one type of material, leads to the arrangement as shown in Table 11. Further assumptions are that 800-g germanium or 300-g $CaWO_4$ crystals are used.

5.4. Readout requirements

5.4.1. Readout of germanium detectors

The readout scheme is the same as in EDELWEISS-III. There are four ionisation channels and two heat NTD channels per detector. For ionisation, the excitation and readout is via the conventional relay scheme [38]. For heat, the excitation is via the usual square excitation scheme, operated at a typical frequency close to 1 kHz. For optimisation of the heat readout, a temperature regulation via a heating resistor on the detector is foreseen. Heat pulses can be injected via either of the two NTD germanium sensor excitation channels.

5.4.2. Readout of TES on CaWO₄ detectors

One phonon and one light channel is read out per detector module. Each tungsten sensor is equipped with a heater. The heater is used to stabilise the operating temperature and to periodically inject heater pulses for continuously monitoring the energy calibration at a set of discrete energies and for measuring trigger efficiency close to threshold. The heater is also used to inject large heater pulses, so called control pulses (about one control pulse every 10 s), serving to control the operating temperature of the TES. The DAQ measures the pulse height of the resulting detector pulses in response to the control pulses and provides a heating signal to stabilise the amplitude of the detector pulses at a constant value. Signal shapes of phonon and light channels are very similar. In CRESST, signals are converted with 16 bit ADCs at a sampling rate of 100 kHz.

Cabling for both types of detector are presented in detail in Section 6.5.

5.5. Detector calibration

The EURECA experiment will require several low and high intensity radioactive sources to perform different kinds of calibrations: energy calibrations to determine the energy scale for phonon and ionisation channels, Compton calibrations with low-energy electron recoils to define the electron recoil band and measure the discrimination power, and neutron calibrations to define the nuclear recoil band, and measure detection and cut efficiencies. In addition, gamma-ray sources will be needed to discharge electrodes periodically and thus restore sensitivity to the ionisation readout channel.

Our experience with currently running experiments shows that [133]Ba provides the most efficient Compton calibration (highest ratio of low-energy to high-energy events). A large number of crystals and

the compact structure of the cryostat will require several sources positioned around the cryostat, each having different intensities. Low intensity (∼1 kBq) sources will provide calibration of the crystals close to the cryostat walls whereas gamma-rays from higher intensity sources (∼10 kBq and greater) will be able to penetrate to the centre of the cryostat. We also consider the use of ∼1–10 kBq ^{60}Co sources for calibration of the crystals close to the centre of the cryostat. The exact position and intensity of sources will be optimised for a specific geometry of the cryostat and crystal configuration. Energy calibration and measurement of energy resolution will be carried out using ^{133}Ba sources (276 keV, 303 keV, 356 keV and 384 keV lines). The germanium detectors will also benefit from unavoidable residual ∼10 keV x-ray photons from ^{68}Ge produced via cosmogenic activation on the surface. They will provide energy calibration and resolution measurements at low energies. For germanium detectors, high-intensity (>100 kBq) ^{60}Co sources will be used to remove the charge accumulated on the surfaces of the crystals. Another possibility is to use a distributed LED system with light delivered through a system of fibres to keep possible radioactive contaminants of LEDs and associated components far from the crystals. Neutron sources (≥100 Bq) will also be placed around the cryostat providing nuclear recoil events in all crystals for calibration of the nuclear recoil band and efficiency measurements.

During science data runs all sources will be stored in small sealed containers on wires, on the inner surface of the water tank far from the detectors so the radiation does not compromise the sensitivity of the experiment. During calibrations or charge removing periods containers with sources will be remotely moved along wires close to the cryostat to irradiate the crystals. Central and peripheral detectors will be calibrated at different times using high- and low-intensity sources, respectively (high-intensity sources will saturate the DAQ of the nearby crystals preventing their calibration to be done at the same time as for central detectors).

6. Electronics and cabling

Table 12 summarises the key numbers for the electronics under the baseline option.

Table 12
Key numbers of the EURECA electronics requirements

Electronics and Cabling	Baseline option
Power requirements	
Room temperature	7.5 kW
100 K level	30 W
2 K level	1.5 W
500 mK level	1.5 mW
50 mK level	30 µW
10 mK level	0.5 µW
Space requirements [dm^3]	
Room temperature	2300
100 K level	17
2 K level	11
500 mK level	1.5
50 mK level	2.5
10 mK level	4

The cabling system can be divided into two sections. One is cryogenic cabling, crossing temperature levels, and all this is to be installed on the detector towers. The second part is a long (>3 m) cabling section, maintained close to ambient temperature, linking the detector tower cabling to the external electronics positioned outside the water shield. The temperature levels for heat sinking of the cabling are governed by the cryostat-side and the detector-side temperature levels, as listed in Table 5, and by the temperature of the front-end JFET-based electronics, running at a temperature of ∼100 K. The power listed in Table 12 for the room temperature level is generated outside the cryogenic vacuum space, whereas all other power generation is within the cryogenic vacuum enclosure.

6.1. Introduction and scope

This section deals with extracting and processing signals from the cryogenic detectors (see Section 5) up to their presentation in digital form to the DAQ. It also deals with the control of the detector biases and the monitoring of all operating conditions that might affect detector performance. It excludes however processing of muon veto data, cryogenic systems data, and any environmental monitoring.

Overall, as for any low background experiment, electronics must also provide a negligible source of radioactivity. Additionally, mounting of first stage amplifiers should take account of their associated power output, and the implications for heat loads with the cryogenic design. Cabling requires a trade-off between reducing thermal conduction (high resistivity) and limiting electronic noise (low resistivity); room temperature and cryogenic cabling differ in this respect as detailed below.

An analysis of how to best streamline and unify the reading out of various sensors, such as NTD-Ge sensors, electrodes for measuring ionisation, QET or TESs shows that much of the hardware is common and, if designed into the system, could be reconfigured to suit the individual detector requirements through running different firmware (can be switched through appropriate command) and, if necessary, a keyed connector, which could be part of the tower cabling or a sensor-specific minor piece of hardware. As a concrete example, the latter two sensors (QET and TES) require installation of a SQUID, acting as impedance converter, which is then read out by the same differential amplifier that is used in a direct manner for reading out high-impedance sensors. Control, excitation and bias voltages/currents can be used for different purposes and their distribution is a matter of the cabling and a minimal set of front-end components. With this approach, the entire EURECA readout can be viewed as a high-impedance readout system and the specifics of electronics and cabling that are individual to the various sensors are confined to a small space and placed near the detectors and towers.

6.2. Room-temperature cabling

Room-temperature cabling will connect the front-end electronics inside the cryostat, situated on the detector towers close to the detectors, to the electronics outside the cryostat and shielding at room temperature. This section of cabling has to bridge the width of the water tank (∼3 m). There are two options for access ports (pipes); one is a straight pipe (or more) that will contain the retractable cable assembly, the other employs a bend of ∼1 m radius in the tube to avoid direct line of sight in order to avoid neutron channels. The former option would see the pipe fully filled with shielding material to avoid direct line of sight and to replace the water the pipe displaced. A similar scenario may be possible for the bent pipe design.

This first section of cabling does not bridge temperature levels and thus the cabling material is not critical. It can be carried out with coaxial cables or shielded Kapton/Apical designs with copper tracks to keep the resistance down. Inside the cryostat, the cabling is terminated on a mechanically robust connector to match that on the actual detector tower. Termination of the cable on one end (still to be decided whether this should be nearer the towers or nearer the external electronics) is on a vacuum barrier to allow the transition from the inner vacuum of the cryostat to the electronics outside. Various solutions for such connectors exist. Keeping the resistance levels low for this long section of cabling is important for any kind of electronics.

6.3. 100 K electronics

The front-end electronics will be kept flexible to be able to read out ionisation channels and NTD-Ge sensors from ionisation-heat bolometers and SQUID impedance converters from other types of detectors. This part of the electronics is mounted on the actual detector towers, following the idea that a tower with its detectors and front-end readout system can be operated independently.

The general idea is to use JFET input stages as already done in EDELWEISS, but to design the first stage in such a way that the true function (whether readout of NTD-Ge, SQUIDs or ionisation channels) is determined by the cabling attached to it on the detector side, and/or a reconfiguration of the room temperature section of the electronics. Designing the hardware sections of the electronics such that everything is identical from the inputs at the 100 K level via the room temperature electronics and digitisation stage to the interface to the DAQ is a major advantage in flexibility of running different detectors in terms of cost and maintenance.

In addition to the tried and proven 100-K electronics, use of HEMTs could avoid a 100-K stage for the electronics altogether, but significant research into the practicability of using HEMTs at the 2-K temperature stage will be necessary to demonstrate that they provide the same reliability and overall performance as the existing approach.

6.4. Cryogenic cabling

This deals with the cabling from the room temperature level to the 100-K level and from the 100-K level down to the actual detectors and towers. Thermal properties are quite important here and so are radioactivity issues, at least for cables close to the detectors. This section of cabling is shorter than the room temperature section and will be made of either Axon [39] coaxial cabling or a laminated Kapton/Apical design with stainless steel tracks. Heat load and cabling capacitance will be important. Tables in Section 6.6 detail the number of cables between different temperature stages for different numbers of germanium and $CaWO_4$ detectors. Since the exact ratio of detector technologies is not critical for this CDR, and the contribution of cabling is not the dominant heat load, the precise number of cables will be somewhere between those figures provided.

6.5. Special considerations for each sensor type

The direct readout of NTD-Ge sensors is done in differential mode. Single-ended readout of electrodes for ionisation is sufficient, but channels could be grouped in a logical way, for example using the same bi-FETs as are used for differential readout in a logical way for two single-ended ionisation signals. Relay configuration and avoiding resistors of high values ($>10 \, M\Omega$) should allow reliable operation and could avoid electronic components at a 2-K or 4-K level. There is scope for further rationalisation, especially in light of also incorporating the possibility of reading out a SQUID impedance converter.

For EDELWEISS FID800 detectors, there are two pairs of wires for two NTD-Ge and four ionisation signals. Hence eight wires per 800 g, or 10 per kg. Associated with each wire is a JFET input stage, causing a heat load of ~1 mW per JFET, or ~10 mW per kg. This value could be a factor of two smaller in an optimistic scenario, or a factor of up to five higher, if speed and ultra-low noise are a concern. For the cabling between the 100 K level and room temperature, each FET requires two wires, and in addition there are bias and feedback wires, resulting in a total of 36 wires per kg detector material.

For CRESST scintillation detectors (300 g each), two SQUID readout channels (one phonon and one light) are required. In addition, a reference resistor is required at the 10 mK level (this could be installed at a higher temperature level, but requires careful consideration of readout currents and impedance of the TES). The wiring is as follows:

- TES to reference resistor: 4 wires (one pair for bias and TES readout and one pair for heater).
- Reference resistor to SQUID: 6 wires (one pair for bias, one for readout and the heater pair).
- SQUID to 100-K stage: 10 wires (one pair for TES bias, one for TES heater, one for SQUID bias, one for SQUID signal, one for SQUID feedback).
- From 100 K to room temperature, this results in 12 wires (the SQUID voltage will be amplified by a JFET pair).

Given existing 300 g detectors (each with phonon and light sensor) require multiplying the above numbers of wires with 6.66, giving 26, 40, 66 or 80 wires per kg detector. Increasing the mass of individual detectors by a factor of 2.5 would reduce this number to the same level as for EDELWEISS-style detectors. Regarding the heat load to the 100 K stage, based on 300 g detectors, 14 JFET per kg are required, resulting in 14 mW per kg (or 6 mW with larger detectors).

A similar analysis of requirements presented here for EDELWEISS/CRESST-style detectors can also be done for CDMS-type detectors.

Also, for CRESST-style detectors, superconducting wiring between the TES, the reference resistors and the SQUID may be necessary, or alternatives could be explored.

6.6. Implications to cryogenics – thermal loads

At the 10-mK level, the heat load is almost exclusively from wiring. To achieve acceptable heat loads from wiring, additional temperature levels between 10 mK and 2 K are required. Here, 0.5 K and 50 mK have been chosen. For NTD-Ge sensors, no additional electronics components are required at this temperature level. In case of TES, the reference resistors should be mounted at this temperature level (although higher temperature levels may be possible) and the power produced by them has to be taken into account. However, given the ~1 μA bias currents and tens of mΩ reference resistor values, this gives with 3332 such detectors (two sensors per detector, 500 kg) ~1 nW, a negligible contribution.

At the 2-K level there could be a contribution from the shunt resistors in the SQUIDs, if installed there. At this temperature level the contribution from SQUIDs is negligible. The heat load from cabling is the dominant contribution.

At 100 K, the dominant contribution to the heat load is the front-end electronics and the cabling. For an all-EDELWEISS FID800 scenario (maximum number of JFET for 1,000 kg detector mass), this is 10 W for the most likely case, but could be up to several tens of W, depending on speed and noise levels required. 20 W for the electronics alone is assumed adequate at this temperature level.

At room temperature, experience with existing electronics suggests that ~5 W per kg detector mass is required for either detector type. This is a rather crude and uncertain estimate and will have to be refined further when designs or prototypes for the EURECA electronics become available. Overall, this figure will have to be multiplied by ~1.5 to take into account the power dissipation of linear power supplies. 7.5 kW is thus the likely power requirement at room temperature.

For heat loads from cabling we consider a composite of Kapton/Apical with glue layers and stainless steel conductors. The signal tracks are in the middle of the cable and there is a screening layer on either side. Overall the composite is ~0.85 mm thick and the track pitch is 0.5 mm. The thickness of the stainless steel layers is 18 μm. The three scenarios discussed below are EDELWEISS detectors (Table 13), CRESST detectors (based on 300 g per module, Table 14). The EURECA scenario is based on scintillation detectors also achieving a mass per module of 800 g and enough cabling to allow total flexibility in detector installation (Table 15).

Heat sinking of this cable type, given its flat shape is easy to achieve with clamping between copper plates. Stacks of cables can be made

Table 13
Heat load from cabling for all detectors being of type EDELWEISS FID800.

From	To	Length	10^3 wires	Heatload
300 K	100 K	0.4 m	36	7.8 W
100 K	2 K	0.2 m	10	0.6 W
2 K	0.5 K	0.1 m	10	0.9 mW
0.5 K	0.05 K	0.2 m	10	18.0 μW
0.05 K	0.01 K	0.1 m	10	0.3 μW

Table 14
Heat load from cabling for all detectors being of type CRESST 300 g.

From	To	Length	10^3 wires	Heatload
300 K	100 K	0.4 m	80	17.3 W
100 K	2 K	0.2 m	66	3.8 W
2 K	0.5 K	0.1 m	40	3.6 mW
0.5 K	0.05 K	0.2 m	40	72.0 μW
0.05 K	0.01 K	0.1 m	40	1.2 μW

Table 15
Heat load from cabling for EURECA (800-g detectors) – maximum flexibility for installation of ionisation-heat and scintillation-heat detectors.

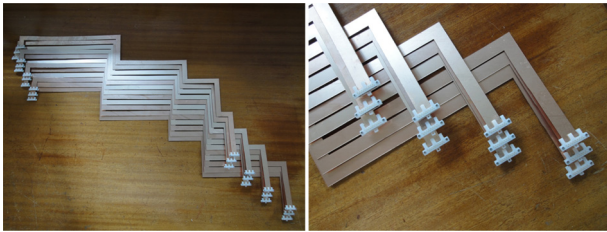| From	To	Length	10^3 wires	Heatload
300 K	100 K	0.4 m	36	7.8 W
100 K	2 K	0.2 m	26	1.5 W
2 K	0.5 K	0.1 m	16	1.5 mW
0.5 K	0.05 K	0.2 m	16	29.0 μW
0.05 K	0.01 K	0.1 m	16	0.5 μW

Figure 14. An example of prototype laminated Kapton/Apical cabling with connectors as installed on the EDELWEISS cryostat for validation for future use in EURECA.

to keep the routing tidy and space requirements low.

All the above figures are estimates and can be adjusted by using different lengths of cabling and/or different/additional temperature levels for heat sinking.

6.7. Cabling and connectors

6.7.1. Laminated cabling

The cabling is either stainless steel or copper as conducting material and Kapton/Apical (or other polymers) with intermediate adhesive/glue layers. On both large faces of the cable, a solid layer of conductor is installed to act as shielding. Copper cables are used near the detectors for reason of radio-purity and for the long section at room temperature to keep the resistance low, while the stainless steel version is used where the cable has to bridge temperature gradients. A typical cable has 18 μm thick layers of metal, the track width is 100 μm and the pitch is 0.5 mm. To keep the electronic capacitance at acceptable levels of ~40 pF/m, the thickness of the shielded cable overall should be ~0.85 mm. Some of these dimensions may change slightly in the process of achieving the optimal design. As such, each wire occupies a cross section of 0.5 mm × 0.85 mm, or 0.425 mm^2. With some extra space between cables, which, in practice is always required, 0.5 mm^2 per wire is a good estimate. Fig. 14 shows an example of a prototype laminated Kapton/Apical cabling with connectors.
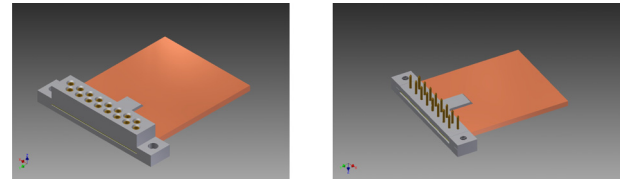

Figure 15. The Kapton/Apical cabling with connectors – plug and socket – attached. Any of the components are made internally and thus full control over radio-purity levels can be exercised by the EURECA collaboration.

6.7.2. Low-radioactivity connectors

The connectors use MillMax pins, suitable for 1 mm pitch. The pins and sockets are housed in Delrin bodies of ~3.5 mm height, each. Allowing for material around the pins to hold them at a pitch of 1 mm and for space to hold the connectors together, the volume occupied by a pin/socket combination for a single wire is ~5 mm^2 × 2 × 3.5 mm, or 35 mm^3. Fig. 15 shows an example of such a solution.

6.8. Space requirements, radioactivity and EMC

6.8.1. Space requirements

Based on the above considerations, the space requirements can be grouped broadly into two areas: the electronics and the cabling. The current design assumes that the cabling will be part of the towers and that any heat sinking etc. will be done on a per tower basis rather than bulk on the cryostat.

For the cabling, the estimate is based on the EURECA scenario with 36,000 wires from the room temperature electronics down to the 100 K level, 26,000 wires down to the 0.5 K level and 16,000 wires towards the 10 mK level. This gives cross sections for the wiring of 180 cm^2, 130 cm^2 and 80 cm^2. This is for the cabling only. In positions where heat sinking to temperature levels is required, these figures will have to be multiplied by ~3. These numbers look large, but not impossible when dividing each by the number of towers. Then, more manageable numbers (per tower) of few cm^2 emerge.

In the following, a few items and scenarios are discussed (starting from nearest to the detectors):

Reference resistors (required for TESs at the 10-mK level): based on existing CRESST reference resistor boxes (which act in addition as heat sinks), but envisaging closer packing: 1 cm^3 per two channels. Assuming 800 g detectors, this is 1250 cm^3 for 1 tonne (a maximum scenario). This figure should be doubled to allow access space for the connectors to cabling, giving a total of 2500 cm^3.

SQUID impedance converters (required for TESs at the 2-K level): each SQUID device is composed of the actual SQUID chip, which is not large (a pcb, approximately 8 × 10 mm^2 and 3 mm high), a pcb holding a transformer and a few passive components, and a niobium shield, housing the SQUID chip. Overall, the whole assembly can be accommodated in a volume of 3 cm^3 per readout channel. With 2 channels per 800-g detector, this gives 7500 cm^3 for one tonne. Care has to be taken with the actual installation position of these SQUID assemblies as the materials are not radio-pure.

Electronics at 100 K is needed for all detectors: this is largely the front-end FETs, relays and passive components. Working on the assumption of 14 JFET channels and 4 relays per kg of detector, the likely space requirement at this level is ~8000 cm^3 for the electronics alone. Realistically, this should be doubled for access to the connectors. Heat sinks are estimated as three times the cabling cross section times a length of 2 cm.

Table 16 gives an overview of the space requirements for individual components at the various temperature levels. As far as cabling is concerned (running between temperature levels) the volumes for these are attributed to the lower temperature level. Most of this space (except at the 300 K level) will be required in individual towers (see

Section 5.3).

For the 300-K section, this cabling is largely the 3.5 m needed from the centre of the cryostat to the outside of the water shield. It is mainly the volume of the tubes linking the cryostat to the outside electronics. The size of the electronics is estimated, based on existing installations and doubled to allow space in between for cooling. The working assumption is that per kg detector mass, the room temperature electronics (reading out the front-end, carrying out digitisation of signals and providing detector bias and control voltages/currents) occupies about 1 dm^3. This results in 1250 dm^3 for the electronics. In addition, power supplies are needed, likely to occupy a further 1 m^3. Room temperature electronics will be placed outside the water tank, so only minor space limitations apply.

6.8.2. Radioactivity

The radioactivity requirements are dealt with in Section 8 and all components will have to be assessed accordingly. Most critical are obviously the connectors near the detectors, the Kapton foils for terminating the detector wiring and the Kapton cabling leading to the next level of electronics. A few mBq/kg are tolerable near the detector and the limitation of materials selected for their low radioactivity makes it likely that this requirement can be met.

There are, however, composite materials like circuit boards and components which must be placed in the vicinity of the detectors. Such materials do not meet the lowest level of tolerable radioactivity and there is little choice in, or chance for, identifying a component of suitably low radioactivity. For these cases the relevant component will have to be installed behind appropriate shielding. Such shielding is shown in sketches of possible detector tower layout, for example in Fig. 13.

6.8.3. EMC considerations and grounding

These considerations are vitally important for low-noise operation of cryogenic detectors. It is also an area that needs careful planning from the start as retro-fitting would be rather difficult, time-consuming and costly in terms of funding as well as detector performance. There exist general guidelines, but these need to be interpreted to be correct for the actual situation. Considerations relating to the external setup are listed in Section 3. Here the focus is on the detectors, the front-end electronics and the cryostat, up to the point at which digital signals are transmitted via optical fibres to the digital DAQ.

The detector compartment is an all-metal vacuum container and as such represents a Faraday cage which shields well against electric fields, but not so much against magnetic fields. It is therefore important to avoid large currents flowing across the walls of the Faraday cage by accidentally (or through poor design) introducing multiple ground points. In case of the inner vacuum of a cryostat this is not too difficult to achieve as it is normally isolated anyway and only connected to the outside world through a number of access ports and cryogenic tubing, all attaching to it in close proximity from each other. For the EURECA cryostat, this will be an area of careful planning based on the experience gained with the existing experiments.

Any signals in and out of the Faraday cage will have to be filtered and are ideally differential around a potential as near as possible to the system ground so that the ground does not act as a return path for any of the signals. This is not difficult to achieve for floating sensors. Such sensors are not grounded, but should operate differentially around the ground from the front-end electronics, through which this scheme is continued to the next stage of electronics comprising the main detector bias and digitisation. The cabling between the front-end and the main electronics is potentially long and should be carried in its own shielding, the connections of which will have to be carefully controlled and connected with care to retain 360° shielding on the main board via a connector. The number of connectors should be minimised as these are always a problem for cross-talk and loss of electromagnetic immunity.

The components on the main electronics board should all be fitted onto the board rather than using piggy-pack boards. Implementation of a very high standard of board layout and routing is paramount. This is especially true for the decoupling between noisy digital components and the low-noise analog sections. These need different, yet common approaches to implementing grounding and shielding, and past experience has shown that this is a highly critical area. Digitisation is implemented on these boards and signal transmission to the digital DAQ is accomplished via optical fibre links, greatly enhancing EMC.

The power supplies should be linear ones and heavily filtered. Soft-switching diodes in the rectifiers have proven vital for low-noise performance. It is also important to keep the chassis ground separate from the analog ground for best performance.

6.9. DAQ – digitisation and detector bias

The room temperature electronics can be grouped broadly into devices that establish the detector operating parameters, the back-end analog electronics to the front-end (nearer to the detectors) and devices that are concerned with the digitisation of the signals emerging from the analog electronics. The electronics covered in this subsection is situated away from the detectors at the periphery of the water shield and have a manageable cable length (∼3 m). The interface to the DAQ should be implemented via optical fibre links to avoid ground loops and interference from digital noise. There is a clear advantage in grouping the components together as described, avoiding multiple clocks (risk of beat frequencies) or transporting signals through connectors (expensive, prone to introducing crosstalk and noise). Invaluable experience exists already from iterations on BoloBoxes for EDELWEISS-detector readout and the CRESST detector bias and readout system. As such, implementing a multi-channel system for EURECA should not pose a new challenge but will be a further progression (and further optimisation) of existing technologies. Advances in technology with multi-channel 16-bit ADC ICs and corresponding DAC with up to 40 channels in one IC lend themselves for the design. A further advantage is that the operating voltages for such devices seem to decrease, mainly driven by the need to keep power and cooling requirements manageable. Optical fibre links can run at 100 MB/s without any problem, or even higher, and have the great advantage of fully decoupling systems.

7. Data acquisition system and

analysis

7.1. Data acquisition

In this section we describe the online processing of digitised signals from the various EURECA data channels. The main data flow comes from the bolometer array and we anticipate around 5000 electronic channels from bolometers. The exact number of channels will depend on the relative amount of scintillation and ionisation detectors, as well as on the final detector design for both technologies. For each channel, 16-bit digitisation will be needed to cover the dynamic range from sub-keV to MeV energies, the former corresponding to the detector thresholds and the latter being needed to characterise several sources of background. Since the heat, ionisation and light signals have different time responses, the sampling rate will depend on the type of the channels. A sampling frequency of 100 kHz is needed for ionisation, and 1–10 MHz may be considered in order to resolve the time structure of charge deposition. Signals from low-frequency thermal sensors, such as NTDs, are well resolved with a sampling of ∼1 kHz, but they may be modulated to reduce the effect

Table 16
Space requirement for EURECA – maximum flexibility for installation of ionisation-heat and scintillation-heat detectors.

Level	Cabling	Heat sinks	Electronics	Total
300 K	63 dm^3	–	2,250 dm^3	2,300 dm^3
100 K	7,200 cm^3	1,080 cm^3	8,000 cm^3	16.3 dm^3
2 K	2,600 cm^3	780 cm^3	7,500 cm^3	10.9 dm^3
0.5 K	800 cm^3	480 cm^3	–	1.3 dm^3
0.05 K	1,600 cm^3	480 cm^3	–	2.1 dm^3
0.01 K	800 cm^3	480 cm^3	2,500 cm^3	3.8 dm^3

Table 17
Key figures for EURECA data acquisition and analysis

	DAQ and analysis
Number of channels from bolometers	∼5000
Dynamic range	16 bits
Common clock	10 MHz
Dataflow	∼5 TBytes/month

of low-frequency noise, so that a sampling rate of 100 kHz before demodulation is foreseen.

All these channels will be handled by a DAQ, operated at room temperature, which will be designed to be flexible, scalable, and adapted to both commissioning and detector validation runs as well as to WIMP search conditions. A possible implementation could be based on a system developed in-house, which connect front-end boards (first level trigger, FLT) to a readout board (second level trigger, SLT) through a proprietary backplane. These DAQs are in use in other experiments (Auger, KATRIN) and will be characterised within EDELWEISS-III. A total of 10–15 DAQ crates would be required for EURECA. They would be cooled by air circulating fans and need 400 W of power each.

7.1.1. Online data processing

The DAQ will be capable of carrying out several data reduction and analysis functions, starting from the digitised signals, written to memory in an intermediate buffer. In the simplest configuration, the data streams are directly transmitted to the control computers or written to disk. In most situations, a trigger is applied on some of the data channels, and events are then built and stored to disk. Dark matter searches require sub-keV thresholds, and therefore dedicated trigger algorithms will be used to reach this goal. A possibility for regular updates on algorithms will be provided, owing to ongoing adaptations of trigger requirements. As a starting point, for FID detectors, the trigger will be similar to the one developed within the highly adaptable SAMBA acquisition software used in EDELWEISS: the heat channel time-domain signals are filtered using bandpass filters adapted individually to the noise on each channel, and convolved with pulse templates that too are specific to each channel. A threshold is then applied to these processed time-domain signals. The value of the threshold is automatically adjusted as a function of the current baseline conditions of each channel. After a trigger, all traces from heat and ionisation channels for a given tower, or sub-group, of detectors are written to disk in a well-documented binary format.

The DAQ system will be interfaced to computers via a LAN: these computers will allow operatives both to control the DAQ and to monitor online the resulting data, in particular via a dedicated monitoring software producing quality-control plots and via the real-time visualisation of the time-domain signals from individual detector channels. These computers will also permit to control and modify all parameters relative to running conditions, including critical detector biases.

7.1.2. Acquisition for ancillary detectors

In addition to the main bolometer data flow, the stream from ancillary detectors must also be handled. In particular, a dedicated acquisition system will be devoted to the ∼100 PMTs inside the water tank surrounding the cryostat to be used as an anti-coincidence veto against muon-induced neutrons.

All bolometers and PMT channels will be synchronised to a common clock, whose operation is vital for the identification of muon-induced background events. This clock must distribute a 1-PPS signal and a common 10 MHz signal along with other control signals. It will be synchronised to a GPS receiver in order to record the accurate UTC time of events.

7.2. Data analysis and simulation

This section deals with data storage and processing, the hardware and infrastructure needed to access all data banks, as well as the software developments to analyse data offline. It presents the procedures of defining and implementing analysis cuts as well as the large variety of simulation packages needed to model different background components, calibration sources and potential WIMP signals.

The topics, described briefly below, are standard approaches in astroparticle physics experiments and the analysis of data from dark matter searches. It is obvious that analysis and simulation tools will be developed according to the experimental progress. Thus, for the sake of completeness of this report, the following describes a generic procedure for data analysis and modelling of signals and background.

7.2.1. Offline storage and computing

The raw data will be first stored on site using external disks, accessible through the local network from the monitoring computers. The volume of data flow will depend on the chosen event building algorithms; it will be driven by ionisation channels of FID bolometers because of their number and large sampling frequency with respect to phonon channels. Based on the experience from EDELWEISS-II, around 5 TBytes of data per month are anticipated. The raw data will be transferred outside the laboratory using an optical fibre network provided by the host laboratory, and stored at a computing centre such as the IN2P3 Lyon computing centre (CC-IN2P3). At least one other location will be used as a mirror. Raw data from ancillary detectors and monitoring devices will be treated in the same way.

An easy access database will be established, with all relevant links to experimental raw data and slow control parameters and with appropriate secured access to all collaboration members. It is expected that the access to raw data will take place through this database. An example of implementation is already used in EDELWEISS-III, based on the CouchDB database [40]. The computing resources used for offline processing will be provided by computing centres and member institutions. Most of the CPU usage will be dedicated to pulse fitting operations. Based on the experience from EDELWEISS and CRESST, the total anticipated CPU for data processing will be very easily provided by computing centres such as the CC-IN2P3.

7.2.2. Data reduction

Data reduction will comprise mostly the offline processing of raw bolometer traces and their precise calibration. There are already data reduction tools developed for pre-EURECA experiments, such as the Oxrop set of tools, the KData framework [40] and other EDELWEISS and CRESST data processing software. These existing analysis tools will be further developed, integrated and adapted for a specific implementation for EURECA. It is foreseen that a significant effort to organise and direct the adaptation of these tools will be needed. The data reduction processes will require multiple databases containing input data needed for the data reduction analysis (such as pulse shape templates), output calibration coefficients, and the meta data associated with the raw and calibrated data files.

7.2.3. Analysis, simulations and WIMP sensitivity

The analysis will be done by groups from different institutions within EURECA, providing multiple, independent analysis chains for cross-checks on the analysis of physics runs. Coordination between analysis groups will define the analysis principles and standard cuts. For WIMP search data, blindness procedures will be imposed in order not to bias the different cuts, which will be set using only calibration data or background data incompatible with WIMPs (for example multiple scattering events).

A substantial effort in simulations will be dedicated to the modelling of signals generated by WIMPs in both types of detectors, and to background processes such as gamma, neutron, alpha and beta radioactivity from materials in the detector vicinity, or muon-induced backgrounds. All these simulations will allow the optimisation of the experimental geometry, e.g. detector placement, shielding, or distribution of calibration sources. Common geometry packages and software tools will be developed to allow an integrated view on all aspects of MC simulation and to incorporate simulated events into the data sets to be analysed with software tools developed for data reduction. A major aim of simulations will be to provide estimations of background intensity for a given WIMP search.

The main outcome of analysis will be the derivation of constraints in the physical parameter space of WIMP mass and its cross section for elastic scattering on nuclei, either in the form of exclusion limits or of a measurement of these parameters. This will require detailed knowledge of form factors and quenching of the ionisation/scintillation signals for nuclear recoils. Theoretical models of spin-dependent and spin-independent interactions will be used, as well as specific models of WIMP halos and their systematics.

Finally, a combination of EURECA data and results from the LHC experiments at CERN will provide complementary constraints on various models of new TeV-scale physics such as generic supersymmetric scenarios or extra dimensions.

The EURECA detectors will also be able to address other physics topics. Alternate dark matter models will be explored such as inelastic-scattering dark matter, isospin-violating WIMPs and axions. In fact, EURECA data will provide a relevant insight into all new physics models which predict low-energy, low-rate interactions on a solid target.

8. Provision of low-background environment

The EURECA experiment with $\sim$1 tonne of target mass requires unprecedented improvements in materials' radio-purity and operating detectors deep underground under extremely clean conditions. External and internal shielding together with an active veto system are needed to suppress radiogenic and cosmogenic backgrounds. This Section summarises the results of our studies with additional information provided in Appendix G.

The primary goal of the EURECA experiment is to discover WIMPs. The aim is to achieve a sensitivity at a level of 10^{-10} pb or below for the cross section of spin-independent WIMP-nucleon interaction. This requires a suppression of the background in the nuclear recoil band down to $\sim$1 event/tonne/year in the region of interest (ROI) ($\sim$10–50 keV) keeping a significant fraction of expected nuclear recoils from WIMPs.

This target background event rate is directly transferred to a similar limit on the single nuclear recoils which is the prime background for a sensitive dark matter experiment. The target background rate also imposes a limit on the gamma-ray induced background prior to discrimination. Owing to a powerful discrimination against gamma-ray background, the upper limit on the tolerated gamma-ray induced rate at low energies is about $10^5 - 10^6$ events/tonne/year or $\sim$0.03 events/kg/day/keV in the ROI. This assumes a gamma-ray background discrimination power of about 10^5 or better in the ROI or about 10^4 per keV at threshold which is expected to be as low as 5–10 keV. Similar discrimination power against surface beta-events is also required. EDELWEISS-II has already demonstrated a rejection factor of more that 10^4 against surface events and more improvements have been recently shown with a new design of interleaved electrodes, to be fully deployed in EDELWEISS-III. Possible lower discrimination power at very low energies can be compensated by reducing slightly the efficiency for accepted nuclear recoils, still providing good sensitivity to WIMPs.

For the CRESST experiment, a discrimination of gamma and beta induced events to nuclear recoil events of at least 10^5 is achieved above and close to the region of interest at 46.5 keV for the internal ^{210}Pb γ-line. This discrimination power can be increased further by improvements in resolution for the light detector and through better radiopurity of the detector crystals. In the next run of the experiment, it will have to be shown that the background related to ^{210}Po decays is removed if the detectors are completely surrounded by scintillating surfaces.

Table 18 gives some of the key features of the required and expected EURECA low-background environment.

Table 18

Key features of the required and expected EURECA low-background environment: required thickness of shielding, radioactivity of major components and expected background event rates before discrimination.

Low-background environment	
External shielding	3 m of water
Inner shielding	Cu – 15 cm, CH_2/acrylic – 20 cm
Required	
U/Th in Cu of the cryostat	$\leq$0.02 mBq/kg
U/Th in materials inside inner shielding	$\leq$10 mBq/kg
Expected before discrimination	
Gamma rate	$<6.1 \times 10^5$ events/tonne/year at 20-200 keV
Neutron rate	<1 event/tonne/year
Rate of surface events	$\sim$7 $\times 10^6$ events/year

8.1. Background from radioactivity

Existing data on material radio-purity were first used to calculate the expected background rate in EURECA from the most massive components. Full details are given in Appendix G. Some important conclusions can be made based on the results of these simulations. The most radio-pure copper known at present – NOSV from Norddeutsche Affinerie (Germany) [41] with contamination levels of <1.6 ppt for U, <5.6 ppt for Th, <2.8 ppb for K and <10 µBq/kg of ^{60}Co will produce an electron recoil event rate which can be rejected by a detector with 10^{-5} discrimination factor. The expected nuclear recoil event rate is much less than one in a tonne of target per year. Due to higher contamination levels, no more than a few kg of stainless steel or any other materials with concentrations of about 1 ppb of U/Th can be placed

near the detectors. Special care should be taken to avoid material with higher than 1 ppb concentrations of U/Th next to the target volume.

Previous experience with the EDELWEISS and CRESST cryogenic experiments revealed that there is a number of components (connectors, cables, cold electronics) which have to be placed close to the detectors and certainly within the shielding, see Section 6. This imposes strong restrictions on the radio-purity of some components which are positioned next to the detectors, for instance, cables which should have contamination levels of less than 1 ppb U/Th with special care to be taken about Rn progeny – ^{210}Pb. Also, it became apparent that an inner shielding made of ultra-pure copper and acrylic/ polyethylene is required to protect detectors from radiation originating in connectors and cold electronics. They should also be made of radio-pure materials. This inner shielding is similar to what has already been realised in the EDELWEISS experiment. Our initial simulations and estimates based on the radioactivity measurements of existing components (cables, connectors, PCBs, FETs) show that 15 cm of Cu, 10 cm of acrylic and 10 cm of polyethylene combined with a careful selection of the material and components will suffice to attenuate the background from these components down to the level expected from the Cu vessels. We plan to install copper shielding as the most radio-pure material closer to the detectors followed by 10 cm of acrylic and then 10 cm of polyethylene. Polyethylene is not as clean as acrylic, so an additional acrylic layer is needed to shield the detectors from neutrons produced in polyethylene. More details on these simulations are presented in Appendix G.

Detailed simulations of background from various components have been carried out using GEANT4 for the baseline geometry of the EURECA setup. The results of the simulations for Ge detectors as a target are reported in Table 19. Since the exact contaminations of the components are not known yet, we either assumed the typical concentrations for specific materials, or took those measured for the EDELWEISS-II/III and CRESST experiments. The background rates are given for the 20–200 keV energy range. The threshold of 20 keV corresponds to single hit events and to at least one hit in multiple hit events. It is assumed that if at least one more hit in multiple hit events has energy greater than 10 keV, this multiple hit event will be rejected. For a 15 (10) keV threshold for single hit events, the neutron rate will be higher by 20% (40%) whereas gamma-induced background will not change much if we assume that the cosmogenic activation of Ge will be kept at a minimum by storing Ge detectors underground. If the energy threshold for the second hit in multiple hit events is reduced from 10 keV down to 3 keV with simultaneous reduction of the threshold for single hit events down to 10 keV, the rates of single hit events will be very similar to the original rates shown in Table 19. All values in Table 19 are preliminary and approximate. They will be updated as soon as more details of the design become available and measurements of the contamination for different materials are carried out. The simulations performed so far confirm the conclusion of the early modelling described in Appendix G: with an inner shielding made of 15 cm of ultrapure Cu, 10 cm of acrylic and 10 cm of polyethylene the background radiation from all components will be suppressed to a level that will not compromise the target sensitivity of the experiment (below 10^{-10} pb).

The gamma-ray background event rate in scintillating bolometers, such as $CaWO_4$, at low energies (10–50 keV) is smaller by a factor of three compared to a similar rate in Ge. The neutron background in scintillators is 50% smaller than in Ge and most events are oxygen recoils. This is due to the difference in interaction cross-sections on different targets (see Table 27 in Appendix G for a comparison between background in Ge and $CaWO_4$). With a powerful discrimination between oxygen and tungsten recoils in $CaWO_4$, most of the neutron background events will be rejected.

To reach the target sensitivity, a high radio-purity of all materials and components has to be achieved. This requires many material samples to be screened with sensitivities at the edge of existing technologies. It will also require a large number of operations with these materials to be developed for all stages of the experiment, from the purchase of the raw materials up to the final assembling.

A low-background environment at the EURECA host laboratory will consist of large storage areas, dedicated clean rooms, Rn trapping facilities ($\sim$mBq/m^3 of air) and high sensitivity Rn monitors. The storage of materials underground at LSM and at shallow depth in various institutions will prevent cosmogenic activation which produces, in particular, radioactive isotopes of ^{68}Ge and ^{65}Zn in Ge detectors, giving rise to lines around 10 keV – close to the expected energy threshold of the experiment. This issue is addressed in Section 3.1 and Appendix B. We also consider copper electro-forming for some essential components as an option. The University of Zaragoza and the Canfranc underground laboratory have developed a technique for copper electro-forming. A workshop located in the surface building of the Canfranc laboratory would allow the manufacturing and the underground storage of specific copper pieces.

8.2. Material selection and low background facilities

Material selection based on their radio-purity is a key factor which determines the background event rate and hence the sensitivity of dark matter experiments. This issue is currently under investigation by the EURECA Collaboration. We have identified existing high purity Ge (HPGe) detectors in Germany, France and Spain which could potentially be used for material screening in the EURECA project. The HPGe detectors in Germany, placed at a shallow depth of 15 m.w.e., could be used in preliminary screenings to select the samples to be measured in the French or Spanish detectors, which are placed underground at Modane and Canfranc. EDELWEISS is currently using a dedicated low-background n-type coaxial HPGe diode of 210 cm^3 with archaeological lead shielding that offers 1.6 litres of maximum volume for a material sample. At Canfranc underground laboratory, a low-background p-type HPGe detector of 1 kg mass is running with a volume of 5 litres available for material samples.

One HPGe detector of 2 kg, with a background close to that estimated in Table 25, needs 450 days to check the samples of copper, Cu–Ni alloy and acrylic. This can, at least in part, be performed in parallel with design and construction of EURECA components. Massive samples of more than 20 kg are required and most time consuming are copper and background measurements. The two HPGe detectors of 1 kg that the collaboration owns in Canfranc and Modane can screen other less critical components such as cables, holders (Kapton), screws, connectors and polyethylene. The mass of the samples should be around 2.5 kg (screws), 10 kg (polyethylene) and less than 0.5 kg for the remaining ones. Typical measurement time is 25 days per sample and detector, therefore we can check 20 samples in 250 days. Electrodes and FETs can be measured at shallow depth with the HPGe detectors of the Technical University of Munich, requiring samples of the order or less than 50 g and a few days per sample. The radio-purity of water is not assessed by HPGe detectors because a low-radon water supply and water radon monitoring are planned, see Section 3.2.6.

The detection limits of the French and Spanish detectors, for instance, for copper samples of 18 kg (2 litres) and 100 days of measurement time are 0.2 mBq/kg for the gamma emitting daughters of U and Th, 1 mBq/kg for ^{40}K, 0.1 mBq/kg for ^{60}Co (EDELWEISS HPGe) and 0.03 mBq/kg for ^{60}Co (Zaragoza HPGe). EDELWEISS has also access to a larger mass HPGe detector at LSM able to reach detection limits below mBq/kg levels.

To fulfil EURECA requirements for radio-purity of materials it is essential to purchase ultra-low background HPGe detectors of 2 kg (minimum) to increase the efficiencies of our present underground detectors. Their shielding must be carefully selected to get lower background and the sample capacity should be increased, specially for the measurement of low density materials. It would be desirable that

Table 19

Expected background event rates due to gamma-rays and neutrons in one tonne of Ge. The rates are given in an energy range of 20-200 keV (before discrimination for gamma-induced events). Only single hits were counted. The calculations assume a secular equilibrium in the U/Th decay chains. The first seven rows show the contribution to the background event rate from materials close to the detectors (inside the inner shielding). The next four rows show the effect from components which will be positioned behind the 15-cm Cu shielding. Other rows show the contribution to the background rate from components which will be protected by additional 20-cm-thick inner neutron shielding made of acrylic (10 cm) and polyethylene (10 cm) and placed behind a 15-cm-thick inner Cu layer.

Source	Material	Mass kg	Contaminations U/Th, ppb	Gamma-rays events/tonne/year	Neutrons events/tonne/year
Screens, Cu parts	Cu	3000	<0.002	$<5.3 \times 10^5$	<0.2
Support rods	Cu-Ni alloy	200	0.01	1.3×10^4	0.05
Cables, 10 mK	Cu, Kapton	6	0.5	1.8×10^4	0.08
Holders	Kapton	0.4	1	2.4×10^4	0.02
Holders	Acrylic	1	0.01	60	0.002
Screws	Cu, Zn	6	0.4	1.4×10^4	0.14
Electrodes	Al	0.0002	200	240	0.02
Connectors	Cu, Delrin	2	1	<20	0.02
Cables	Cu, Kapton	4	0.5	<20	0.02
Neutron shielding	Acrylic	200	0.01	<50	0.004
Neutron shielding	CH_2	150	0.1	<300	0.007
Electronics	FR4	2	200	<800	0.11
Water shielding	Water	0.4 kt	0.001	<80	<0.001
Muon-induced	All	–	–	–	<0.3
Total				$<6.1 \times 10^5$	<1.0

Table 20

Saturation activities of long-lived isotopes activated in natural Ge at sea level. ^{68}Ga ($T_{1/2} = 1.1$ h) is in equilibrium with ^{68}Ge.

Isotope	^{57}Co	^{54}Mn	^{68}Ge–^{68}Ga	^{65}Zn	^{60}Co
$T_{1/2}$ (days)	272	312	271	244	1925
Saturation activity (μBq/kg)	21	37	290	350	34

Table 21

Number of events at 10–50 keV in 0.5 t Ge per year from long-lived cosmogenic isotopes after one day exposure to cosmic rays at sea level. The contribution from the peaks has been estimated assuming a FWHM of 1 keV.

		^{57}Co	^{54}Mn	^{68}Ge–^{68}Ga	^{65}Zn	^{60}Co	Total
Continuum		19	23	19	100	19	180
Peaks	9 keV				100		100
	9.7 keV			240			240
	10.4 keV			**8400**			**8400**
	15 keV	13					13
	21 keV	110					110

Table 22

Heat load from elements within the cryogenic system. The contribution to the 50 mK stage from the mechanical supports will be re-evaluated if metallic struts are used. The design cooling power figures are those listed in the main text in Table 4.

Stage	60 K	1.8 K	500 mK	50 mK
Power consumption	[W]	[W]	[mW]	[μW]
Mechanical support	370	1.1	3.4	85
Cryo-line	300	0.5		
Detector towers	30	1.5	1.5	30
Dilution refrigerator		0.6		
TOTAL	700	3.7	4.9	115
Design cooling power	2200	10.0	50.0	600

these new gamma spectrometry systems were similar to or preferably better than GEMPI at Gran Sasso laboratory (LNGS) providing a sensitivity below 0.1 mBq/kg for the U/Th decay chain, a few tens of mBq/kg for ^{40}K and about 10 μBq/kg for ^{60}Co with a large volume for a sample material (>20 kg).

However, HPGe spectroscopy cannot provide accurate measurements of U/Th whereas for the evaluation of the neutron flux, the parent isotopes, in particular ^{238}U (giving spontaneous fission), are important. Other instruments and methods for measuring very low levels of contaminations, such as advanced radiochemistry, inductively coupled plasma mass spectrometry (ICP-MS), and neutron activation analysis (NAA) should also be used to assess concentrations of U and Th in a sample. We acknowledge the achievements of the BOREXINO [42], CUORE [43] and EXO [44] collaborations and plan to use a similar approach. These methods are complementary depending on the nature and size of the sample. NAA and ICP-MS have already proved to be well-suited for very small samples. But these methods do not check the total activity of a sample and have to be combined with a high sensitivity gamma-counting facility. More details are given in Appendix G.

The European-funded ILIAS project started compiling an online database [45] containing the results of radio-purity measurements for different materials and components. The measurements of radio-purity of materials using HPGe detectors and mass-spectrometry are currently ongoing for the upgrade of the EDELWEISS experiment. A large number of materials and components tested for EDELWEISS-III, which pass the criteria for EURECA, will be used later in the construction of EURECA. The EURECA collaboration will continue the development of the database of material purity.

Table 23
Heat load onto the 10 mK stage. The design cooling power is 20 μW.

Item	[μW]	Remarks
Detector cryo-unit (struts)		
Heat released from Cu support	2.6	700 kg Cu with 0.1 ppm H_2
Structural relaxation in Cu supports	10.4	
Detector electrical loading	0.2	1250 detectors
Cable conduction	1.0	1250 detectors
Heat released in detectors	0.6	1250 detectors
TOTAL	15.3	

Table 24
Maximum specific activities in the copper of the cryostat.

	U chain	Th chain	^{40}K	^{60}Co
μBq/kg	20	20	80	10

Table 25
Maximum allowed background counting rates for the main lines of the natural radioactive isotopes and ^{60}Co for a 2-kg HPGe detector devoted to screen the copper of the EURECA cryostat

Chain	Long-lived isotope	Nuclide	keV	Counts/day
^{232}Th	^{228}Th	^{212}Pb	238	0.64 ± 0.22
	^{228}Th	^{208}Tl	583	0.26 ± 0.06
	^{228}Ra	^{228}Ac	911	0.18 ± 0.05
	^{228}Ra	^{228}Ac	969	0.13 ± 0.04
	^{228}Th	^{208}Tl	2615	0.14 ± 0.04
^{238}U	^{226}Ra	^{214}Pb	295	0.14 ± 0.08
	^{226}Ra	^{214}Pb	352	0.33 ± 0.09
	^{226}Ra	^{214}Bi	609	0.30 ± 0.06
	^{226}Ra	^{214}Bi	1120	0.04 ± 0.02
	^{226}Ra	^{214}Bi	1764	0.07 ± 0.03
		^{40}K	1461	0.10 ± 0.03
		^{60}Co	1173	0.35 ± 0.07
		^{60}Co	1332	0.28 ± 0.05

8.3. Surface treatment

Cryogenic Ge detectors, having very good rejection power against gamma-ray induced backgrounds, have faced limitations to their sensitivity in the past because of near-surface events due to electrons coming from beta-decays of the radioactive isotopes (for instance ^{210}Pb) located on the surfaces of the detectors or copper caps. Alpha decay of radioactive atoms present on the surfaces mainly due to ^{222}Rn exposure can also produce surface events in the nuclear recoil band. Although these events have been successfully rejected in the past from a sample of WIMP-like events thanks to the fiducialisation (e.g. interleaved arrangement of the electrodes in EDELWEISS – ID technology, resulting in a rejection power of better than 10^4 in the ROI) and better performance has recently been demonstrated with the new FID detectors in EDELWEISS-III, an increase of the target mass in EURECA by more than 2 orders of magnitude, requires very careful consideration of this background and improvement in the treatment of surfaces of Ge detectors and copper caps. Surface events caused by β-particles do not pose much of a problem for bolometers based on $CaWO_4$ or other scintillators which record heat together with scintillation.

The rate of surface beta events in EDELWEISS-II was measured to be ∼400 events/m²/day. This implies that the surface beta rate in EURECA can be ∼5 × 10^6 events/year for 800 g detectors. With a beta rejection power of 1.7 × 10^4 at 90% C.L. already demonstrated in EDELWEISS-II [6,24] we may have up to 300 background events per year in the nuclear recoil band at 20–200 keV from surface beta events after all cuts. The rate of surface alpha events in EDELWEISS-II was about ∼200 events/m²/day leading to an expected rate in EURECA of up to ∼2.5 × 10^6 events/year for 800 g detectors. With a rejection power similar to that for beta events, we may have up to 150 events per year from surface alphas leaking to the nuclear recoil band at 20–200 keV.

New FID detectors with improved rejection power to surface events compared to EDELWEISS-II ID detectors will allow us to reduce the rate of surface background events after cuts by at least an order of magnitude. Further reduction will be achieved by improved cleaning.

We have identified new cleaning methods [46] and have developed procedures to validate their efficiencies. Within these procedures, samples of Cu have been exposed to artificially high levels of Rn, various cleaning methods have been applied and we are now investigating which cleaning method provides better reduction.

We are also in the process of collecting the available information on the emanation rates of radon from different materials and estimating expected effects in the detectors.

Finally, we are in contact with the CDMS collaboration who are currently developing a low radioactive background-screening detector for low energy beta-emitting contamination on surfaces, the so-called beta cage. Such a detector is essential to identify beta emitters in materials. The collaborative work with CDMS has already been started on these issues.

8.4. Muon-induced neutrons

Another potential source of the background is related to high-energy cosmic-ray muons able to cross the rock above the laboratory and produce neutrons nearby the detector which will then give signals in the detectors. LSM, being the deepest operational underground laboratory in Europe, offers a unique opportunity to reduce this background down to a very low level. Nevertheless proper simulations are required to estimate the residual event rate due to muon-induced neutrons and design the active veto system. At present, the water tank, suggested as a passive shield around the cryostat, is expected to be instrumented with PMTs providing a capability of detecting Cherenkov light from muons and muon-induced cascades. Here we briefly summarise the results of the simulations of muon-induced neutrons for EURECA.

Muons were transported from the surface down to the underground site and generated around the laboratory hall using the MUSIC and MUSUN codes [47]. Muons were passed then to GEANT4 [48] which transported initial muons and all particles produced by muons in rock and materials in the laboratory. All particles were transported down to the detectors and their energy depositions in water and detectors were recorded. Fig. 16 shows the spectra of energy depositions from muon-induced events in the detectors.

The background that can mimic a WIMP event consists of single nuclear recoils only. We have found 12 single nuclear recoil events at 10–50 keV in 7.4 years of running about one tonne of Ge leading to a rate of 1.6 ± 0.5 events/year. All other events in the detector were found to be multiple hit events containing energy depositions from muons and secondaries (gammas, electrons, hadrons) in muon-induced cascades. A similar rate was obtained for a set-up with approximately half Ge and half $CaWO_4$ detectors. Single nuclear recoil events were dominated by the high-energy oxygen recoils for $CaWO_4$ detectors. This result does not assume any anti-coincidence between the events in the main target with energy depositions in water. In reality, the water tank(s) will be equipped with photomultiplier tubes and act as a water Cherenkov veto system. In this case, our simulations, based on 11.7 years of detector live time, revealed no events in
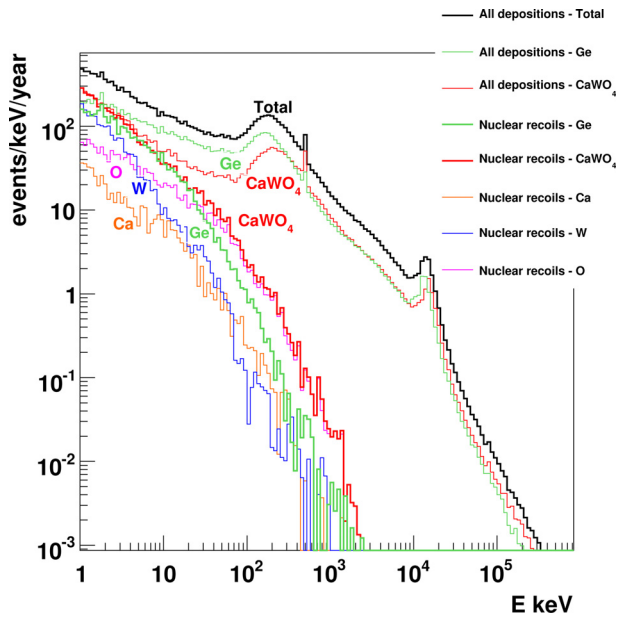
Figure 16. Spectra of energy depositions induced by cosmic-ray muon events in 506 kg of Ge and 576 kg of CaWO$_4$. Also shown are the spectra of nuclear recoils for both types of detectors and for individual elements in CaWO$_4$. All spectra are given *before* the single-hit selection (see text). At 511 keV, the single escape peak of positron annihilation is visible, the broad peak at about 15 MeV is due to muon energy deposition in the detectors.

Figure 17. Original plan for the layout of two water tanks with the building, accommodating cleanrooms, control rooms and other infrastructure, placed between them.

anti-coincidence between the target and the veto (with a veto threshold of 0.2 GeV) leading to an upper limit on the background event rate at 90% CL of 0.3 events/year in one tonne of target. A factor of two uncertainty in neutron production by GEANT4 can increase this upper limit. However, it is clear from these results that the muon-induced background is not a limiting factor for a tonne-scale detector located at the LSM with a water Cherenkov veto system if the veto system has a threshold of 0.2 GeV or below. Initial estimates of Cherenkov light production show that the minimum number of PMTs required to achieve 0.2 GeV threshold is about 50 for the designed water tank.

9. Conclusion

The Conceptual Design Report presented here gives an overview of how we propose to achieve a tonne-scale dark matter search experiment with a multi-material target. We aim to follow a two-phase approach, whereby an initial 150 kg of detective mass is augmented by an additional 850 kg after one year of operation.

The detectors will be a combination of Ge, giving heat and ionisation signals, and CaWO$_4$ detectors, from which light and heat measurements are made. These will be mounted in a total of up to 12 towers, each able to be extracted without disruption to the others. The towers will be mounted within a 2 m $\times$ 2 m cylindrical cryostat for a detector temperature operation of 10 mK. A layer of shielding above the detectors, consisting of Cu, PMMA and PE, will protect detectors from radioactivity from the first amplification stage.

Cooling of the detectors will be through use of a dilution refrigerator, providing a cooling power of 20 μW to a base temperature of 7 mK. Additional thermal shields will also be cooled by the dilution refrigerator at temperatures of 50 mK and 500 mK. Cooling of additional thermal shields at 1.8 and 60 K will be made by use of a helium refrigerator.

The cryostat will be housed within a large tank containing 400 m^3 of ultrapure water, providing a line-of-sight of at least 3 m of water in each direction, shielding from gammas and neutrons from within the laboratory. The tank will also function as an active muon veto,
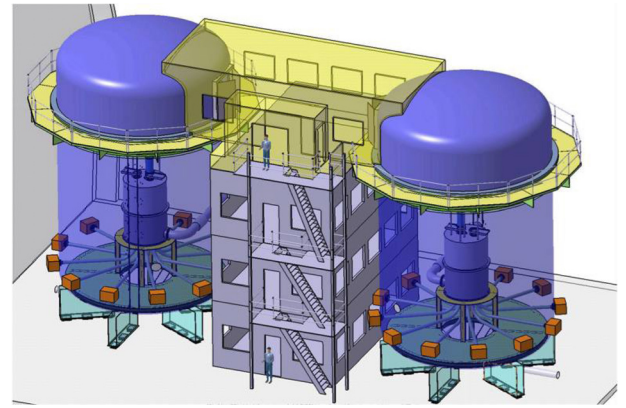
equipped with up to 100 PMTs to detect the Cherenkov emission of through-going muons.

Whilst the ideal site for EURECA is the DOMUS laboratory, formed from the extension to the current LSM, our design allows us to place the experiment in any suitable underground location.

The above-described experiment with properly selected radio-pure materials, shielding and active veto system will probe the dark matter parameter space down to a cross section of $2 \cdot 10^{-11}$ pb corresponding to a WIMP mass of 60 GeV/c^2.

Appendix A. Alternative housing of the experiment

Whilst the baseline design consists of the above-mentioned layout of one cryostat in a water tank, alternatives are also considered. These are briefly presented here.

A.1. Two identical systems

The initial design for EURECA considered using two identical systems each consisting of one cryostat containing 500 kg of detector mass within a water tank. This is shown in Fig. 17. The advantage of such a setup is the capability of using one system for science (long uninterrupted measurements), while the other system could simultaneously be used for initial validation of detectors and further detector R&D for which multiple, shorter runs are required.

Such a setup could be employed if additional space is available. One possibility is shown in Fig. 17, which would allow access to each of the water tanks from a shared cleanroom. Such a layout requires that one tank, the building and the other water tank are placed along the long side of the 15-m wide cavern. Further space would be needed for the water buffer tank, and for two sets of cryogenic equipment. Another option would lead to a much larger cleanroom, the footprint

Table 26
Background event rate per year at 10 – 50 keV due to single nuclear/electron recoils from neutron/gamma interactions in 100 kg of Ge. The event rates for electron and nuclear recoils in the target were estimated in the energy range of 10 – 50 keV, assuming one year of running. The first three columns specify the source of background radiation, its thickness and mass used in the simulations. Individual contaminations for each radioactive isotope considered, are given in the fourth column. The composition and thickness of the shielding between the source of background radiation and the detectors are shown in the fifth column. The last two columns report the rate for electron and nuclear recoils in the target.

Source	δ [cm]	Mass [tonne]	Contamination level	Shielding	e^--Recoil events	n-Recoil events
Concrete	30	1111	1.9 ppm U, 1.4 ppm Th,	20 cm Pb + 50 cm CH_2	-	0.064
				20 cm Pb + 60 cm H_2O	-	0.125
			$2.5\ 10^3$ ppm K	cryostat in water 2 m/ 3m	$1.03 \times 10^5/1300$	-
Stainless steel (laboratory walls)	2	121	1 ppb U/Th, 1 ppm K	1 cm Cu (cryostat vessels)	8×10^5	17.2
Lead (outside the cryostat)	20	200	1 ppb U/Th, 1 ppm K	50 cm CH_2 1 cm Cu (cryostat vessels)	603	-
Polyethylene (outside cryostat)	50	21	0.1 ppb U/Th, 0.1 ppm K	1 cm Cu (cryostat vessels)	2.12×10^5	0.442
Copper (cryostat)	1	0.32	0.01 ppb U/Th, 10 ppb K	none	6677	0.0308
Stainless steel (inner cryostat vessel)	0.5	0.347	1 ppb U/Th, 1 ppm K	none	4.04×10^5	2.54
				5 cm Pb + 10 cm CH_2	5.57×10^3	0.042
				10 cm CH_2 + 5 cm Cu	2.26×10^4	0.130
				10 cm $C_5O_2H_8$ + 5 cm Cu	-	0.521
Lead (inside the cryostat)	5	0.331	1 ppb U/Th	10 cm CH_2	-	0.557
Polyethylene (inside the cryostat)	10	0.336	0.1 ppb U/Th, 0.1 ppm K	none	1.58×10^5	0.288
Polyethylene (inside the cryostat)	10	0.462	0.1 ppb U/Th, 0.1 ppm K	5 cm Cu	1.38×10^4	0.333
Plexiglass (inside the cryostat)	10	0.592	0.1 ppb U/Th	5 cm Cu	-	0.523

δ - thickness.

Table 27
Background event rates per year at 10 – 50 keV due to single nuclear/electron recoils from neutron/gamma interactions in Ge and $CaWO_4$. The simulations have been carried out either with 253 kg of Ge and 288 kg of $CaWO_4$, or with 506 kg of Ge (marked as [†]) and have been re-scaled to one tonne of target of each material. The first three columns specify the source of background radiation, its thickness and mass used in simulations. The composition and thickness of the shielding between the source of background radiation and the detectors are shown in the fourth column. Individual contaminations for each radioactive isotope considered are given in the fifth column. The last four columns report the rate for electron and nuclear recoils for the two targets.

Source	δ [cm]	Mass [tonne]	Shielding	Contamination level	e^--Recoils, events/tonne/year Ge	$CaWO_4$	n-Recoils, events/tonne/year Ge	$CaWO_4$
Concrete	30	1291	3 m H_2O, Cu[§]	Tot	3043	931		–
				U 1.9 ppm	1055	334	–	–
				Th 1.4 ppm	1945	583	–	–
				K 2480 ppm	46	14	–	–
Copper[§]	See text	2.86	–	Tot (U,Th,K)	3.70×10^5[†]	–	1.44/1.60[†]	0.753
				U 0.01 ppb	2.45×10^5[†]	–	1.33/1.48[†]	0.694
				Th 0.01 ppb	9.98×10^4[†]	–	0.105/0.118[†]	0.0569
				K 10 ppb	2.35×10^4[†]	–	–	–
				^{60}Co 10 μBq/kg	7.87×10^3	2382	–	–
Copper(vessels)	See text	2.17	plates, holders	Tot	7.86×10^4[†]	–	0.789[†]	–
				U 0.01 ppb	5.08×10^4[†]	–	0.731[†]	–
				Th 0.01 ppb	2.04×10^4[†]	–	0.058[†]	–
				K 10 ppb	7.47×10^3[†]	–	–	–

δ - thickness.
[†] 506 kg of Ge.
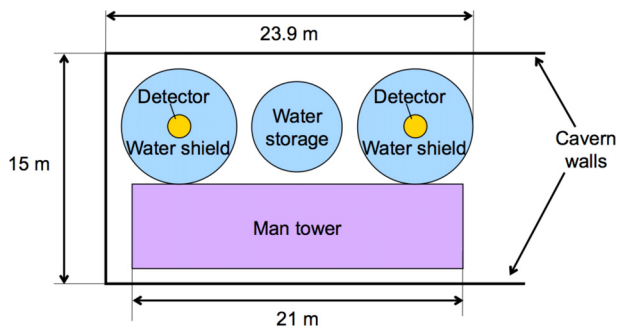[§] Cryostat vessels, plates and holders.

Figure 18. Alternative footprint for the layout presented in Fig. 17. The clearance between either the water tanks or the building, and the cavern sidewalls has been taken as 1 m, which would require modification to the upper parts of the tanks or buildings due to the proposed position of the crane beam.

of which is shown in Fig. 18, although the latter option leaves too little space for clearance around the equipment.

While the volume for each of the cryogenic spaces would be half that of the baseline design, the requirement for 3 m of water shielding would remain. Thus for the detector tower design of 12 storeys of detectors, the diameter of each cryostat would have to be at least 1.5 m, requiring a water tank diameter of 7.5 m, only slightly different from the original 8 m, with the height unchanged at 12 m.

The quantity of water would then be 350 m^3. The size of the water purification plant would be unchanged from the baseline design. Since only one system would be running at any one time, the requirement of one buffer tank for the water would be maintained.

The baseline design was considered more favourable since it leads to a reduced cryogenic plant, reduced DAQ and hardware for the active veto, and employs smaller overall volumes.

A.2. Lead and polyethylene shielding

As presented in Section 3.6, 3 m of water is needed to suppress the gamma flux to a level below the sensitivity of the detector. As an alternative, around 25 cm of Pb would provide an equivalent attenuation of gammas, with around 60 cm of polyethylene (PE) for neutrons.

It would be preferable to place the PE inside the Pb, to limit any additional muon-induced neutrons produced within the Pb. However, this has the less desirable effect of requiring a larger amount of Pb. Under the assumption of a cryostat 2 m in diameter and height, with a 10-cm clearance between each shield, we would require about 27 t of PE and 250 t of Pb for cubic shields. Cylindrical shields could also be considered, requiring less material but are more difficult to manufacture.

Placing the Pb inside the PE would reduce the necessary amount of Pb by a factor of around 2.5, whilst increasing the amount of PE by about 60%. Overall this would reduce the cost of shielding. However, placing lead close to the target would increase the background from muon-induced neutrons, requiring better efficiency for an active veto system.

The footprint for a system using PE and Pb shielding as defined above then reduces to 4 × 4 m^2. If this were to be enclosed within a cleanroom, the height of 4 m, plus clearance for removal of any roof sections of Pb and PE and space for a crane, would have to be considered. Use of Cu, or of Pb–Cu alloy, for the floor section may be preferable due to creep exhibited by Pb under loading.

A sandwich of Pb (outer shielding), polyethylene (middle) and Cu (inner) would provide an optimum solution for the alternative shielding design. An active veto system made of scintillators will either surround the cryostat and the shielding or the cryostat only. In the first case this can also be a water Cherenkov detector. The risk of such a solution for an active shield consists of not hermetically covering the

cryostat (see section below).

A.3. Alternative water tank size

In an extreme scenario, highly compromising the effectiveness of the shielding and hence the sensitivity of EURECA, a non-optimal shielding could consist of only the sides and volume above the detector being water-filled. The shielding below would then be formed by a sufficient thickness of Pb and Cu, equivalent to 25 cm of Pb; and 60 cm of PE. Retaining the option of an internal crane above the water level requiring 1 m, an overall height for the water tank could be reduced to around 7 m. The diameter would remain at 8 m unless a partial water/PE/Pb shield were employed (see above). It would be possible to locate the entrance door at least partially within the water level, since access will only be once the water has been drained out of the tank.

Other alternatives include an option to submerge, completely or partially, the water tanks: digging 5 m down would allow the water storage tank to be of 5.3 m diameter for an overall height of 18.2 m. The tank would then reach the maximum height allowable of 13.2 m, achievable only within the central 10.25 m of the cavern (see Fig. 4). Such a layout would limit the size of materials that could be craned along the hall from the entrance next to EURECA.

Appendix B. Local storage of low-background components

Due to the activation of materials by cosmic rays at the surface we plan to store some materials and components in shielded locations to prevent a build-up of radioactive isotopes by activation.

A measurement of the copper activation by cosmic rays [41] shows that ^{60}Co attains an activity of 10 μBq/kg after 4 weeks at sea level, or after 2 weeks at 1 km altitude. The attenuation length of fast neutrons at shallow depths is 1.6 m.w.e. [49,50], therefore 5 m.w.e. is the minimum shielding required to store the copper for 1 year at sea level, or for 6 months at 1 km altitude. Combining a measurement of the fast neutron flux at 20 m.w.e. underground [51] and the cross section of the ^{63}Cu$(n, \alpha)^{60}$Co reaction, we obtain a saturation activity of less than 0.3 μBq/kg of ^{60}Co at 20 m.w.e., i.e. this depth is absolutely safe and the copper could be stored in places other than the current LSM. Other actions can aid in reducing the copper activation: a shielding of 1 m of polyethylene (PE) (or H$_2$O) around the copper during transport or storage doubles the allowed time for storage; concrete layers over the machining workshop will provide additional protection.

The suppliers of the copper should be relatively close to the laboratory and should send the copper as soon as possible after electrolysis. Travel, by road or railway, should be as fast as possible; a supplier within Europe is therefore preferable. The preferred supplier of copper is Norddeutsche Affinerie (Germany). Their NOSV copper satisfies the strict requirement for radio-purity of a large mass of materials near detectors. The history, including (but not limited to) time span, altitude, and possible overburden, of the exposure to cosmic rays will be recorded. Copper samples from the same batch and travelling together with the main shipment will be measured in a HPGe detector for an independent measurement of activation.

The cosmogenic activation of stainless steel (used in the water tank) is not as critical as with copper. Measurements of stainless steel samples [52,53] show that the natural or anthropogenic (^{60}Co) radioactivity is greater than that induced by cosmic rays. Among the cosmogenic isotopes in stainless steel, only ^{54}Mn (312 d half-life) attains a saturation activity of a few mBq/kg, the remainder are of the order or less than 1 mBq/kg [41]. The water will shield the detectors from the radioactivity of the stainless steel tank.

The depth needed for the underground storage of germanium detectors can be estimated using the measurements of the production of the long-lived isotopes ^{57}Co, ^{54}Mn, ^{68}Ge, ^{65}Zn and ^{60}Co by fast neutrons in Ge enriched with ^{76}Ge [54] and applying these results to

natural Ge. Our results for the saturation activities in natural Ge are shown in Table 20.

We have calculated the background produced by the isotopes given in Table 20 for one day of exposure at sea level (Table 21). The figures can be scaled linearly up to about the half-life of every isotope. Two contributions are listed, the first one for the continuum and the second one for the discrete lines coming from the atomic binding energies after electron captures. For ^{57}Co, the 14 keV nuclear de-excitation energy is added to the atomic binding energies.

The values in Table 21 (except the values given in bold) are upper limits because they are estimated for isolated Ge detectors of 1 kg, i.e. without taking into account that the gammas emitted in a decay could give other signals in neighbouring detectors; the only exception is the peak at 10.4 keV because the electron capture is always going to the ground state of ^{68}Ga.

The required depth for storing Ge detectors underground can be estimated using the data from [55]. The optimum would be to store Ge crystals at the LSM before and after detector preparation and validation as it is already done in the context of EDELWEISS. Storage at shallow depths should be limited to a few weeks. Detector preparation and validation are expected to be completed within a week or so.

The transportation between the manufacturing place, the temporary storing and the underground laboratory, as well as temporary storage, could be done with a movable iron shield as proposed in [56]. The results of [56] applied to natural Ge give a reduction factor of 7.6 for the activation of ^{68}Ge compared to the non-shielded Ge at the surface. The iron shield could be used to extend the storage time at shallow depths.

Appendix C. Power

Estimates for the power consumption by various equipment in the EURECA experiment are presented in Fig. 19. Whilst the given total provides the maximum power, a reduction during operation is expected by 25 kW for the compressor (cryogenics) and by a further 15 kW for water treatment (no RO and reduced flow rate).

Appendix D. Radon

Many models exist to predict the amount of Rn deposition onto surfaces. However, they are generally not in agreement. The conditions of Rn progeny deposition depend on many parameters including Rn density, surface adhesion, ratio of room surface area to volume, aerosol particle density, etc. In an effort to simplify these, a model has been built which agrees with long-term predictions when compared to some models (for instance, [57], hereafter N&Y, and also references therein) and appears to be up to a factor of two higher in deposition than others [58–60]. The factor of two could therefore be considered a worst case scenario, providing a safety buffer.

Deposition of the progeny is linearly proportional to the concentration of Rn in air and the deposition of the long-lived progeny is approximately linear with exposure times for up to about 20 years [57]. There is little difference in deposition of Rn descendants on several common surfaces, such as metal or glass, with the notable exception of polyethylene for which an increase by a factor of 2–4 has been observed [61] over other surfaces.

It should be noted that some measurements have suggested that Rn deposition increases by a factor 20 in low aerosol environments [62] due to the higher unattached fraction. However, other studies [58] have shown that Rn progeny deposition decreases by a factor of 100 within filtered cleanrooms, since the progeny are generally attached to aerosols and are therefore effectively trapped within HEPA filters.

Our model uses the solution of the Bateman equations to scale the initial surface concentration of Rn to obtain a value of ^{210}Po in

Section	Sub section	Item	Power/item kW	No. items	total kW
Cryogenics					
		Compressor	75	1	75
		1.8-K pump	2	1	2
		Gas handling unit	20	1	20
		Electronics	2.2	2	4.4
		Water/air cooling pumps for above			30.4
		TOTAL			**131.8**
Low Background					
Water shield cycling purification		Pumps	2.2	2	4.4
		RO & EDI	20	1	20
		Degassing column	2.2	1	2.2
	monitoring	Flow meters	0.1	5	0.5
		Resistivity meters	0.072	3	0.216
		Pressure gauges	1.2E-3	5	0.006
		PC + monitor	0.4	1	0.4
		Solenoid valves	0.0336	5	0.168
	PMTs	Total per channel	0.01	200	2
		HV supply	Included in above		
		Pre-amps	Included in above		
		DAQ	Included in above		
Rn control system for air			30	1	30
		Compressor (22 kW included)			
		Air dryer	Included in above		
		Cooled charcoal	Included in above		
	Rn monitor	PC + monitor	0.4	6	2.4
		Pump	2.2	6	13.2
		Detective element			
Cleanroom		Overpressure fans	0.22	8	1.76
		Laminar flow cabinet	0.85	2	1.7
		Ultrasonic bath	5.2	1	5.2
		Bonding machine for crystals	1	1	1
		Crane, 1 t	1.5	1	1.5
	Neutron monitors				
		PC + monitor for readout	0.4	6	2.4
		Water/air cooling pumps for above			26.7
		TOTAL			**115.8**
Slow Control					
		Control PCs	0.3	3	0.9
		Slow con system			
		DAQ (per channel)	0.01	150	1.5
		DAQ subracks	0.4	15	6
		Bolometer bias supply	Included in above		
		Pre-amps	Included in above		
	Computing	DAQ, per machine	0.3	5	1.5
		monitors	0.08	2	0.16
		printers	0.072	2	0.144
		Oscilloscopes	0.3	2	0.6
		NI control boards	1.92	3	5.76
		Cooling for electronics			5.0
		TOTAL			**21.5**
Safety					
		UPS supplies	TBD		
		Fire equipment	TBD		
		Alarms	TBD		
		Emergency lighting	TBD		
		Water emergency egress pumps	2.2	1	2.2
		Water emergency egress valves	0.0336	1	0.0336
		Mass spec in vacuum jacket	0.072	1	0.072
		PC + monitor for mass spec	0.4	1	0.4
		TOTAL			**2.7**
		GRAND TOTAL			**272**

Figure 19. Estimate of the power consumption of the EURECA setup.

agreement with that of N&Y at long times. Linear scaling of the initial Rn concentration, and of surface area, then allows predictions to be made for the quantity of all Rn progeny at any time, assuming a perfectly clean surface at an initial time.

Assuming an internal surface area facing each 800 g Ge detector of 250 cm^2, as in EDELWEISS-III, a total of 1 t of Ge detectors leads to a total internal surface area of 31 m^2. This is for a total of 1250 Ge detectors, whereas the current design has space for 1368. For an initially clean surface exposed to 100 mBq/m^3 of Rn for 90 days, we would expect to obtain 40 μBq/m^2 of ^{210}Pb, giving rates of 3.3 α/day/m^2 from ^{210}Po and 6.6 β/day/m^2 from ^{210}Pb and ^{210}Bi once equilibrium is reached, after about 2 years.

Appendix E. Cryogenics

E.1. Cooling systems

A system similar in some respects to that proposed for EURECA is that of the NeuroSpin cryostat [32]. NeuroSpin is a 17 *T* nuclear magnetic resonance imaging system located at Saclay, France. Similarities lie in the use of a Claudet bath, HELIAL series refrigerator and separation of cryostat and heavy plant by a 200-m cryo-line. The general layout is shown in Fig. 20. The cryostat is designed to provide a mixed mode with liquid helium and cooling power of up to 190 W at 4.2 K and of 900 W at 40 K with pressurised helium at 15 bar, circulating at
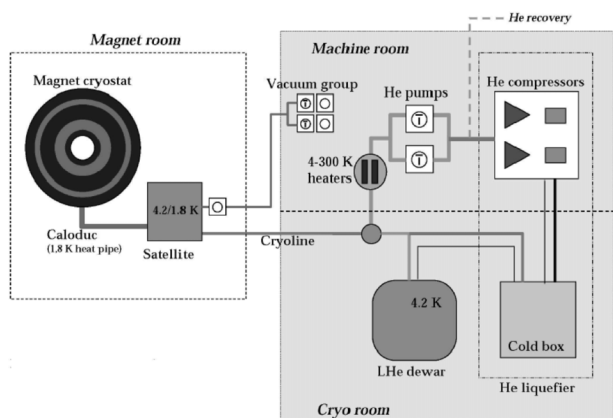
Figure 20. NeuroSpin general layout with the superfluid helium heat pipe [32].

Figure 22. Claudet bath principle.

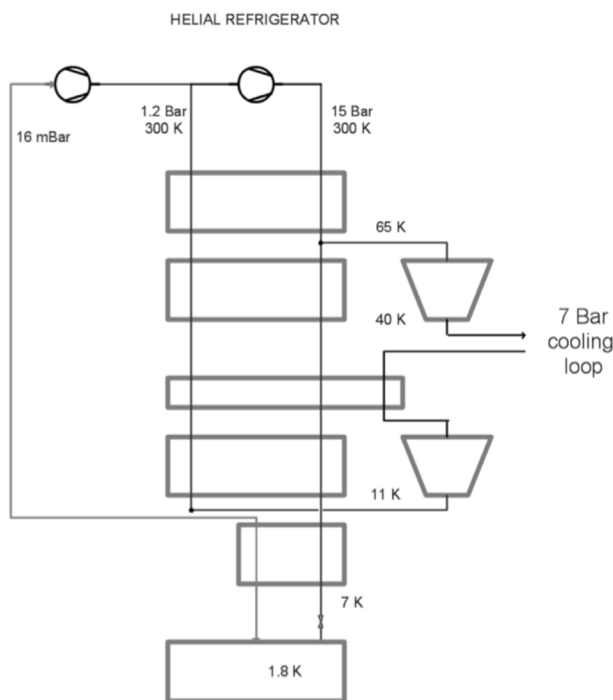**Figure 23.** A prototype design for possible heat exchanger elements for EURECA.

Figure 21. A possible process flow for the EURECA refrigerator with a direct expansion at 1.8 K (the Claudet bath is not shown here).

a rate of 40 g/s. A Claudet bath is added to supply pressurised He II (1.8 K, 1.25 bar).

The Claudet Bath [63] is a solution to create a superfluid He heat pipe. It offers the advantage of cooling to 1.8 K without boiling He which otherwise can cause microphonic noise in cryogenic detectors. Pressurised to well above the saturation pressure, the He II is a highly conductive material that creates a perfect isothermal link without any vaporisation of the liquid. The heat is removed by the surrounding liquid He, creating a classical pumped bath at the saturation pressure of the He II (see Fig. 21). The He II is provided by pressurised normal liquid He at 4.2 K cooled by conduction within the liquid bath. A porous material is used to avoid the conduction by the superfluid phase below the lambda point (2.17 K). An overview is shown in Fig. 22.

E.2. Heat exchanger elements

Dilution refrigerator performances are limited by the counterflow heat exchanger used in the low temperature part (below 1 K). At the
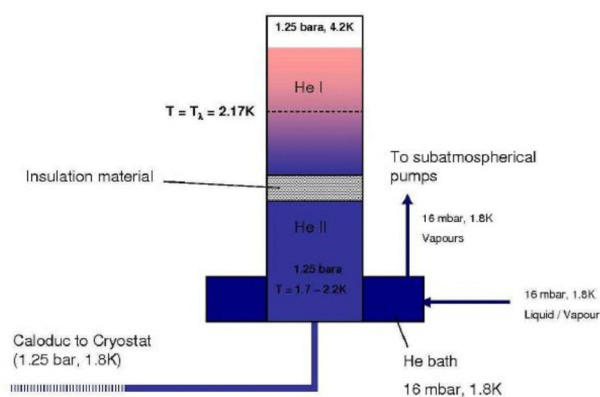
lowest temperature, the Kapitza resistance limits the performances of the heat exchange between the wall material and the liquid He. The effective contact surface can be greatly improved by using sintered materials made from Ag or Cu. This technique is used to create discrete heat exchangers for use below 100 mK. The number of such heat exchangers and the design of the flow section have to be optimised for the required ^{3}He flow and low-temperature performance. Fig. 23 shows a possible design of such a discrete heat exchanger consisting of two separate boxes, thermally linked, with powder in each. A dedicated study has been started to find the best material and to produce a design compatible with the low-radioactivity requirements of EURECA.

E.3. Power budget contributions

Tables 22 and 23 summarise the heat load or power consumption of the different components in the cryogenic system.

Appendix F. Simulations of gamma-ray and neutron background from the laboratory walls

Initial simulations were aimed at determining the thickness of the passive shielding required to suppress the gamma-ray and neutron fluxes from laboratory walls to a level that would allow the EURECA detector with a tonne-scale target mass to reach a sensitivity of 10^{-10} pb for the WIMP-nucleon spin-independent cross-section. A simplified geometry of the cavern (30 × 12 × 12 m^3) and the detector was used. An internal layer of 30 cm of concrete, covering the rock face, was included. The simulations were done for different targets: a) 103 kg of Ge; b) 506 kg of Ge; c) 506 kg of Ge plus 576 kg of CaWO$_4$. The target was surrounded by two Cu shields, both of 5 mm thickness. Figure 24 shows the visualisation of the cavern with the two cryostats in the GEANT4 simulations.

Two possible shielding designs were considered. The default design included two water tanks with immersed cryostats with detectors (only one cryostat for 104 kg of Ge). An alternative design used lead and polyethylene shielding. The alternative design was included in the unlikely case that there is no space for water tanks in the laboratory that will host EURECA.
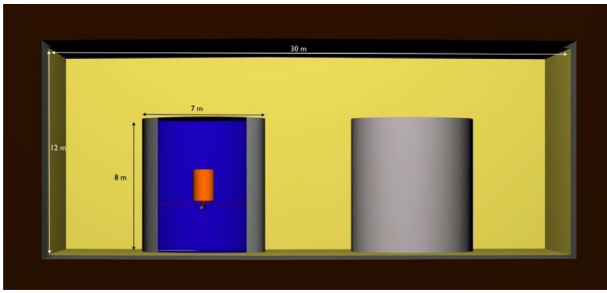
Figure 24. GEANT4 visualisation of the laboratory hall with water tanks and cryostats inside.

Figure 26. Single-hit electron recoil spectrum in about 500 kg of Ge from gamma-rays originated in copper (cryostat, plates, holders).
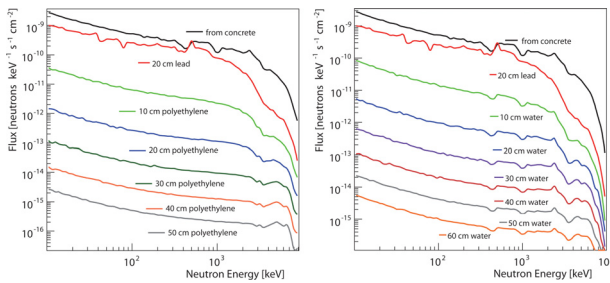

Figure 25. Neutron spectra from concrete behind the lead (20 cm) and polyethylene shielding (left) and behind the lead (20 cm) and water shielding (right). Thicknesses for PE and water are shown next to the curves.

Figure 27. Single-hit nuclear recoil spectra (black curve) from uranium in copper. 250 kg of Ge and a similar mass of $CaWO_4$ were used as a target. Individual contributions for each element reflect the dependence of the spectrum on the atomic mass of the target (see legend for details).

Neutron production by radioactive isotopes was carried out using the SOURCES4 code [64]. The code was modified to extend the energies of alpha particles up to 10 MeV from the original upper energy cut at 6.5 MeV [65]. Many more cross-sections of (α, n) reactions have been added to the code library [66–68]. The newly added cross-sections have been calculated using the EMPIRE-2.19 code [69]. Significant improvements have been made to the calculations of the (α, n) cross-sections and branching ratios [68,70].

The CH_2-containing plastics, polyethylene and polypropylene, have traditionally been used as a standard neutron shield. Simulations of neutron transport, carried out using the GEANT4 toolkit [48] show that about 60 cm of CH_2 (behind lead shielding) would be sufficient to suppress the neutron flux below the sensitivity of a tonne-scale detector. Water is also very efficient as a neutron shield. The difference between the water and polyethylene is mainly in the material density and in the relative fraction of hydrogen. Figure 25 shows the attenuation of the neutron flux in polyethylene and water, respectively. Neutrons were produced in the concrete of the laboratory walls and transported through polyethylene and water with GEANT4. About 75 cm of water would provide a similar shielding capability as 60 cm of CH_2. A much greater thickness of water is needed to shield from gamma-rays.

With an isotropically produced photon background within 3 m of rock and 30 cm of concrete, simulations show that the concrete layer is responsible for more than 95% of the gamma (and electron) flux beyond the shielding with the event rate dominated by the Th decay chain. To reduce the background from the walls, the concrete constituents can be selected. To achieve efficient gamma-ray flux attenuation, a thickness of 3 m of water is required, leading to a size of a water tank of about 8 m in diameter and 8 m in height for a tonne-scale experiment.
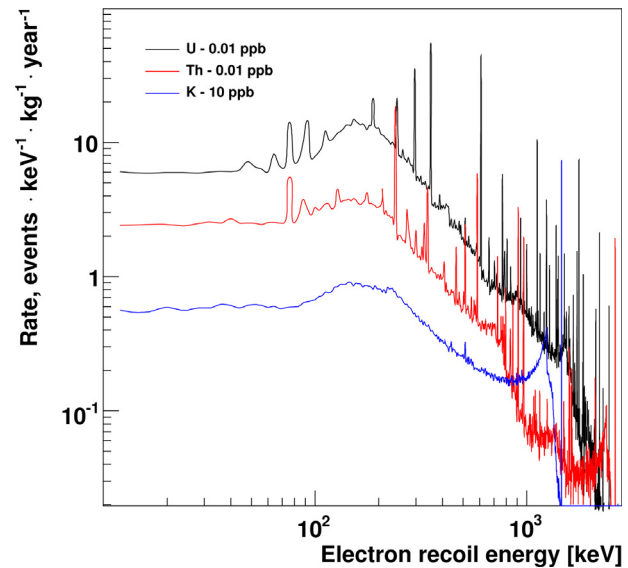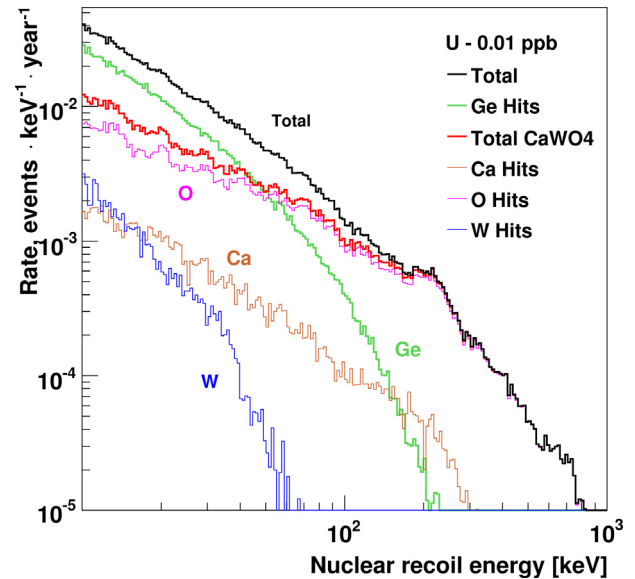
Appendix G. HPGe detectors and background simulations

G.1. Other options for external shielding

We are considering the primary option of water shielding against gamma-rays and neutrons. This has the advantage of low-cost construction and operation with an additional opportunity to equip the water tank with PMTs, converting it into an efficient active veto system against cosmogenic background. We understand, however, that not all underground sites are (or will be) suited and equipped to host a large 8 m diameter × 8 m high water tank and a water purification plant. To not compromise the sensitivity of the EURECA experiment we have also investigated the possibility of having a more conventional shielding consisting of lead, polyethylene and copper. The results of these studies are shown in Tables 26 and 27. We conclude that an alternative to the 3 m water shielding would be 25 cm of lead and 60 cm of polyethylene with additional inner shielding of 15 cm

of Cu and 15 cm of CH_2 (similar to the standard design option).

G.2. HPGe detectors for material selection

Monte Carlo simulations identified the copper of the cryostat as one of the most critical materials for the success of EURECA. Table 24 shows the maximum specific activities of the nuclei in U and Th chains, ^{40}K and ^{60}Co. The production of ^{60}Co through the reaction $^{63}Cu(n, \alpha)^{60}Co$ requires special care in the manufacturing of the copper and in its transport, storing and machining.

The quality control of successive batches of copper implies the measurement of small contaminations with HPGe detectors in underground laboratories, just at the frontier of the current technology of ultra-low background measurements. These measurements are necessary but not sufficient, because to evaluate accurately the gamma and neutron background from copper or any other material or component, measurements of the gamma-ray lines from the radioactive isotopes and the mass-spectrometry measurements of U/Th should be carried out. Since the gamma-ray lines from U/Th decay chains come from U/Th daughters and the radioactive equilibrium is frequently broken, HPGe spectroscopy cannot provide accurate measurements of U/Th whereas for evaluation of the neutron flux, the parent isotopes, in particular ^{238}U (giving spontaneous fission), are important.

The sensitivity of HPGe detectors is determined primarily by the background event rate. We have estimated the maximum allowed background counting rate (Table 25) of a 2-kg HPGe to get the detection limits (90% C.L.) of Table 24 for a copper sample of 59.6 kg and 100 days of measurement time.

The rates in Table 25 have been computed with the following hypotheses:

- The sample does not attenuate the peaks. It means that we assume that the origin of the background peaks is mainly located inside the detector holder, end cap, preamplifier or any other component close to the HPGe crystal.
- The ^{222}Rn activity inside the shielding must be as low as possible and constant. Filling totally the sample volume in every measurement could be the safest way to achieve low Rn concentration. Combining the peaks of ^{214}Pb and ^{214}Bi we obtain a reliable value of (or upper limit on) the activity of ^{226}Ra.
- The detection limits for the long-lived ^{228}Ra and ^{228}Th are 30 μBq/kg. We attain a value of 20 μBq/kg if we assume equilibrium for the ^{228}Ra and ^{228}Th branches and we combine the peaks of the Th chain.

There are some degrees of freedom in the rates of the Table 24 because the detection limits are estimated combining the peaks of one or more isotopes and, therefore, different sets of rates can give the same detection limit. The statistical uncertainties place lower bounds on the detection limits of 15, 14, 48 and 7 μBq/kg for U, Th, ^{40}K and ^{60}Co, respectively. The detection limits can be improved by measuring similar samples in similar ultra-low background systems.

G.3. Background from different components

Initial simulations of the gamma-ray and neutron production, transport and detection have been carried out for a simplified detector geometry as described in Appendix F. For the simulation of particle transport and detection, the GEANT4 [48] toolkit was used. Gamma-rays have been generated with GEANT4 whereas neutrons have been produced using modified SOURCES4A (see Appendix F for details). Materials with potentially large masses in EURECA have been included in the first set of simulations. The prime goal of this modelling was to identify materials which can be used in large quantities near the detectors (inside the shielding) and to answer the question whether a tonne-scale cryogenic experiment can achieve ultra-low background level so it can reach a sensitivity to the WIMP-nucleon cross-section as low as 10^{-10} pb or below.

We have considered copper as the main material for the cryostat and have also checked whether a large mass of stainless steel can be placed nearby the detectors. The results for 100 kg of Ge (approximate mass of EURECA Phase 1) are presented in Table 26 whereas the results for a larger mass target are reported in Table 27 [68,70]. Figs. 26 and 27 show example spectra of electron recoils and nuclear recoils in different targets if original gamma-rays and neutrons were produced in copper (cryostat, holders, plates).

References

[1] P.A.R. Ade et al. (Planck Collaboration) submitted to Astronomy & Astrophysics arXiv:1303.5076 (2013).
[2] M. Drees, G. Gerbier, Dark Matter, in: J. Beringer et al. Review of particle physics Phys. Rev. D 86 (2012) 010001.
[3] D. Hooper, S. Profumo, Phys. Rept. 453 (2007) 29.
[4] A. Birkedal, Phys. Rev. D 74 (2006) 035002.
[5] S. Chatrchyan, (CMS Collaboration). J. High Energ. Phys. 03 (2013) 037.
[6] E. Armengaud, (EDELWEISS Collaboration). Phys. Lett. B 702 (2011) 329.
[7] E. Armengaud, (EDELWEISS Collaboration). Phys. Rev. D 66 (2012), 051701(R).
[8] G. Angloher, (CRESST collaboration). Eur. Phys. J. C72 (2012) 1971.
[9] A. Brown, Phys. Rev. D 85 (2012), 021301(R).
[10] Z. Ahmed, Phys. Rev. Lett. 102 (2009) 011301.
[11] Z. Ahmed, Phys. Rev. D 84 (2011) 011102.
[12] D. Akimov, Phys. Lett. B 709 (2012) 14.
[13] E. Aprile, Phys. Rev. Lett. 107 (2011) 131302.
[14] SuperCDMS Proposal, 25 kg (7-ST@Snolab), retrieved from http://dmtools.brown.edu (Accessed: 3 October 2012).
[15] E. Aprile et al. e-Print: arXiv:1206.6288v1 [astro-ph].
[16] Maurer Söhne, http://www.maurer-soehne.com/, Seismic viscous dampers MHD and MHD-R
[17] G. Burghart, PhD Thesis, CERN and Technical University of Vienna (2010), http://cdsweb.cern.ch/record/1266865
[18] S. Fukuda, Nucl. Instrum. Meth. Phys. Res. A 501 (2003) 418.
[19] K.-H. Ackermann, (GERDA Collaboration). Eur. Phys. J. C 73 (2013) 1.
[20] C. Arpesella, (Borexino collaboration). Astropart. Phys. 18 (2002) 1.
[21] C. Mitsuda, Nucl. Instrum. Meth. Phys. Res. A 497 (2003) 414.
[22] B.A. Johnson. Corrosion of Metals in Deionized Water at 38 °C (100 °F). Washington D.C.: NASA, May 1969, NASA TM X-1791.
[23] L. Pattavina, Low Energy Alphas, EDELWEISSinternal note, unpublished (2011).
[24] A. Broniatowski, Phys. Lett. B 681 (2009) 305.
[25] G.A. Vermeulen, PhD Thesis, Leiden (1986).
[26] A. Nucciotti, J. Low Temp. Phys. 167 (2012) 528.
[27] P. Wikus, T.O. Niinikovski, J. Low Temp. Phys. 158 (2010) 901.
[28] P. Wikus, Dilution Refrigeration of Multi-Ton Cold Masses, PhD Thesis, CERN and Technical University Vienna (2007), http://cdsweb.cern.ch/record/1036217
[29] A. Nucciotti, J. Low Temp. Phys. 151 (2008) 662.
[30] M. Martinez, In Proc. In: Low Temperature Detectors LTD 13. AIP Conference Procs. 1185 (2009), 693.
[31] Air Liquide HELIAL series, http://www.airliquide.com/
[32] S. Crispel, P. Bredy, F. Gratiot, D. Grillot, H. Lannou, C. Matileri, G. Flavien, D. Deshildre, T. Roussel, The Cryogenic System for NeuroSpin Laboratory: Main Features and Refrigerator Commisioning CEC/ICMC Conf. Proc. (2011).
[33] P. Kittel, A.L. Spivak, L.J. Salerno, Thermal conductance of gold plated metallic contacts at liquid helium CEC/ICMC Conf. Proc. (1991).
[34] L.J. Salerno, P. Kittel. Thermal Contact Conductance. NASA, Ames Research Center, February 1997, NASA TM 110429.
[35] N. Coron et al., in proceedings of "Identification of Dark Matter 2010", PoS(IDM2010)054.
[36] E. Armengaud, (EDELWEISS Collaboration). J. Phys.: Conf. Ser. 375 (2012) 012004.
[37] A. Erb, J.-C. Lanfranchi, Growth of High-Purity Scintillating CaWO_4 Single Crystals for the Low-Temperature Direct Dark Matter Search Experiments CRESSTII and EURECA, CrystEngComm (2013). http://dx.doi.org/10.1039/C2CE26554K.
[38] B. Censier, A. Benoit, G. Bres, F. Charlieu, J. Gascon, J. Gironnet, M. Grollier, R. Guichardaz, A. Juillard, L. Lauro, J. Minet, B. Paul, L. Vagneron, The EDELWEISS Collaboration, EDELWEISS Read-out Electronics and Future Prospects, J. Low Temp. Phys. 167 (2012) 645. http://dx.doi.org/10.1007/s10909-012-0568-9.
[39] AXON Cable SAS http://www.axon-cable.com/
[40] G.A. Cox, (EDELWEISS Collaboration). Nucl. Instrum. Methods A 684 (2012) 63.
[41] M. Laubenstein, G. Heusser, Appl. Rad. Isot. 67 (2009) 750.
[42] C. Arpesella, Astroparticle Physics 18 (2002) 1.
[43] C. Bucci, Eur. Phys. J A 41 (2009) 156.
[44] D.S. Leonard, Nucl. Instrum. Methods A 591 (2008) 490.
[45] P. Loaiza et al. http://radiopurity.in2p3.fr
[46] M. Wójcik, G. Zuzel, In Proc Topical Workshop on Low Radioactivity Techniques: LRT 2006, AIP Conference Procs. 897 (2007) 53.
[47] V.A. Kudryavtsev, Comp. Phys. Commun. 180 (2009) 339.
[48] S. Agostinelli, (GEANT4 Collaboration). Nucl. Instrum. and Meth. in Phys. Res. A

506 (2003) 250.

[49] G. Cocconi, V. Cocconi Tongiorgi, Phys. Rev. 84 (1951) 29.
[50] J.F. Ziegler, IBM J. Res. Develop. 40 (1996) 19.
[51] M. Chen, V.M. Novikov, B.L. Dougherty, Nucl. Instrum. Methods A 336 (1993) 232.
[52] http://radiopurity.in2p3.fr/search.php?Material=Steel
[53] W. Maneschg, Nucl. Instrum. Methods A 593 (2008) 448.
[54] S.R. Elliott, Phys. Rev. C 82 (2010) 054610.
[55] G. Heusser, Ann. Rev. Nucl. Part. Sci. 45 (1995) 543.
[56] I. Barabanov, Nucl. Instrum. Methods B 251 (2006) 115.
[57] D. Nikezić, K.N. Yu, Radiat. Meas. 41 (2006) 101.
[58] J. Benziger, Nucl. Instrum. Methods A 582 (2007) 509.
[59] A. Pocar, PhD Thesis, Princeton University (2003), http://borex.princeton.edu/public-docs/theses/pocar_phd.pdf
[60] V.E. Guiseppe, In Proc Topical Workshop on Low Radioactivity Techniques: LRT-2010 1338 (2011) 95, AIP Conference Proc.
[61] E.O. Knutson, C.V. Gogolak, P. Scofield, G. Klemic, Radiat. Prot. Dosim. 45 (1992) 313.
[62] A.C. George, E.O. Knutson, K.W. Tu, Health Phys. 45 (1983) 439.
[63] G. Claudet, Cryogenics 26 (1986) 443.
[64] W.B. Wilson, SOURCES4A: A code for calculating (α, n) spontaneous fission, and delayed neutron sources and spectra, Technical report LA-13639-MS Los Alamos (1999).
[65] M.J. Carson, Astroparticle Physics 21 (2004) 667.
[66] R. Lemrani, Nucl. Instrum. and Meth. in Phys. Res. A 560 (2006) 454.
[67] V. Tomasello, V.A. Kudryavtsev, M. Robinson, Nucl. Instrum. and Meth. in Phys. Res. A 595 (2008) 431.
[68] V. Tomasello, M. Robinson, V.A. Kudryavtsev, Astroparticle Physics 34 (2010) 70.
[69] M. Herman, R. Capote, B. Carlson, P. Obložinský, M. Sin, A. Trkov, H. Wienke, V. Zerkin, EMPIRE: Nuclear Reaction Model Code System for Data Evaluation, Nucl. Data Sheets 108 (2007) 2655, Empire 2.19 User's Guide, www.nndc.bnl.gov/empire219/downloads.html.
[70] V. Tomasello. PhD Thesis, University of Sheffield (2010).

Glossary

ADC: analogue-to-digital converter
ANR: Agence Nationale de la Recherche
ASPERA: Astroparticle European Research Area
BGO: bismuth germanium oxide
BMBF: Bundesministerium für Bildung und Forschung
CC: computing centre
CDM: cold dark matter
CDMS: Cold Dark Matter Search
CERN: Organisation Européenne pour la Recherche Nucléaire
CL: confidence level
CPU: central processing unit
CRESST: Cryogenic Rare Event Search with Superconducting Thermometers
CUORE: Cryogenic Underground Observatory for Rare Events
DAQ: data acquisition
DB: database
DOMUS: Deep Observatory for Multidisciplinary Underground Science
DR: dilution refrigerator
EDELWEISS: Expérience pour Détecter les WIMPs en Site Souterrain
EDI: electrodeionisation
EMC: electromagnetic compatibility
EURECA: European Underground Rare Event Calorimeter Array
EXO: Enriched Xenon Observatory
FEA: finite element analysis
FID: fully interdigitised
FLT: first level trigger
FR4: flame retardant fibreglass
FWHM: full width at half maximum
GEANT4: Geometry and Tracking
GEMPI: Max Planck Institute Ge-spectrometer

GERDA: Germanium Detector Array
GPS: Global Positioning System
HAP: Helmholtz Alliance for Astroparticle Physics
HEMT: high-electron-mobility transistor
HEPA: high-efficiency particulate air filter
HPGe: high-purity germanium
HV: high voltage
IC: integrated circuit
ICP-MS: inductively coupled plasma mass spectrometry
ID: interdigitised
IEC: International Electrotechnical Commission
ILIAS: Integrated Large Infrastructures for Astroparticle Science
IN2P3: Institut national de physique nucléaire et de physique des particules
IR: infrared
ISO: International Organisation for Standardisation
JFET: junction gate field-effect transistor
KATRIN: Karlsruhe Tritium Neutrino experiment
KData: Karlsruhe Data Analysis
LAN: local area network
LED: light emitting diode
LHC: Large Hadron Collider
LHe: liquid helium
LKP: lightest Kaluza-Klein particle
LNGS: Laboratori Nazionali del Gran Sasso
LN2: liquid nitrogen
LSM: Laboratoire Souterrain de Modane
LSP: lightest supersymmetric particle
LTP: lightest T-odd particle
LUX: Large Underground Xenon experiment
MICINN: Ministerio de Ciencia e Innovación
MPOD: Myriapoda, voltage supply system
MSSM: minimal supersymmetric standard model
MULTIDARK: Multimessenger Approach for Dark Matter Detection
MUSIC: Muon Simulation Code
MUSUN: Muon Simulation Code for Underground Physics
m.w.e.: metres water equivalent
NAA: neutron activation analysis
NEMO: Neutrino Ettore Majorana Observatory
NTD: neutron transmutation doped
Oxrop: Oxford University ROOT-based data analysis software
OVC: outer vacuum case
PCB: printed circuit board
PE: polyethylene
PMMA: poly(methyl methacrylate)
PMT: photomultiplier tube
PPS: pulse per second
PVDF: polyvinylidene fluoride
QET: quasiparticle-trap-assisted electrothermal feedback
RO: reverse osmosis
ROI: region of interest
ROSEBUD: Rare Objects Search with Bolometers Underground
SAMBA: Système d'Acquisition Multi-Bolomètres sur Apple
SI: spin independent
SLT: second level trigger
SOURCES4: code for calculating (α,n), spontaneous fission, and delayed neutron sources and spectra
SQUID: superconducting quantum interference device
SUSY: supersymmetry
TDR: technical design report
TES: transition edge sensor
UF: ultrafiltration
UHV: ultrahigh vacuum
UTC: Universal Time Coordinate
UV: ultraviolet
WIMP: weakly interacting massive particle
XMASS: Xenon Detector for Weakly Interacting Massive Particles